[redacted]
P. 136

[redacted]

NASA Contractor Report 189648

CHEMICAL VAPOR DEPOSITION FLUID FLOW SIMULATION MODELLING TOOL

Edward T. Bullister

NEKTONICS, INC.
875 Main St.
Cambridge, MA 02139

Contract NAS1-19102

June 1992

National Aeronautics and Space Administration

Langley Research Center
Hampton, Virginia 23665-5225

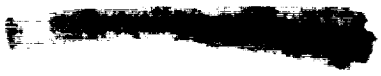

Contents

Chapter 0

INTRODUCTION

OBJECTIVE:

The objective of this project was to enhance the computational fluid dynamics (CFD) code NEKTON to include additional capabilities necessary for chemical vapor deposition (CVD) applications. The major task associated with this was to modify the incompressible code to include compressibility. This was important because compressibility is essential to the accurate solution of CVD problems. Other tasks related to CVD, and specifically, microgravity CVD, included addition of arbitrary body forces for g-jitter, addition of variable properties for temperature-dependent and species-dependent materials properties, and the ability to calculate chemical reactions in multicomponent reactions.

IMPLEMENTATION:

The strategy for the implementation of the capabilities necessary for CVD applications was to introduce sequentially each feature necessary for solution of CVD problems. Each feature added to the code was tested on sample problems to verify

its accuracy.

Nektonics is currently planning to release a NEKTON/CVD code in the context of its next major product release (Nekton 3.0).

ORGANIZATION:

In the following we detail chronologically the implementation of each individual feature in the form of summaries of the work done in each quarter.

In Chapter 1 we describe the implementation and demonstrate the use of the capability for solving problems involving the "g-jitter" forces. These time-varying forces typically are large in relation to the constant accelerations in microgravity environments.

In Chapter 2 we demonstrate the use of the variable diffusivity of chemical species in NEKTON. We demonstrate the effects of variable diffusivity on mass transfer problems in geometries prototypical in CVD applications.

In Chapter 3 we describe the multibody radiation capability in NEKTON. We describe the module which gives the additional capability of calculation of Gebhart factors through inversion of the shape factor matrices.

In Chapter 4 we show the implementation of the Soret effects in the passive scalars of NEKTON.

In Chapter 5 we describe the implementation of the Motif graphical user interface in NEKTON. We give examples of the use of it for ease of the input of geometries and ease of evaluation of the results.

In Chapter 6 we first give the expansion of the Navier-Stokes equations using perturbations for small Mach numbers. We justify the use of the resulting Low-Mach number approximation for CVD applications and demonstrate its use in compressible

test cases.

In Chapter 7 we present the method of Bussing and Murman for the solution of coupled problems in which the time scales for chemical reactions was much smaller than the diffusive time scales. We demonstrate the use of this point-implicit method in test problems with varying time scales.

In Chapter 8 we show the method for solving the convection-diffusion problem for *nondilute* mixtures of gases. This involves calculation of a convective component of the diffusion process and a mixture-dependent density.

Finally, in Chapter 9 we summarize the work done in this project. We discuss the physical processes important in CVD problems, the approach we used to model these processes, and the results we have achieved.

Chapter 1

Unsteady Body Forces (g-jitter)

OBJECTIVE:

The technical objective to be attained by the close of the first quarter in Phase II was to develop the capability to handle arbitrary fluctuating three-dimensional body forces ("g-jitter").

BACKGROUND:

The motivation for enhancing the simulation capabilities of NEKTON through inclusion of an arbitrary three-dimensional body force stems from the need to accurately handle the prevailing gravity levels in space during materials processing. The recorded g-levels on board the shuttle appear to establish that the direction and magnitude of the gravity vector in space vary with time [1]. Whereas fundamental considerations suggest a minimum residual gravitational acceleration of 10^{-6} of earth gravity in space, current measurement techinques appear to be limited to 10^{-5} g_e. Further more, the lowest frequency of the g-jitter is found to be close to 20 Hz. As the primary driving force for interference of convection with crystal growth in space

is associated with the buoyancy forces in the reactor, it is reasonable to expect that convection in these systems is a complex function of time leading to three-dimensional flow structures. Numerical simulation of crystal growth processes in space (e.g. [2]) are generally based on a uniform magnitude and direction of g. The time-dependant aspect of gravity level has been considered by several researchers [3-6]. It has been shown in ref. [6] that the response of convective systems to time-dependant gravity is controlled by the ratio of vibrating frequency of g to the diffusive time scale in the system, the so-called Wormerley number $W = h^2\omega/\nu$. For $W < 1$ convection in the system follows the time-dependant change in g, and for $W > 1$ the intensity of convection in the melt decreases with W. The formulations developed in refs. [3-6], amongst many others, represent idealizations of the prevailing gravity field in the space. Recently Alexander and colleagues have shown that impulses in g as well as the three dimensional nature of the gravity field can significantly influence the dopant distribution during directional solidification of doped semiconductors [7]. With the continuing advances in accelerometer technology reliable data on g-levels in space can be expected to be available in the near future. As the magnitude and direction of g determines the flow structure in crystal growth systems, the presently developed capability of NEKTON can provide for accurate simulation of convection in crystal growth systems using measured unsteady 3-dimensional g-levels in space.

IMPLEMENTATION :

The gravitational body force was input in the right hand side of the Navier stokes equations in a manner analogous to the handling of the nonlinear convective term. That is, a third order Adams-Bashforth integration scheme was used. This scheme, in addition to providing third order accuracy for the integration of a time-dependant gravitational body force, has favorable stability characteristics. No additional stability constraints beyond the Courant condition were imposed by the oscillating body

force. The user accesses this gravitational body force via 3 FORTRAN functions typed in during problem definition in the preprocessor. Through each of the 3 FORTRAN functions the user can define 3 independent components of the gravitational force, each of which can be either constant or can vary with time according to an arbitrary functional relationship.

The body force was tested using three cases. In each case the steady component of the Rayleigh number, that is, the magnitude of the convective force caused by the steady component of gravity, was 10. In cases b and c a sinusoidally oscillating component of component of gravity, resulted in the oscillating Rayleigh number of 100. The problem was solved for the hemispherical geometry depicted in figure 1. A temperature of 100 was imposed at the seed surface, and a temperature of zero was imposed at the inner surface of the support shaft.

	Case a	Case b	Case c
Wormersley Number	0	0.1	100
Rayleigh Number			
Steady	10	10	10
Oscillating	100	100	100

Here we define the Wormersley number as W=h**2 omega/nu, where h is the sphere radius, omega is the frequency in cycles/time, and nu is the kinematic viscosity. The test cases represent a zero Wormersley number control, a low Wormersley

number, and a high Wormersley number.

For relatively low Wormersley numbers (case b), we expect the dynamic components of the oscilliating force to be of marginal unimportance; we expect a quasi-steady flow at each instant corresponding to the steady flow resulting from a steady gravitational force equal to the gravitational force at that instant.

In the high w limit (case c), we expect a strong interaction between the dynamic component of the oscillating force and the dynamics of the flow regime. In this case, we expect a filtering behavior such that the response of the system in terms of velocity magnitude to decrease with Wormersley number (frequency).

Note that these test cases were run each with a single frequency component of the gravitational force. This in no way reflects a code limitation; the structure of the function input allows for multiple frequencies and directions to be simultaneuosly input. Studies of nonlinear interactions between frequency components are therefore possible with this implementation.

RESULTS:

In figures a, b, and c we plot the axial velocity component at a point on the axis about midway between the crystal surface and the hemisphere surface. In case a the velocity reaches a peak of 0.33e-2 before reaching its steady value of approximately 0.1e-2. This velocity overshoot is caused by the evolution of the temperature field from its initial conditions. As steady state is reached the convection set up by the velocity reduces the temperature difference within the fluid, acting to relieve part of the force driving the fluid. In case b the velocity reaches a steady periodic half-amplitude of 0.1e-2. In case c the velocity reaches a steady periodic half-amplitude of 0.12e-3. There is a clear indication of suppression of the effects of convective force with increasing Wormersley number. For Wormersley number of 0.1, the magnitude of the

oscillating gravitational component needed to be an order of magintude higher than the steady case to achieve com- parable convective velocity magintudes. Increasing the Wormersley number to 100 supresses the convective velocity by an additional order of magnitude.

REFERENCES

1. N. Trappen and F.J. Demond, Porceedings of the Norderney Symposium on Scientific Results of the German Spacelabd Mission D1, Norderney, Germany, 1986.

2. P.M. Adornato and R.A. Brown, J. Crystal Growth, 80 (1987) 155

3. L.W. Spradely, S.W. Bourgeois, and F.N. Lin, AIAA paper, 75-695, 1975.

4. Y. Kamotani, A. Parsad, and S. Ostrach, AIAA Journal, 19 (1981) 511.

5. P.R. Griffin and S. Motakef, Applied Microgravity Technology, II (1989) 121-132.

6. J.I.D Alexander, J. Ouzzani and F. Rosenberger, J. Crystal Growth, 97 (1989) 285.

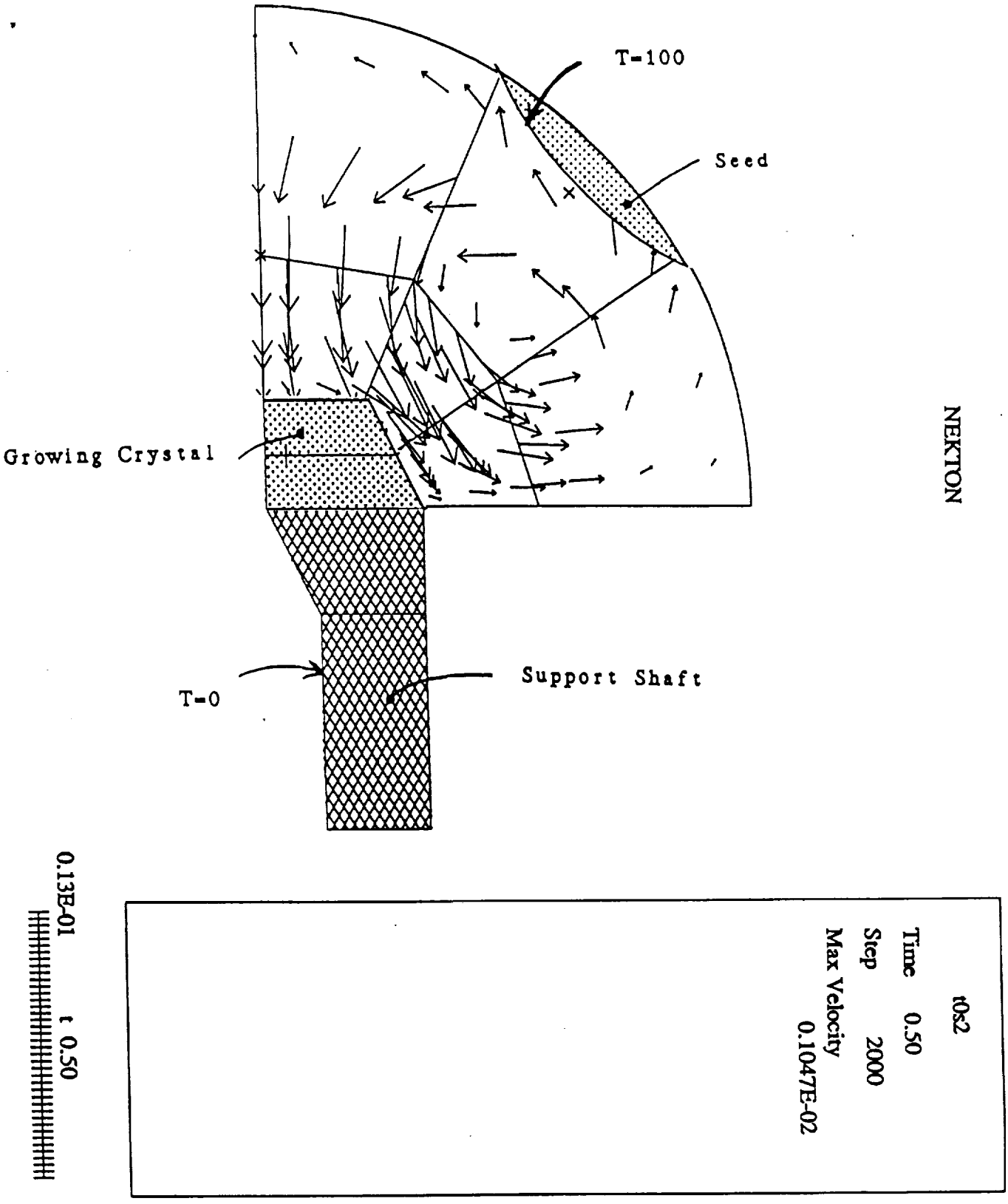
T=100
Seed
Growing Crystal
T=0
Support Shaft
NEKTON
t0s2
Time 0.50
Step 2000
Max Velocity
0.1047E-02
0.13E-01
t 0.50

FIGURE 1

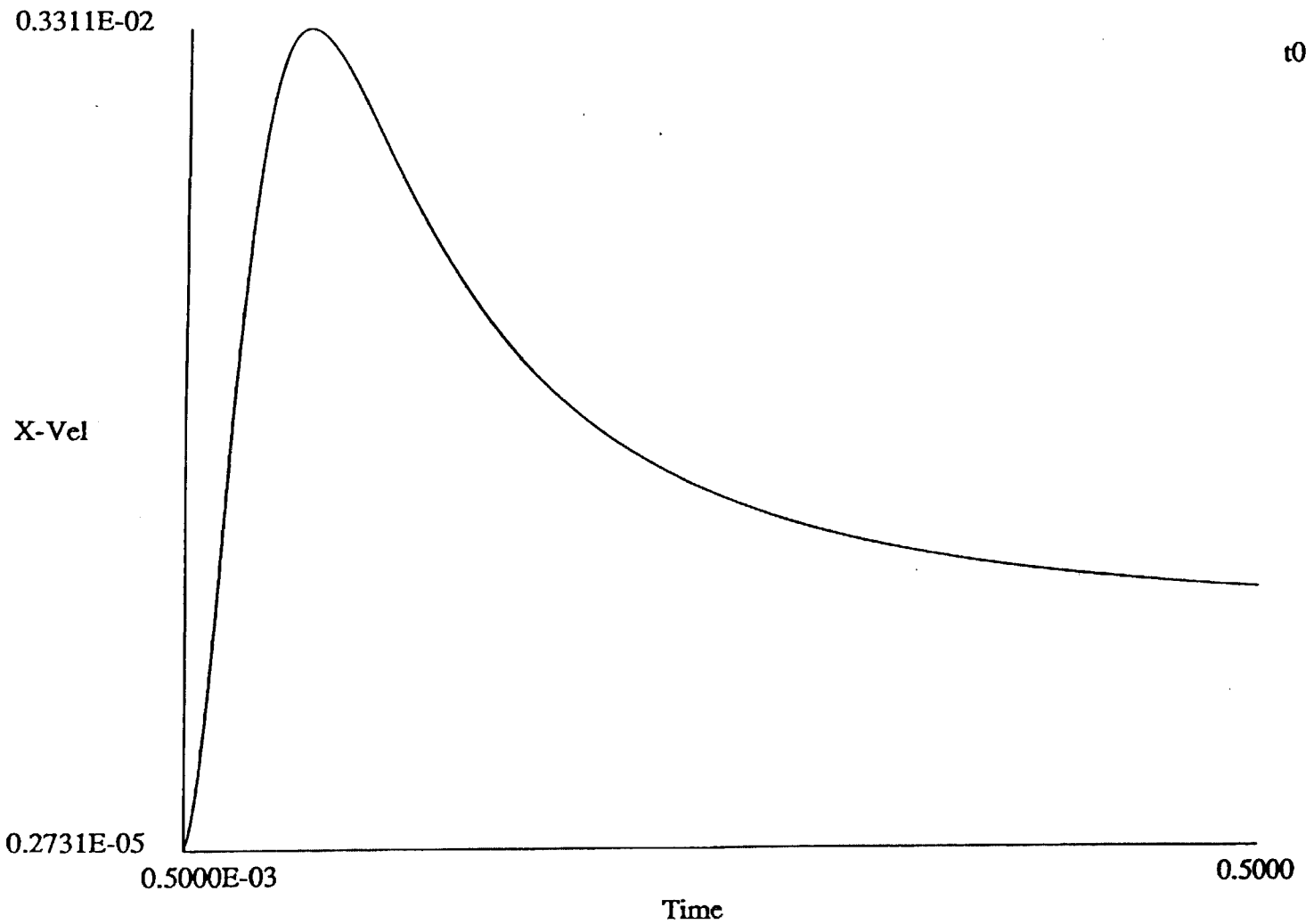

FIGURE a

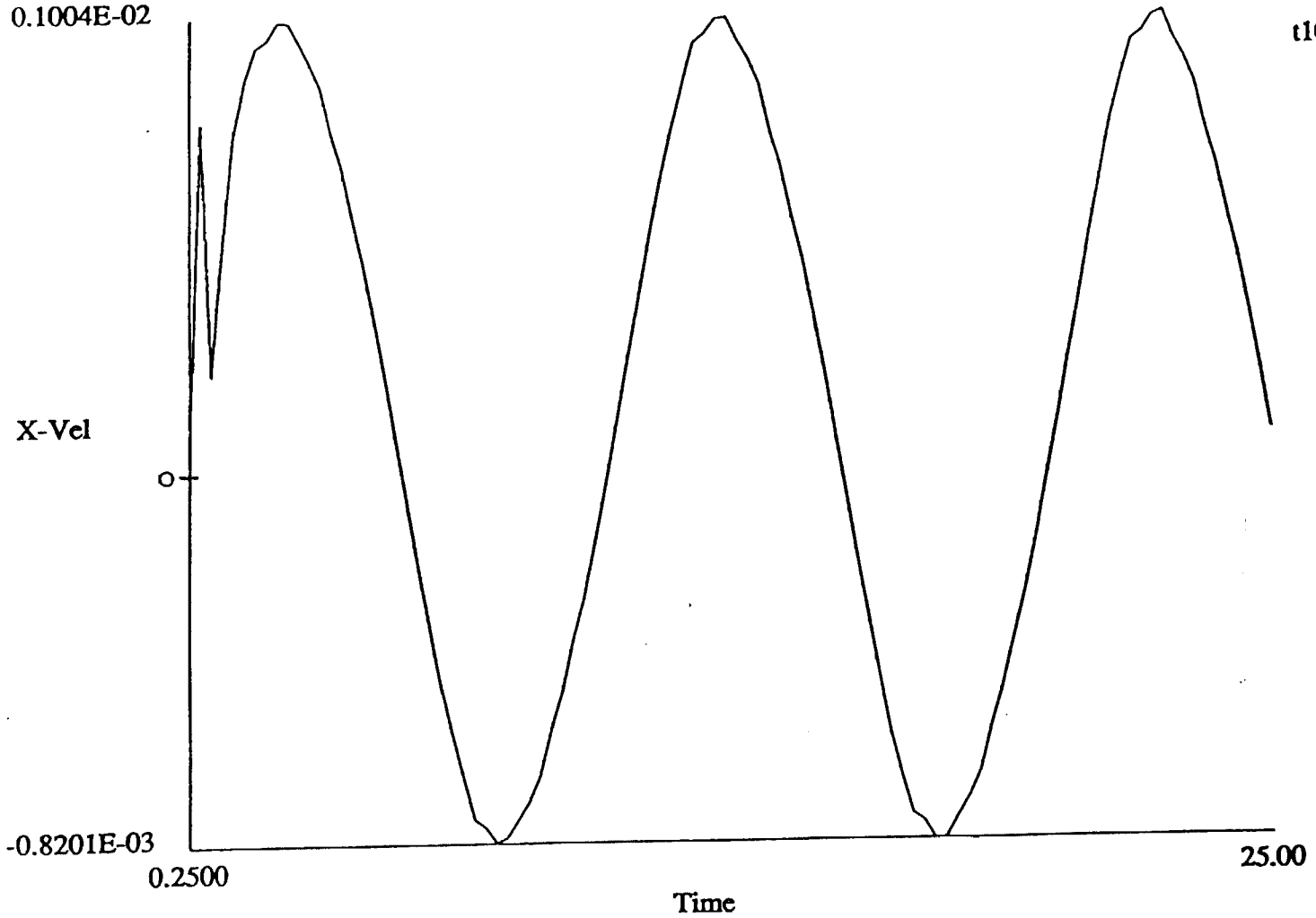

FIGURE b

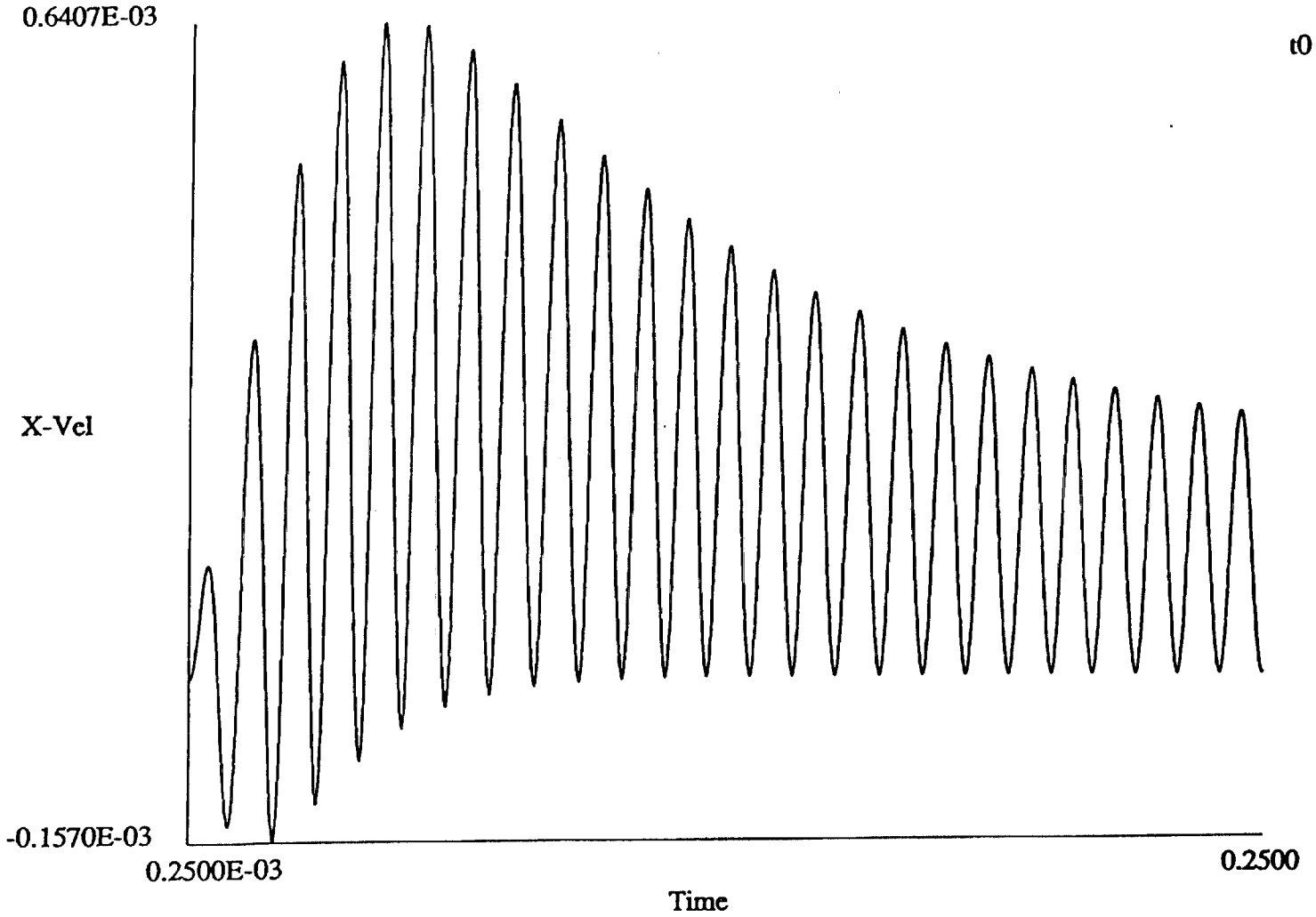

FIGURE C

Chapter 2

Variable Diffusivity

OBJECTIVE:

The objective in quarter 2 was to complete implementation of variable diffusivity of the chemical species within the context of an incompressible NEKTON. We have completed the implementation of this capability in NEKTON. We have run two simulations that demonstrate the effects of variable diffusivity in a prototypical CVD reactor. These simulations also serve as a preliminary invesigation on the effects of variable properties in prototypical CVD applications.

OTHER PROGRESS:

Parallel to the development of new capabilities within the NEKTON solver is the development of the user interface. During this quarter we addressed two aspects of user interface development.

First, we expanded the capability of the PRENEK preprocessor to enable the user to access the new features added to the NEKTON solver. PRENEK now prompts the user for variable or constant properties within the passive scalar fields. This enables a

user to enter, from the keyboard, a FORTRAN function which defines the diffusivity for the chemical species stored within the passive scalar fields. This allows the species diffusivity to vary arbitrarily with temperature.

Second, we enhanced the structure and layout of the user interface to make the package a more useful CVD tool. A modern CVD tool should have an interface which is flexible, and readily accessible to its user without requiring extensive training or programming skills. Toward this goal we have adapted PRENEK and POSTNEK to run through the Motif toolkit for X Windows applications. In figure 1, we show the layout and structure of the Motif- based POSTNEK application. In this figure two windows are brought by POSTNEK, a window for flow control and text display at the top of the figure, and the plotting window below. The top level control of POSTNEK is handled by a menu bar which spans the top of the control and text window. Within the menu bar are sets of cascading pull-down menus which give a top-level, intuitive, and standardized system for control of POSTNEK.

As many MOCVD applications can be treated as quasi-steady problems, we have implemented the steady state solution technique of Sidi and Celestina[1] in NEKTON. The advantages of this addition are twofold. First, solution of the problem requires less input from the user to define the problem. Second, significant savings in cpu time can result from accelerating the convergence to steady state. At the expense of losing accuracy during the transient phase, the accurate steady state solution can be obtained much more quickly. In appendix A we present a more detailed description of this technique.

VARIABLE DIFFUSIVITY:

BACKGROUND: Constant gas properties are assumed within CVD applications in a first examination in order to make the problem more amenable to theoretical analysis and to make numerical investigation simpler. Real CVD applications can have gases in which absolute temperatures vary by a factor of two or more, which result in diffusivities changing by a factor of 3-4.

IMPLEMENTATION :

We have implemented in NEKTON the ability to input gas properties (diffusivity within passive scalars) which can vary locally with temperature and passive scalar concentration. In NEKTON this has required us to change the equation solved for the diffusion operator for passive scalars. Whereas we previously calculated the term as (D*laplacian (concentration), we now calculate the gradient(D*gradient(concentration)). In the latter calculation, the diffusivity D can vary arbitrarily with space without compromising the accuracy of the result.

TEST CASES

We have run two test cases. The purpose of these tests was to demonstrate the impact of variable properties on quantities of interest in a realistic CVD geometry, i.e., concentrations profiles of chemical species and deposition rates.

In test case a we simulate diffusion of TMGa in H_2 using a constant diffusivity based on the bulk temperature of the ambient gas.

In test case b we simulate diffusion of TMGa in H_2 using the dependencies from Moffat and Jensen [2]. This diffusivity varied according to the relation

$$D = \frac{2.23 \times 10^{-5} T^{1.73}}{p} \quad cm^2/sec$$

where D is in cm**2/sec and p is in atm. In figure 2 we show the geometry of the hemispherical reactor in which we perform our simulations. In this geometry the seed material temperature is fixed at 1300 K, while the growing crystal is cooled from below and has a somewhat lower surface temperature. In figure 3 we plot this temperature along line segment a-b defined in figure 4, which runs perpendicularly from the substrate surface toward the reactor wall. In figures 5a and 5b we plot along the same line segment the concentration profiles for test cases (a) and (b), respectively. The profiles for the two cases are qualitatively similar. As expected, the concentration gradient (and therefore, deposition rate) at the surface is steeper in case (b). This follows from the lower local diffusion coefficient in case (b) due to the lower than average local temperature. The net difference in deposition rate is approximately 25 percent.

REFERENCES

1. Moffat and Jensen, Journal of Crystal Growth, 77 (1986) 108-119.

2. Sidi, Avram, and Celestina, Mark "Convergence Acceleration for Vector Sequences and Applications to Computational Fluid Dynamics", NASA Technical Memorandum 101327, ICOMP-88-17.

APPENDIX: STEADY STATE ACCELERATION

Steady State Acceleration

NEKTON uses a semi-implicit approach to solve the unsteady Navier-Stokes equations (or unsteady convection-diffusion equations). If the solution has a steady state, this solution is obtained by a time-integration of the unsteady equations until steady state is reached.

For larger Re-numbers (or Pe-numbers), the number of times steps, $N_t = \tau/\Delta t$, can be large. The reasons for this are: (1) the typical time (τ) to reach steady state is proportional to the Re-number; (2) larger Re-number problems generally require more resolution (smaller mesh size, Δ_x); (3) the time step restriction due to the Courant criterion, $\Delta t < CU/\Delta_x$, is more severe for higher Re-numbers and high resolution meshes. Here U is a characteristic velocity.

In order to speed up the steady Navier-Stokes solver, we have recently implemented a steady state acceleration procedure based on the work of Sidi et al ["Convergence Acceleration for Vector Sequences and Applications to Computational Fluid Dynamics", August 1988]. The main idea is to compute the initial transient behavior, and then apply an extrapolation procedure based on a sequence of (global) solution vectors. Figure 6 shows an example where this strategy was applied, resulting in a speed-up of a factor of 5.

Sidi
Ford
Smith
Celestina

Steady State Acceleration

$$\frac{du}{dt} = \phi(u)$$ semi-discrete N-S eqs.

$$u_* = \lim_{t\to\infty} u(t)$$ steady state

$$u_*^{n,k} = \sum_{j=0}^{k} \gamma^j u^{n+j}$$ extrapolation

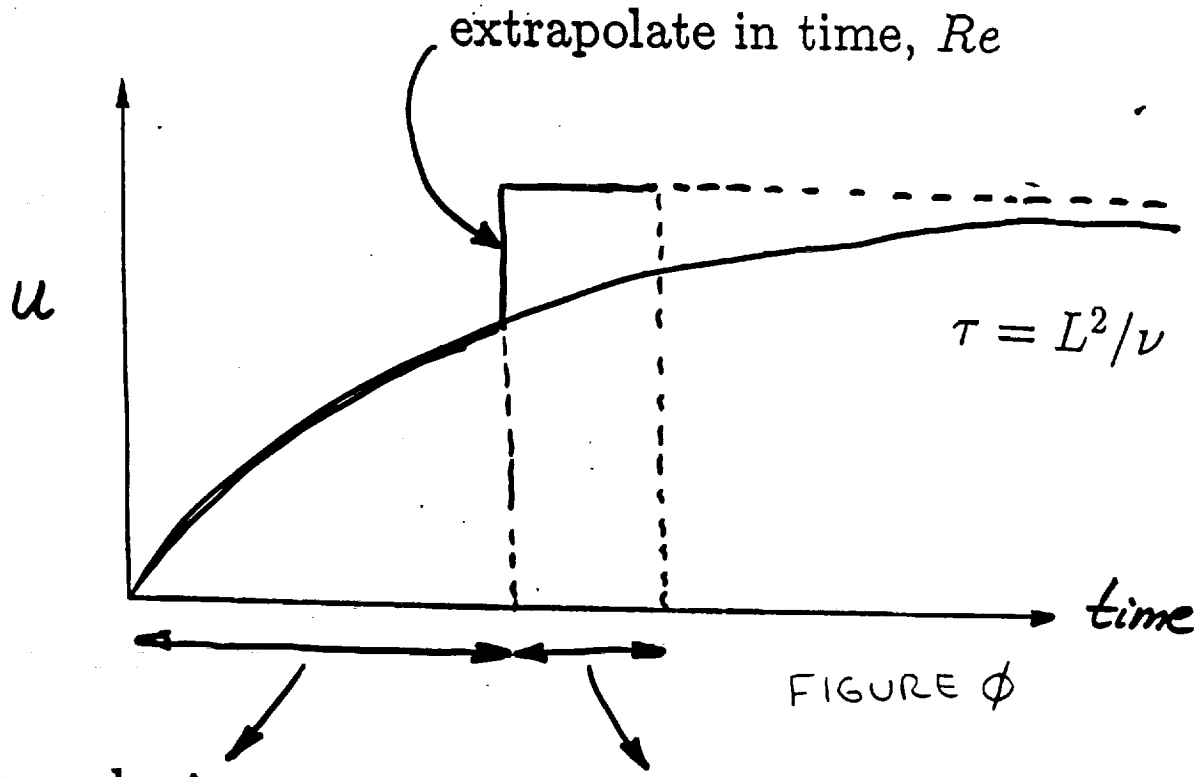

FIGURE ϕ

- low-order in time
- large time step
- loose tolerances
- lower Re, Pe

- increase temporal order
- reduce time step
- optimal tolerances

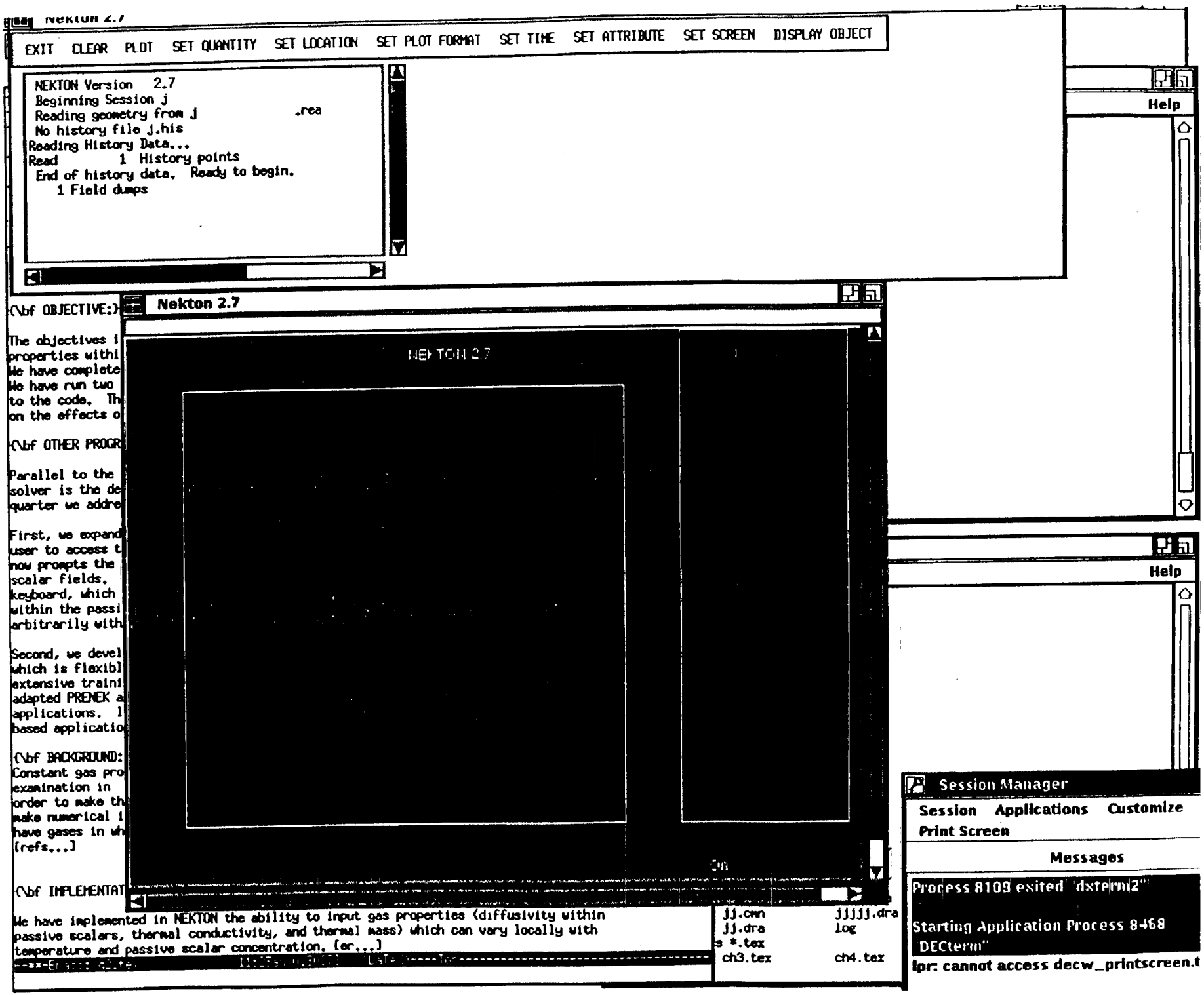
EXIT CLEAR PLOT SET QUANTITY SET LOCATION SET PLOT FORMAT SET TIME SET ATTRIBUTE SET SCREEN DISPLAY OBJECT
NEKTON Version 2.7
Beginning Session j
Reading geometry from j .rea
No history file j.his
Reading History Data...
Read 1 History points
End of history data. Ready to begin.
1 Field dumps
Help
Nekton 2.7
Session Manager
Session Applications Customize
Print Screen
Messages
Process 8109 exited "dxterm2"
Starting Application Process 8468
"DECterm"
lpr: cannot access decw_printscreen.t
jj.cmn jjjjj.dra
jj.dra log
*.tex
ch3.tex ch4.tex

Figure 1

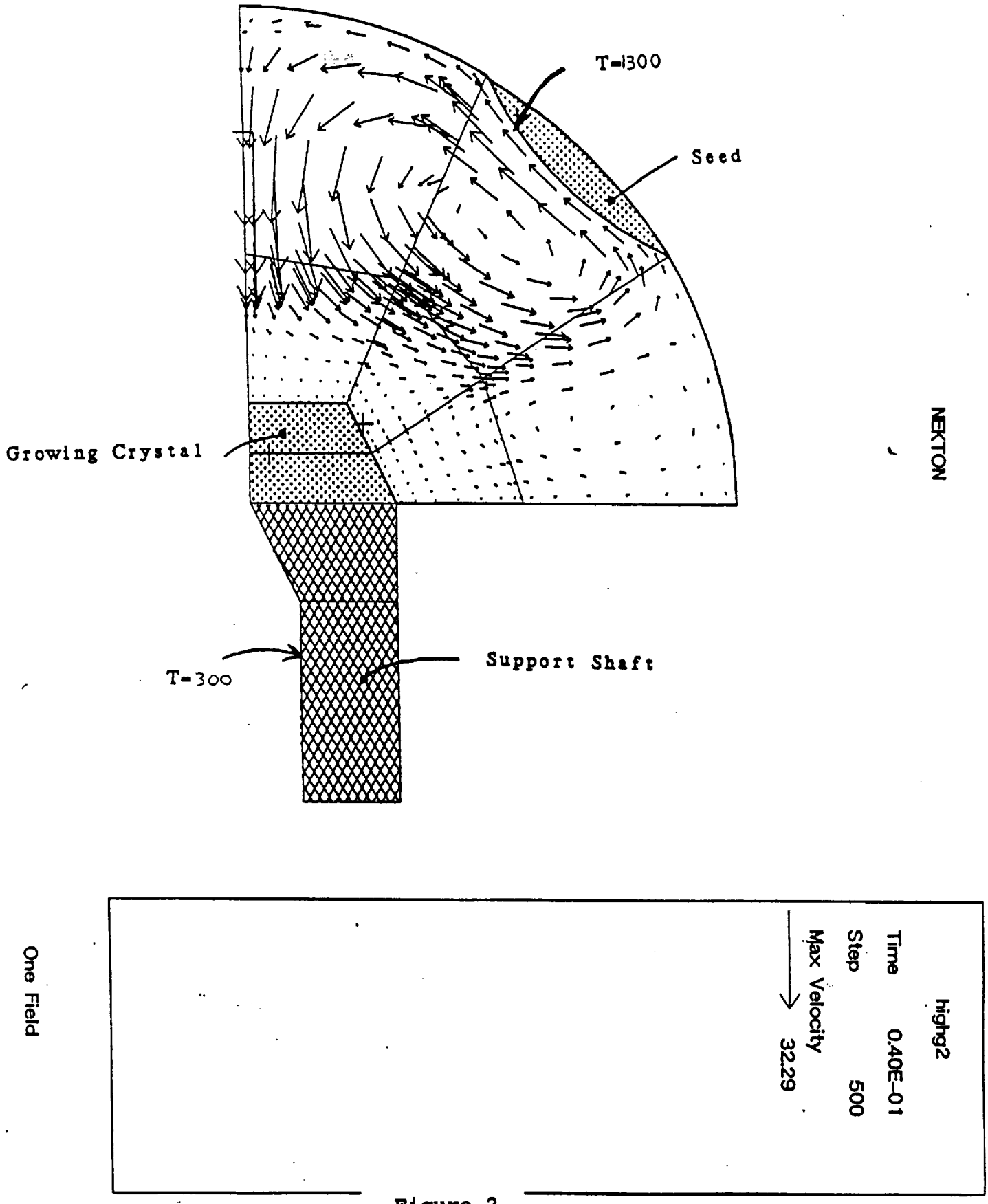
T=1300
Seed
Growing Crystal
T=300
Support Shaft
NEKTON
One Field
high2
Time 0.40E-01
Step 500
Max Velocity
32.29

Figure 2

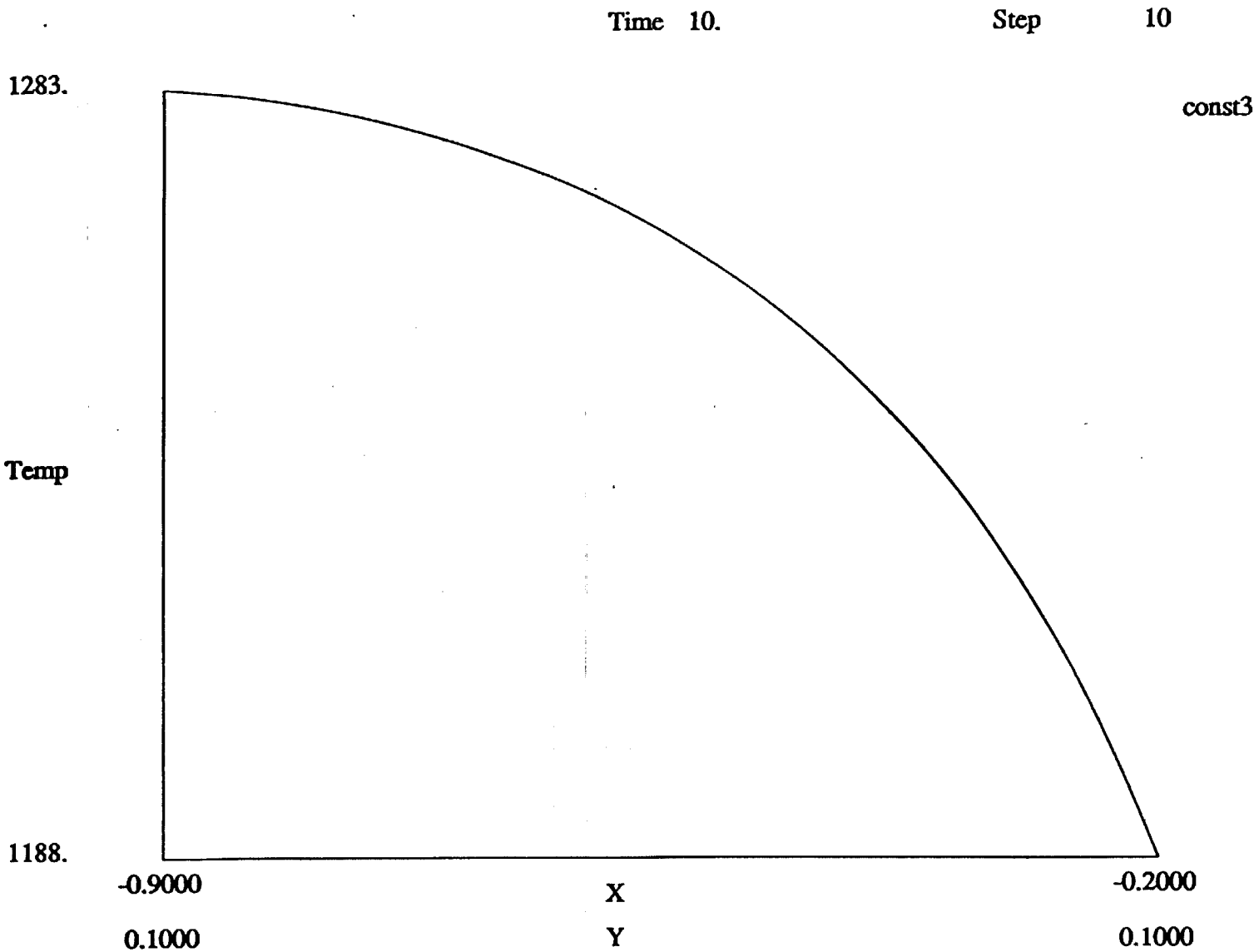
Time 10.
Step 10
1283.
const3
Temp
1188.
-0.9000
X
-0.2000
0.1000
Y
0.1000

Figure 3

Figure 4

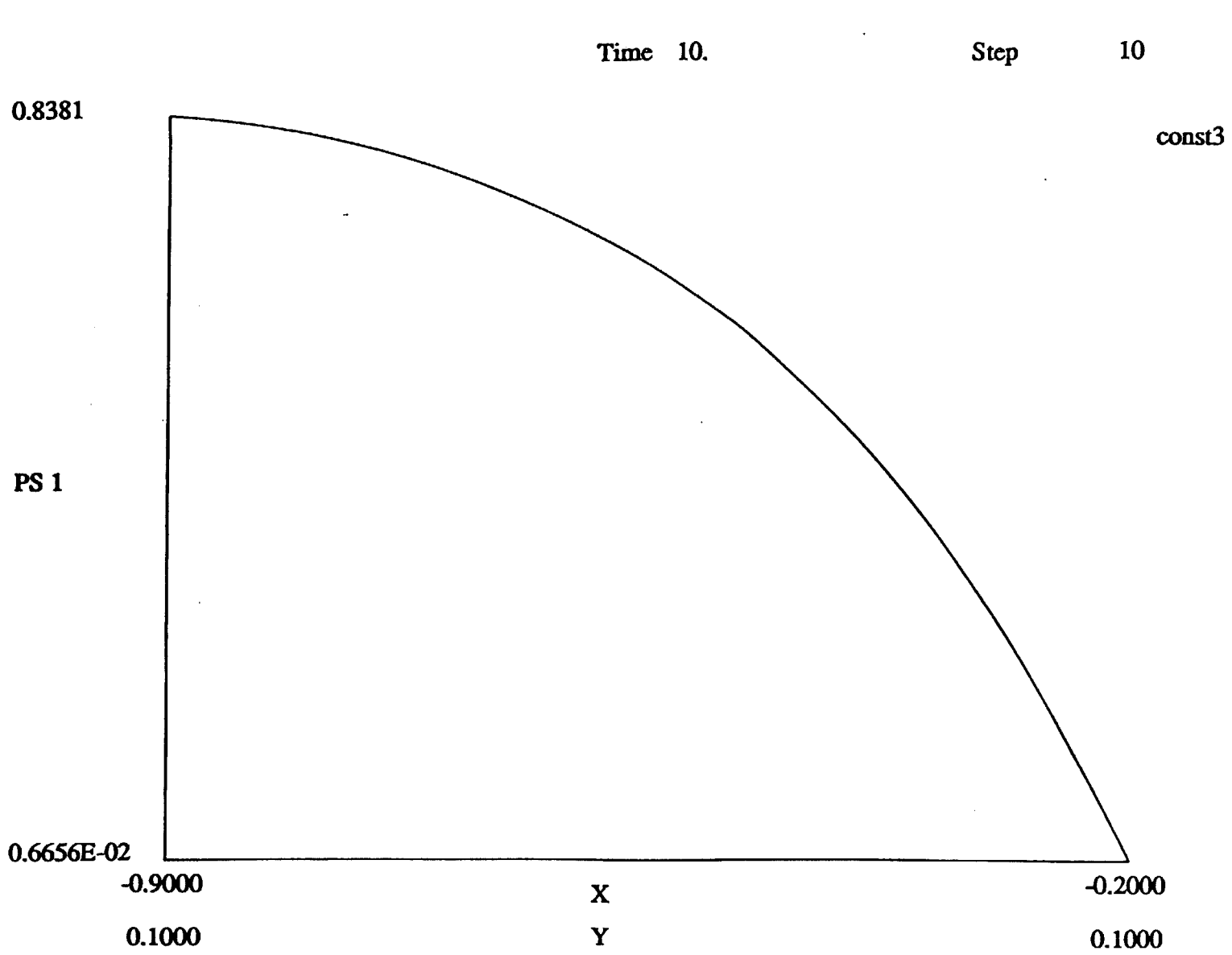
Time 10.
Step 10
0.8381
const3
PS 1
0.6656E-02
-0.9000
0.1000
X
Y
-0.2000
0.1000

Figure 5a

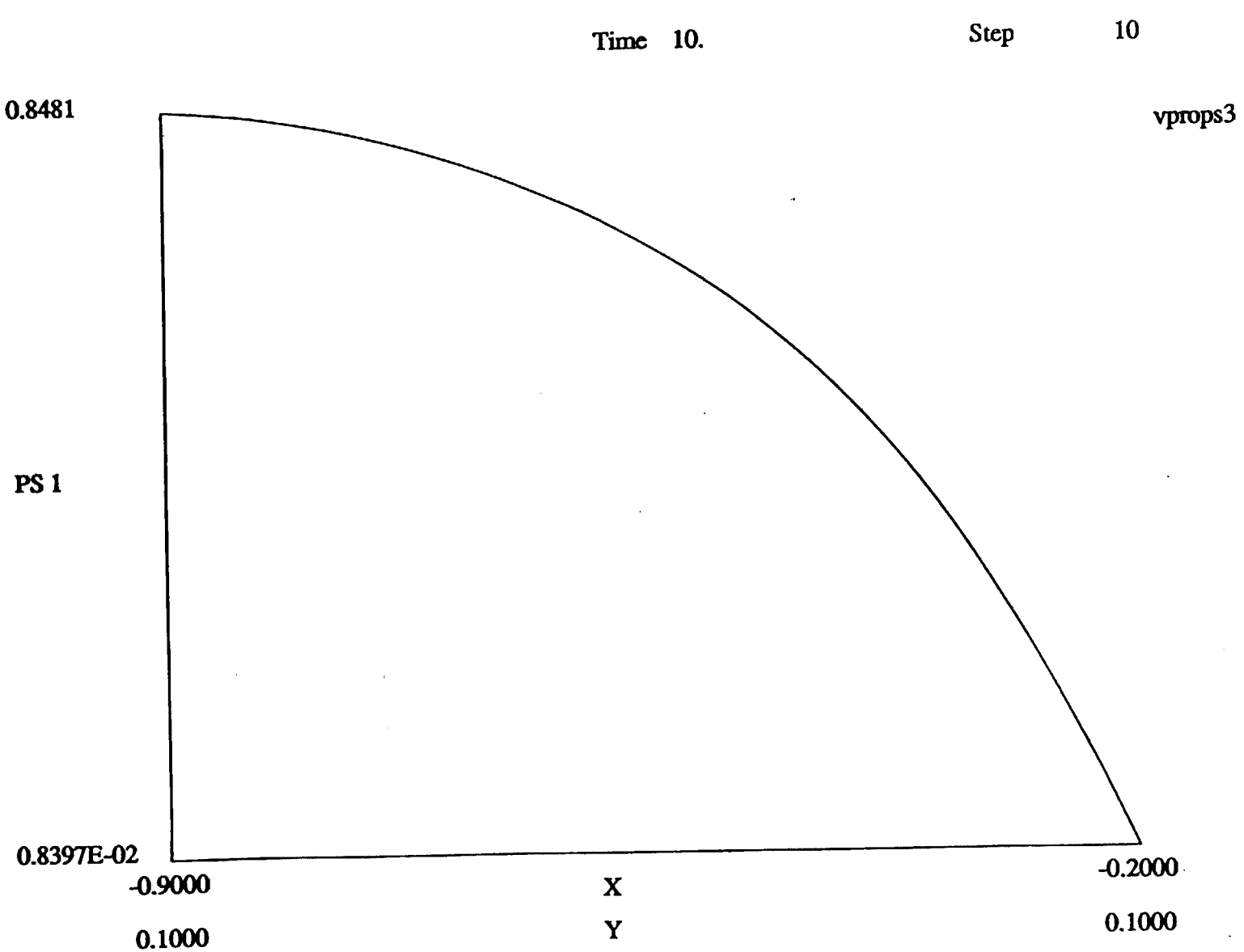
Time 10.
Step 10
0.8481
vprops3
PS 1
0.8397E-02
-0.9000
0.1000
X
Y
-0.2000
0.1000

Figure 5b

Steady State Acceleration

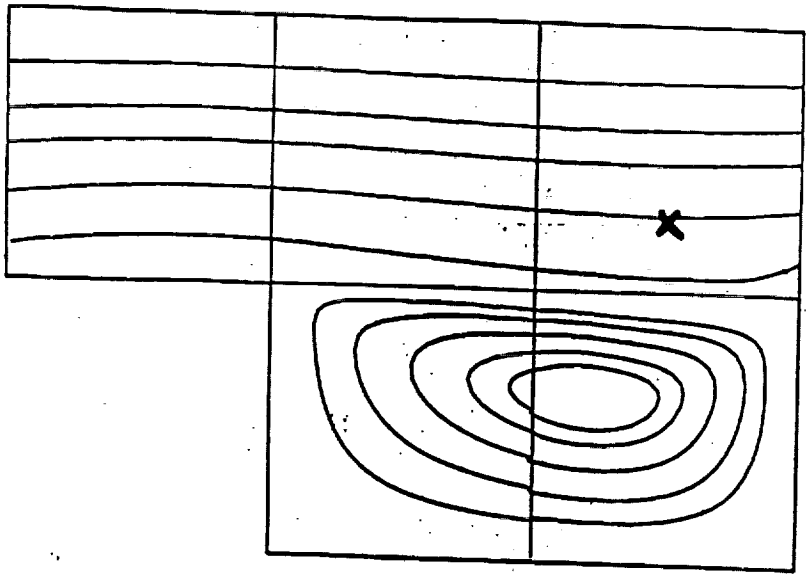

periodic grooved channel

$Re \sim 100$

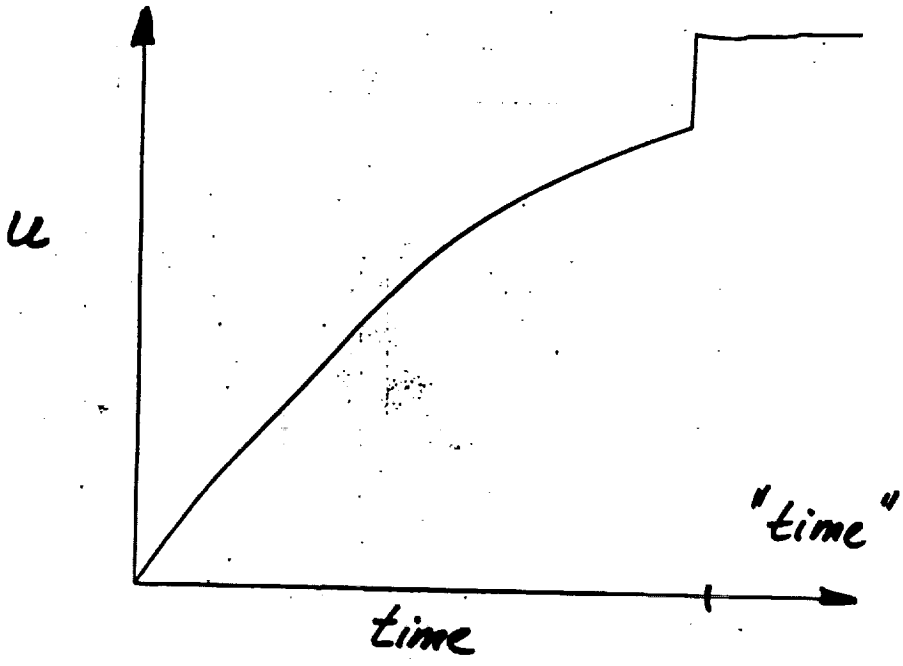

Figure 6

Chapter 3

Multibody Radiation

OBJECTIVE:

The objective for this report period was to implement multibody radiation capability in NEKTON and demonstrate its effects on the thermal calculations in a CVD rotating pedestal reactor geometry.

BACKGROUND:

The high temperatures found inside CVD reactors ensure that radiation will play a dominant role in heat transfer. Therefore, radiation heat transfer cannot be ignored in CVD reactors. Typically, radiation is handled in numerical code with the assumption of single-body radiation, that is, independent radiation exchange between a single isolated body and a nonreflecting environment. This approach breaks down when radiative interaction between components is important, when the environment temperature is unknown, and when the environment cannot be treated as an isothermal black body.

Calculation of multibody radiative exchange allows for the calculation of tempera-

tures and heat exchange rates between multiple bodys with unknown temperatures, arbitrary emissivities and arbitrary relative configurations (shape factors).

IMPLEMENTATION :

As far as we have been able to determine, multibody radiation has not yet been implemented in spectral code. To implement this feature in NEKTON, the goal was to retain the spectral accuracy inherent in the rest of the calculations, to maintain a reasonable operation count, to implement it in a manner that is clean and amenable to easy future maintenance of the code, and to make its use relatively easy for the user.

The spectral accuracy was retained by using an integration technique for the radiative heat flux calculation consistent with the spectrally accurate integration used in other parts of the code. The integrals of heat transfer between elemental edges were done as follows. The temperatures used were those at each Gauss-Lobatto collocation point on each elemental edge involved in the multibody radiation calculation. The area associated with each collocation point for the calculation of shape factors was weighted by the mass matrix. Posing the problem in this manner enabled coupling the spectral code with standard methods for the calculation of radiation heat transfer (shape factors, etc.). The resultant operation count, therefore, was the same (per point) as that for radiation implemented in a lower order finite difference or finite element method.

The shape factors for each point was calculated based on the effective area associated with each collocation point. Each of these areas was set to be a panel and (in 2-D) Hottel's Methods is used to calculate the shape factors. For the axisymmetric cases, the values from a set of standard axisymmetric configurations were adapted to the general case using the algebra governing shape factors. Thus, shape factors are cal-

culated automatically for 2-d or axisymmetric simple (without blocking) enclosures. For more complex systems with blocking of radiation or three dimensional problems, a subroutine is provided in which the shape factors can be input directly by the user.

We chose the enclosure analysis method of Gebhart [1] for the radiative coupling calculation. In this approach, the local emissivities and shape factors are converted into Gebhart factors, which are essentially Green's functions for calculating the net radiative flux to each node due to the sum of the other radiative fluxes.

Calculation of each column $[G_k]$ in the matrix of Gebhart factors is as follows:

$$
\begin{aligned}
G_{1k} &= F_{1-k}\epsilon_k + F_{1-1}\rho_1 G_{1k} + F_{1-2}\rho_2 G_{2k} + \cdots \\
&\qquad + F_{1-k}\rho_k G_{kk} + \cdots + F_{1-N}\rho_N G_{Nk} \\
G_{2k} &= F_{2-k}\epsilon_k + F_{2-1}\rho_1 G_{1k} + F_{2-2}\rho_2 G_{2k} + \cdots \\
&\qquad + F_{2-k}\rho_k G_{kk} + \cdots + F_{2-N}\rho_N G_{Nk} \\
&\cdots\cdots\cdots\cdots\cdots\cdots\cdots\cdots\cdots\cdots\cdots\cdots\cdots\cdots\cdots\cdots \\
G_{Nk} &= F_{N-k}\epsilon_k + F_{N-1}\rho_1 G_{1k} + F_{N-2}\rho_2 G_{2k} + \cdots \\
&\qquad + F_{N-k}\rho_k G_{kk} + \cdots + F_{N-N}\rho_N G_{Nk}
\end{aligned}
$$

where F_{j-k} is the shape factor between points j and k, ρ_k and ϵ_k are the reflectivity and emissivity, respectively, at point k. For column k of [G], the relation is expressed in matrix notation as:

$$[G_k] = \epsilon_k[F_k] + [F]diag[\rho][G_k]$$

Defining [H] = [F] $diag[\rho]$

(1) becomes

$-\epsilon_k[F_k] = [\mathrm{H}]\ [G_k] - [G_k]$

or

$-\epsilon_k[F_k] = ([\mathrm{H}]-[\mathrm{I}])\ [G_k]$

so that

$[G_k] = ([H] - [I])^{-1}\ (-\epsilon_k[F_k])$

$([H]-[I])^{-1}$ is inverted using standard direct (LU) solvers. The direct method is more appropriate here as the matrix is small (it contains only the radiative surface points) and is full. Also, the inverse needs to be calculated only once before performing N back solves to calculate N Gebhart vectors.

Once the Gebhart factors are calculated, we use these to calculate the heat flux between the radiating surfaces:

$Q_k = A_k\epsilon_k\sigma T_k^4 - \sum_{j=1}^{N} A_j\epsilon_k\sigma G_{jk}T_j^4$

where the first term on the RHS represents heat radiated from surface k and the second term represents the heat radiated to surface k from the N surfaces. Here σ is Boltzmann's constant and A_k is the area of surface element k.

This coupled set of nonlinear equations is solved iteratively in conjunction with the conduction heat transfer. The first term is linearized and handled semi-implicitly, similar to the manner in which single body radiation is calculated:

$A_k\epsilon_k\sigma T_k^4 = (A_k\epsilon_k\sigma T_k^3)T_k$

where the $h_r = (A_k\epsilon_k\sigma T_k^3)$ has the form of a nonlinear convection coefficient which is updated during the iteration procedure.

The second term needs to be handled explicitly as a source term on the right hand side of the heat equation, so the procedure becomes, looping over m iterations:

$$[\nabla^2 + h_r^m]T_k^{(m+1)} = F_r \sum_{j=1}^{N} A_j \epsilon_k \sigma G_{jk} (T_j^m)^4$$

While the implicit integration of the first term guarantees unconditional stability, the explicit handling of the sum on the right hand side of the equation does not. In fact there is a relaxation factor $0 < F_r < 1$ applied in the second step

$$T_k^{(m+1)} = T_k^m + F_r(T_k^{(m+1)} - T_k^{(m)})$$

which, unfortunately, is problem-dependent and is adjusted to govern the stability and convergence rate.

TEST CASES

To demonstrate the multibody radiation capability and to show its effects on a CVD reactor, we ran three cases with the geometry of the rotating pedestal reactor shown in figure 1. These demonstrate the competing effects of multibody radiation (figure 2) vs. conduction in the reactor. In each case we fix the temperature at input and input a fixed heat flux just below the pedestal surface. We nondimensionalize using the reactor diameter as the length scale, the inlet temperature as the nondimensional temperature, and the heat flux originating at the pedestal surface.

The radiation cavity consists of the disk shaped surface at flow inlet, the cylindrical reactor wall and the disk shaped pedestal surface. These are modelled using the elemental edges I1 and I2, W1 and W2, and P, respectively (see figure 3). Each of these 5 elemental edges has, in turn, 5 internal collocation points associated with its fourth-order polynomial. Each collocation point has an effective area based on its spectral weighting function.

A typical velocity field through such a cavity is plotted in figure 4.

The calculation of shape factors is done within the multibody radiation module of NEKTON based on the coordinates of each collocation point and its normal vector. This 25x25 shape factor matrix is inverted according to equation [1] to generate the Gebhart factor matrix. This matrix is full, including diagonal entries, since with nonunity emissivities each node can "see" the effects of its own emittance through reflections from other surfaces. Thus, for this problem, 625 radiation exchange paths are followed.

Note that the radiation boundary conditions are superimposed upon the other boundary conditions; this allows flexibility in combining radiation with other mechanisms of heat transfer. The heated pedestal, for example, inputs a net of one unit of flux irrespective of the radiational and conduction exchange within the cavity.

We run three cases with this geometry and set of boundary conditions. In case emiss0, the emissivities of all radiating surfaces is set to 0. In case emiss05, the emissivities are set to 0.5. In case emiss1 the emissivities are set to 1.

The case with emissivity of 0.0 (figures 5a, 5b, 5c) is effectively a conduction problem, as no radiational exchange can occur.

The case with emissivity of 0.5 (figures 6a, 6b, 6c) exercises the full multibody radiational capability with multiple reflections between all surfaces.

The case with emissivity of 1.0 (figures 7a, 7b, 7c) is effectively a set of single body radiational exchanges, as no reflections are allowed to occur.

The effects of the multibody radiation on the resultant temperature on the overall solution can be measured by the the peak temperature. This peak temperature appears near the center of the heated pedestal. It is reduced from 1.58 to 1.26 to 1.19

as the emissivity is increased from 0.0 to 0.5 to 1.0, demonstrating the effects of the increasing influence of radiative heat transfer. Moreover, the increased radiational component of the heat transfer causes a cooling of the center for more uniform temperature profile across the pedestal surface, as the center of the pedestal has the most direct view of the coolest radiating surface, the inlet.

Note that in figure 5c, an essentially linear wall tempreature profile reflects the nature of the solution to the conduction problem. In figure 6c and 7c we see the devitation from this as the effects of the fourth power dependence of radiation and the direct interaction between the distant radiative surfaces causes a steeper increase in temperature profiles immediately downstream of the inlet.

REFERENCES

1. Gebhart, B: Surface Temperature Calculations in Radiant Surroundings of Arbitrary Complexity- For Gray, Diffuse Radiation, Int. J. Heat Mass Transfer, vol. 3, no. 4, pp 341-346, 1961.

2. Seigel and Howell, Thermal Radiation Heat Transfer, Appendix E.

3. Holman, J.P. Heat Transfer, McGraw-Hill, 1976.

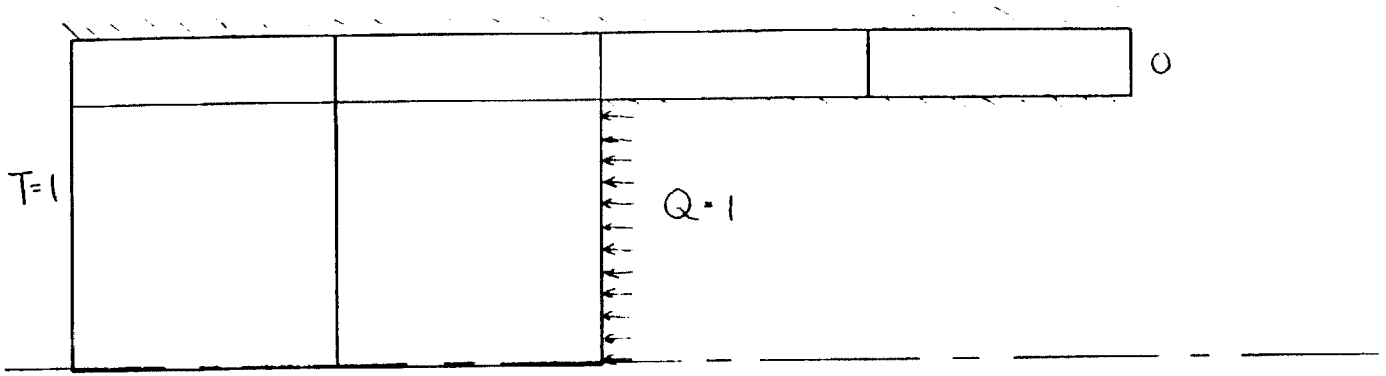

Figure 1 Non-Radiative B.C.'s

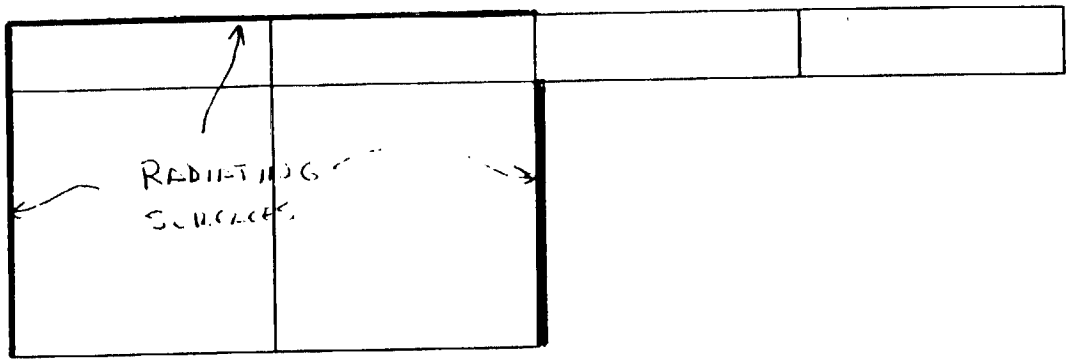

Figure 2 Multi Body Radiation B.C.'s

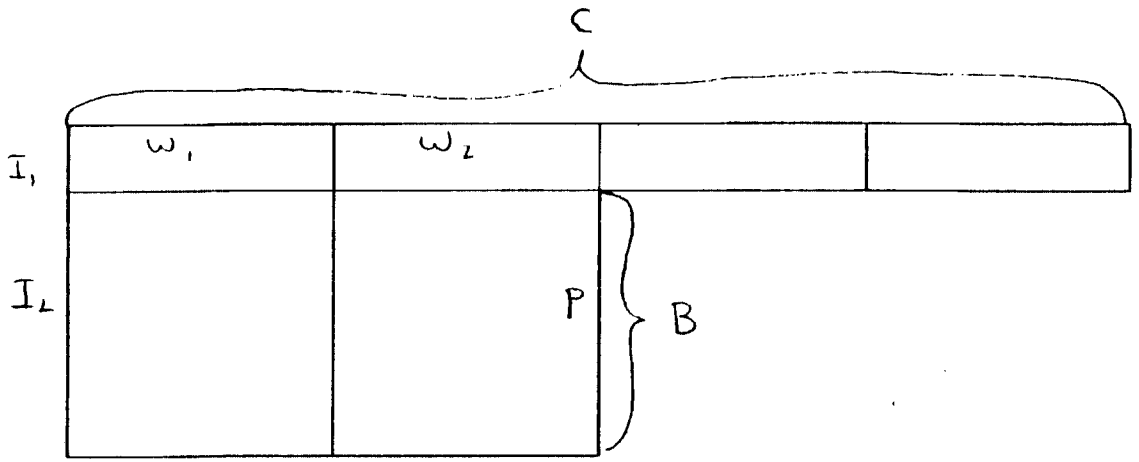

Figure 3 Plotting Segments

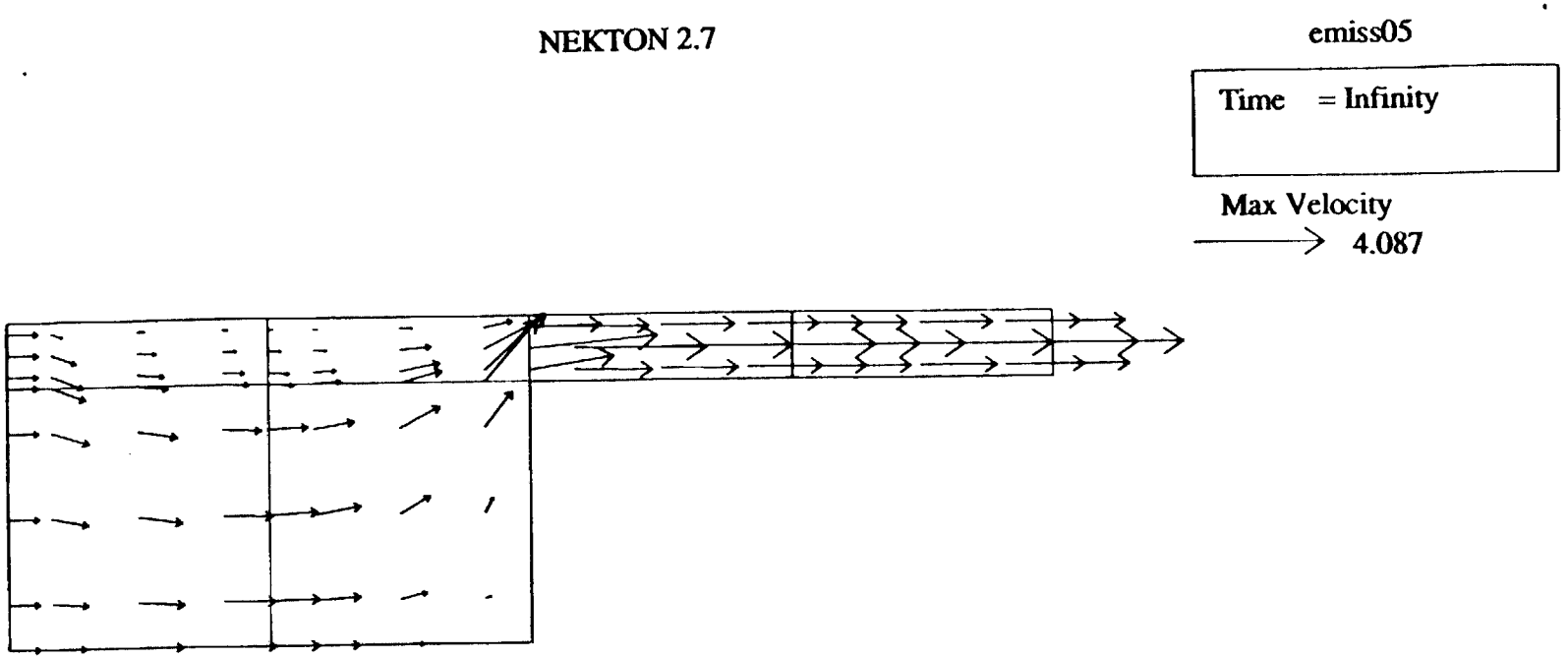

Figure 4 Velocity Vectors

NEKTON V 2.7	Session Name: emiss05
	Postnek Results
	Dec 17 16:06 1990

NEKTON 2.7

emiss0

Time = Infinity

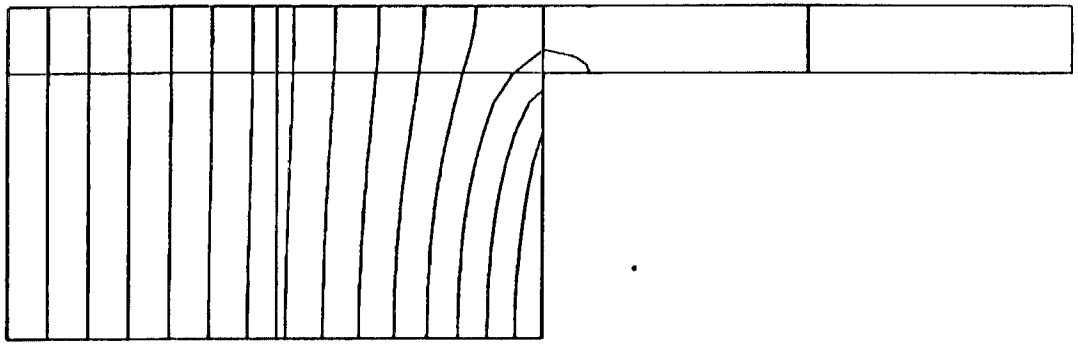

Tmax= 1.578

1.000
0.929
0.857
0.786
0.710
0.642
0.571
0.500
0.429
0.357
0.286
0.214
0.143
0.071
0.000

Tmin= 1.000

Figure 5a e=0 Temperature Contour

NEKTON V 2.7	Session Name: emiss0
	Postnek Results
	Dec 17 17:02 1990

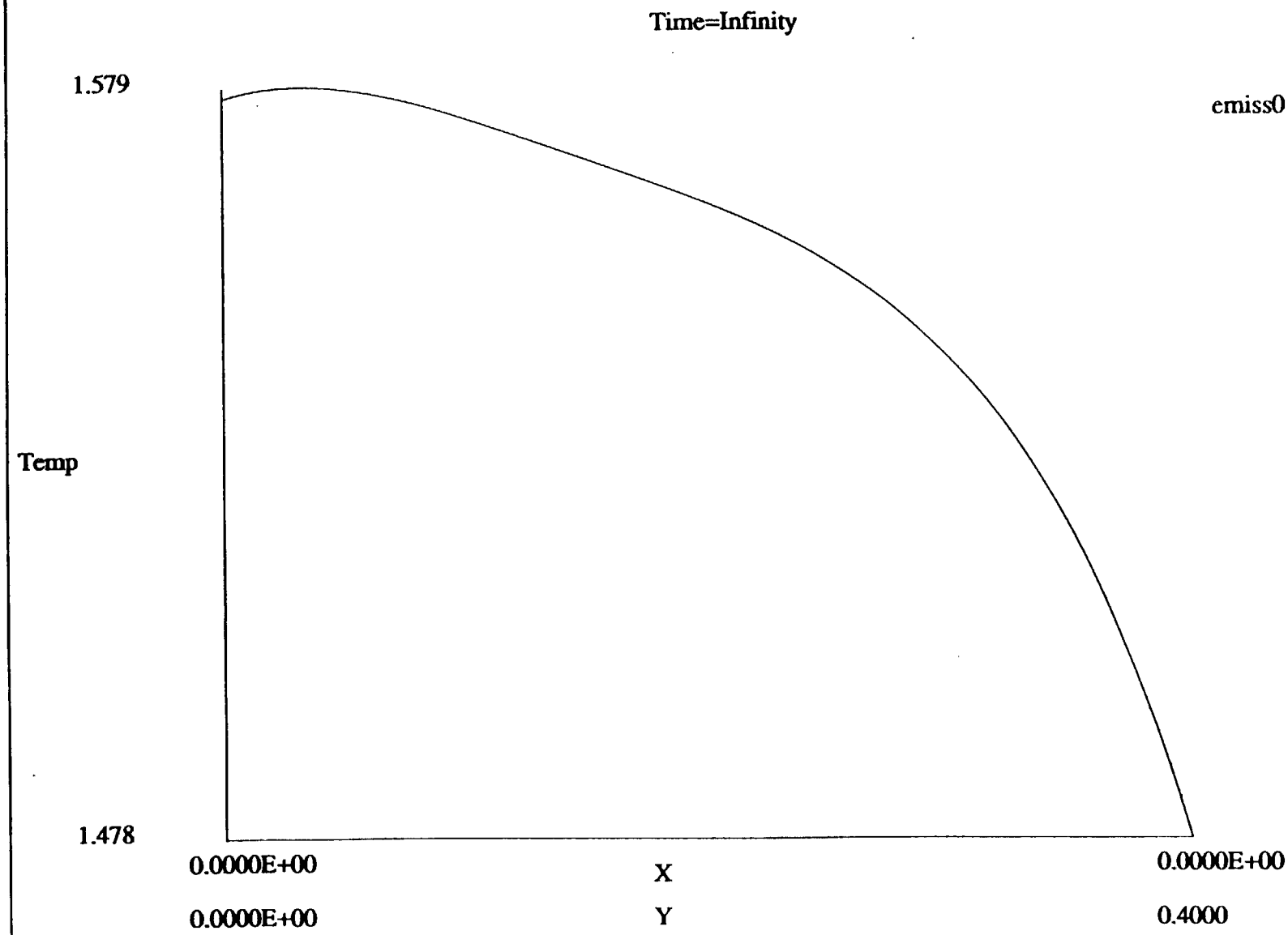

Figure 5b e=0 Temperature Profile along B

NEKTON V 2.7	Session Name: emiss0
	Postnek Results
	Dec 17 17:02 1990

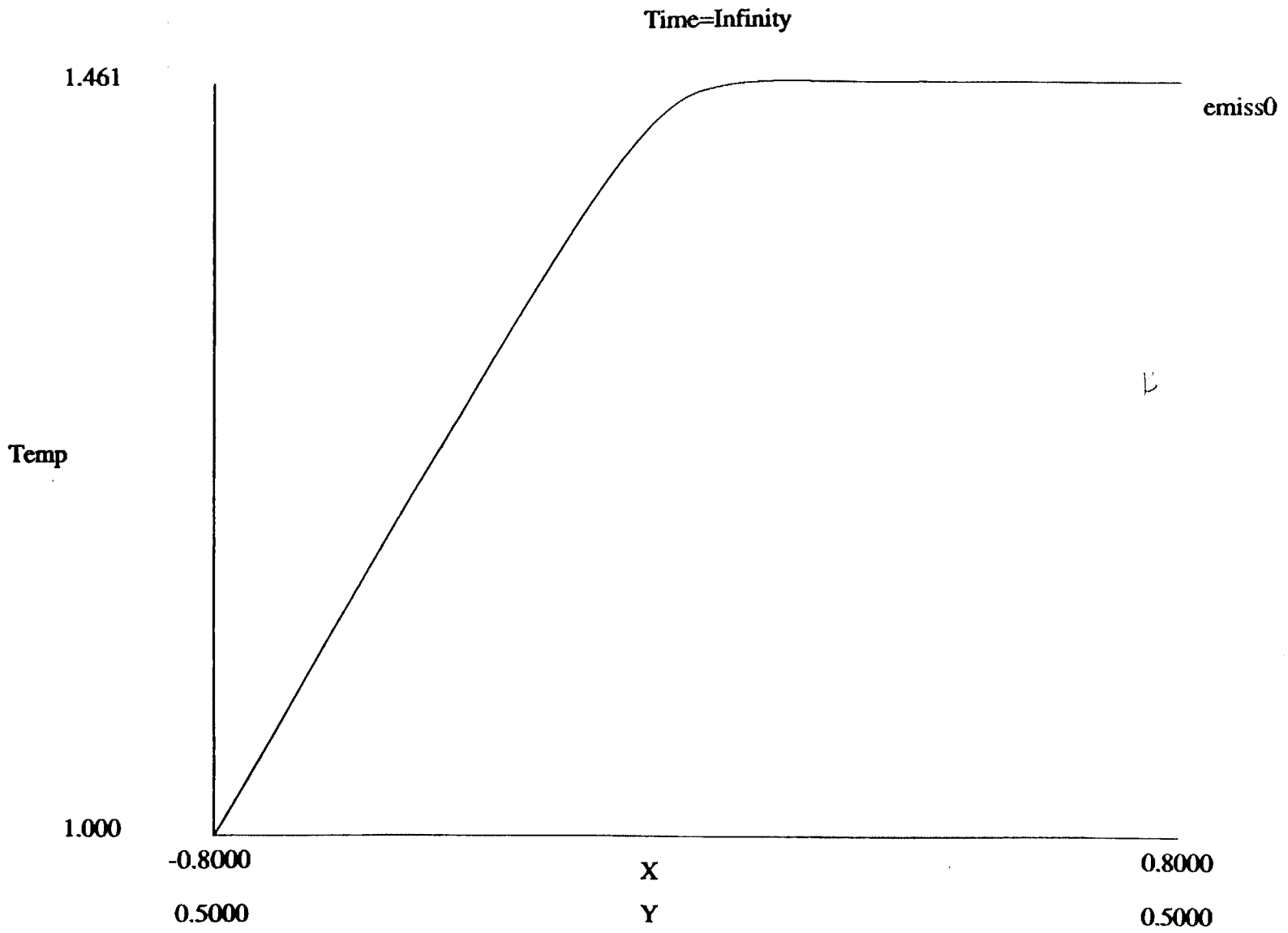

Figure 5c e=0 Temperature Profile along C

NEKTON V 2.7	Session Name: emiss0
	Postnek Results
	Dec 17 17:02 1990

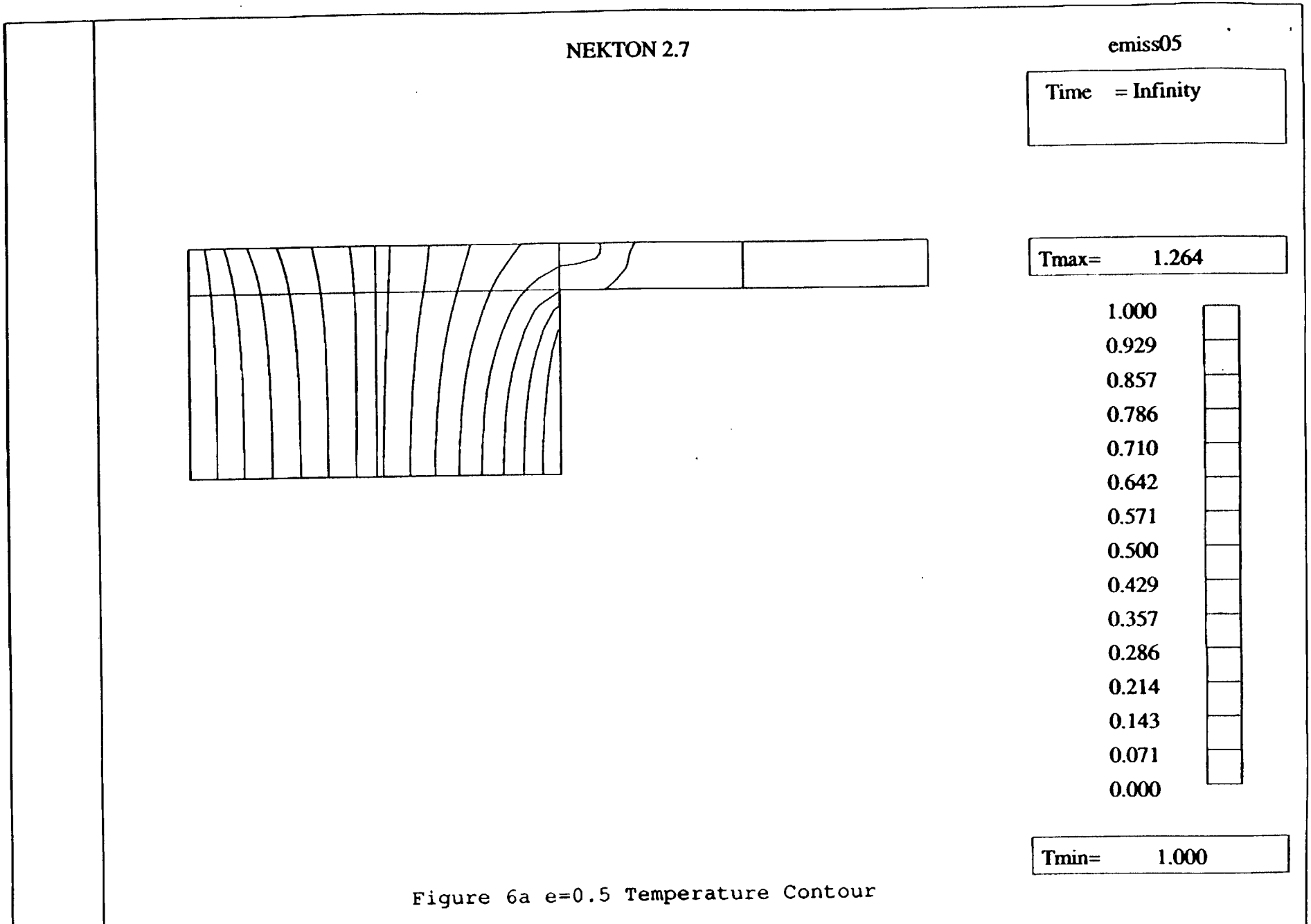

Figure 6a e=0.5 Temperature Contour

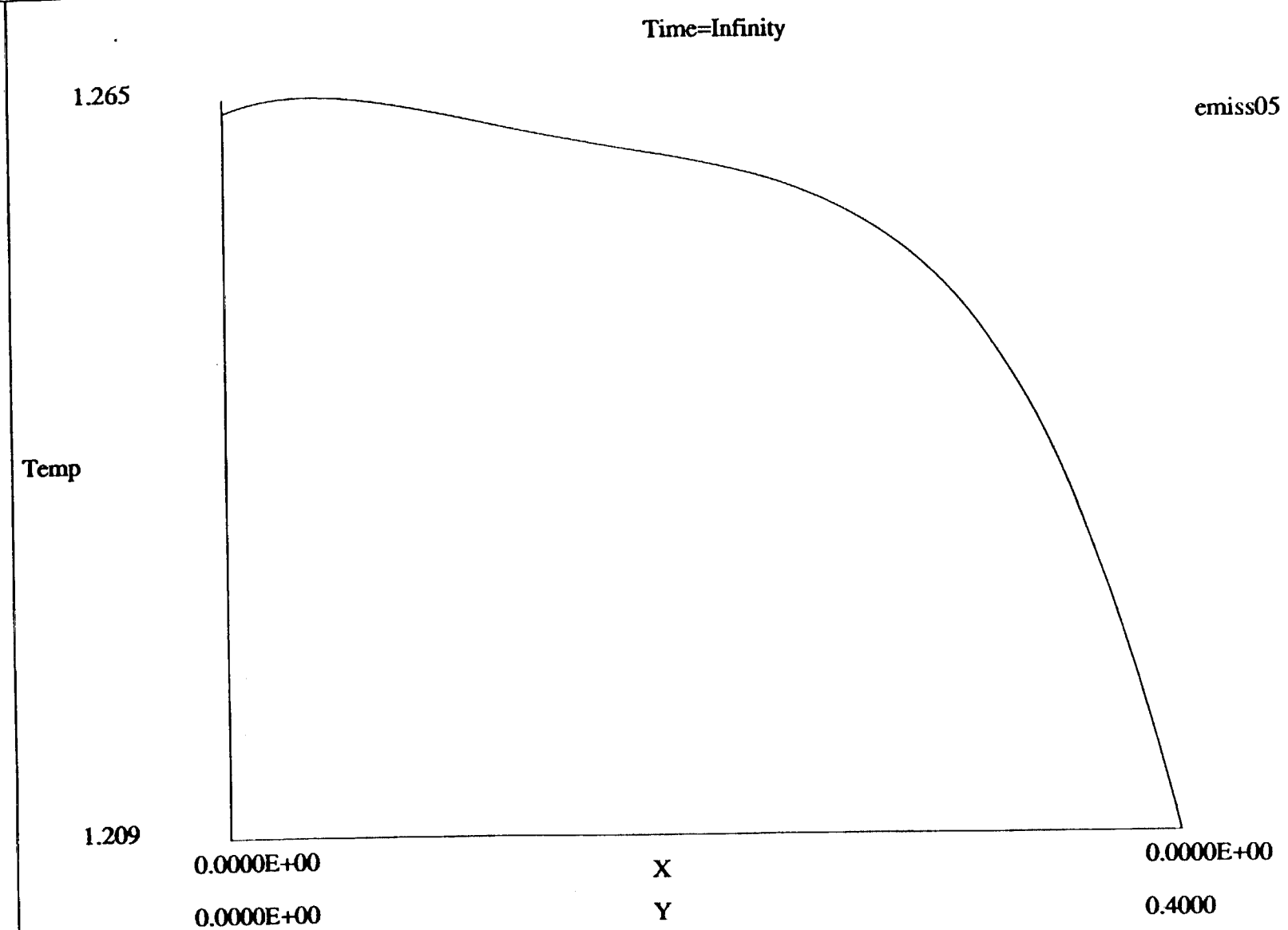

Figure 6b e=0.5 Temperature Profile along B

NEKTON V 2.7	Session Name: emiss05
	Postnek Results
	Dec 17 15:44 1990

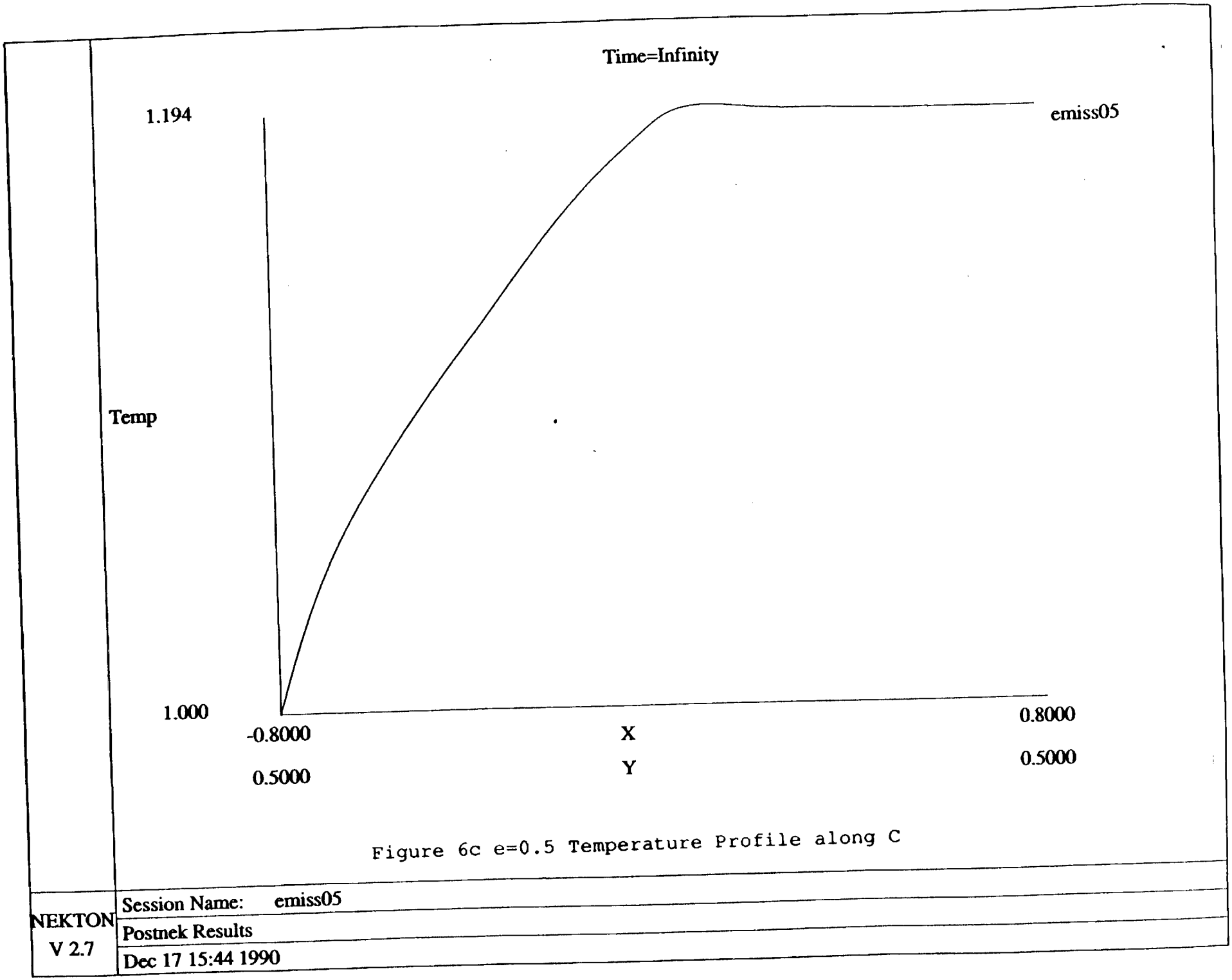

Figure 6c e=0.5 Temperature Profile along C

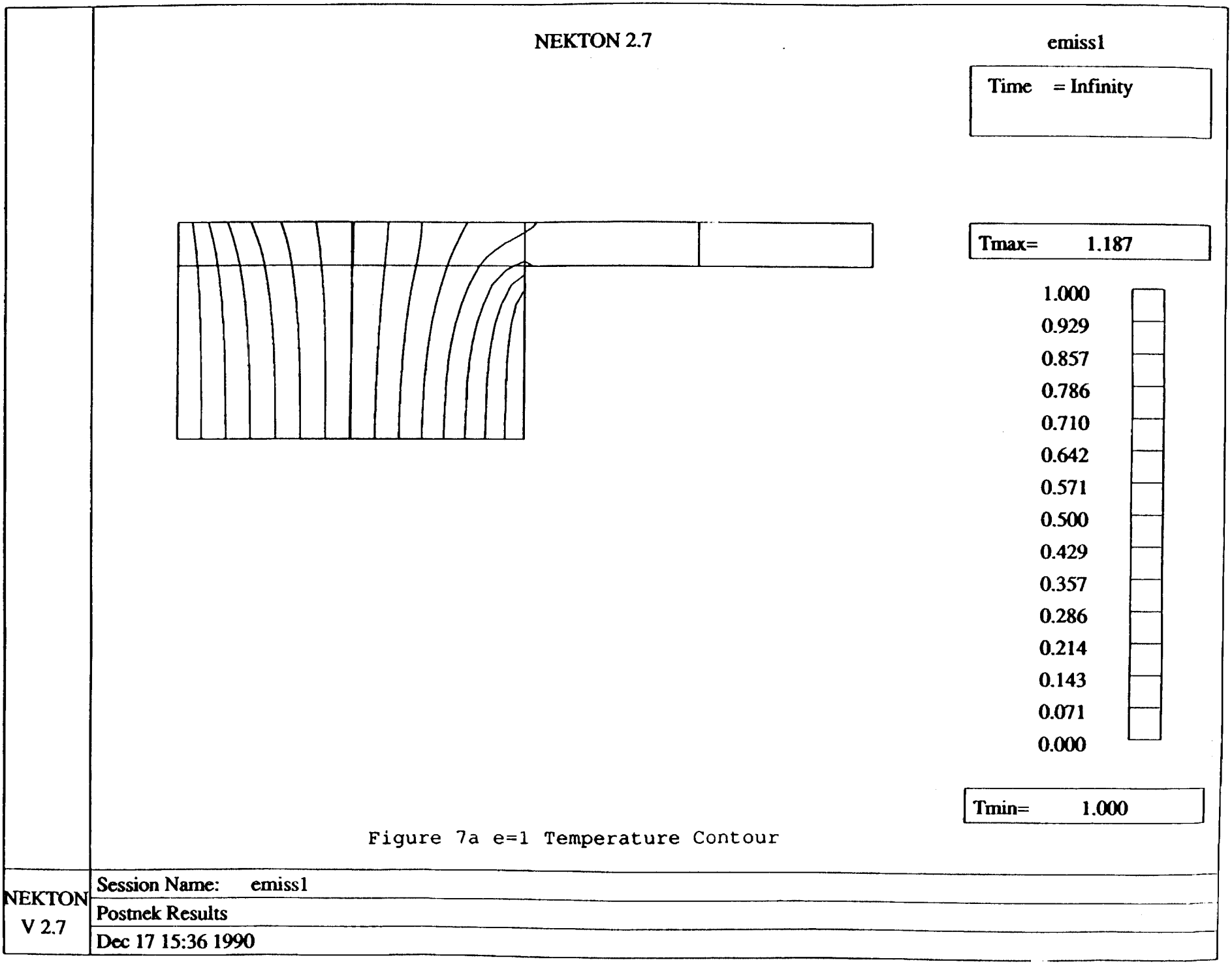

Figure 7a e=1 Temperature Contour

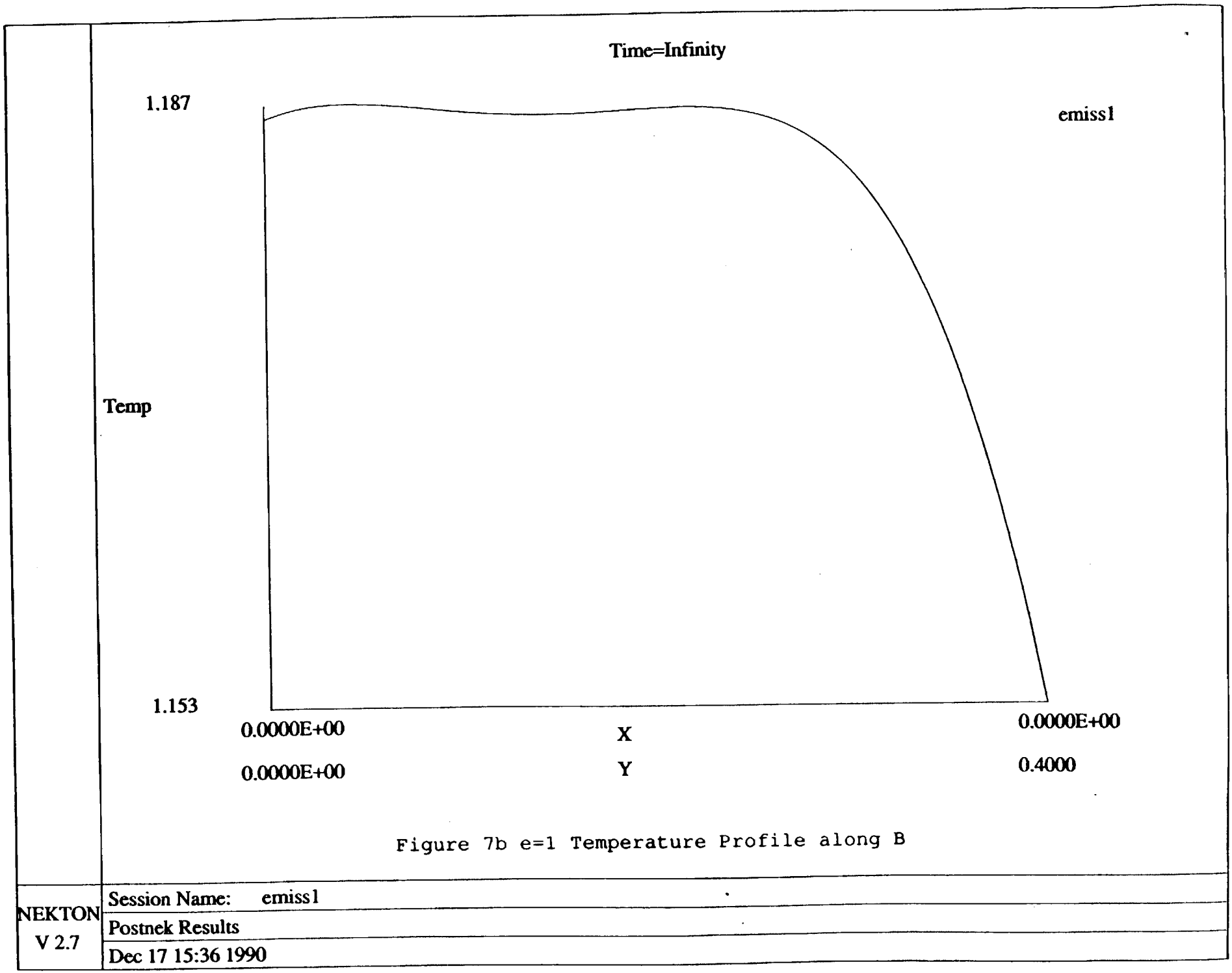

Figure 7b e=1 Temperature Profile along B

NEKTON V 2.7	Session Name: emiss1
	Postnek Results
	Dec 17 15:36 1990

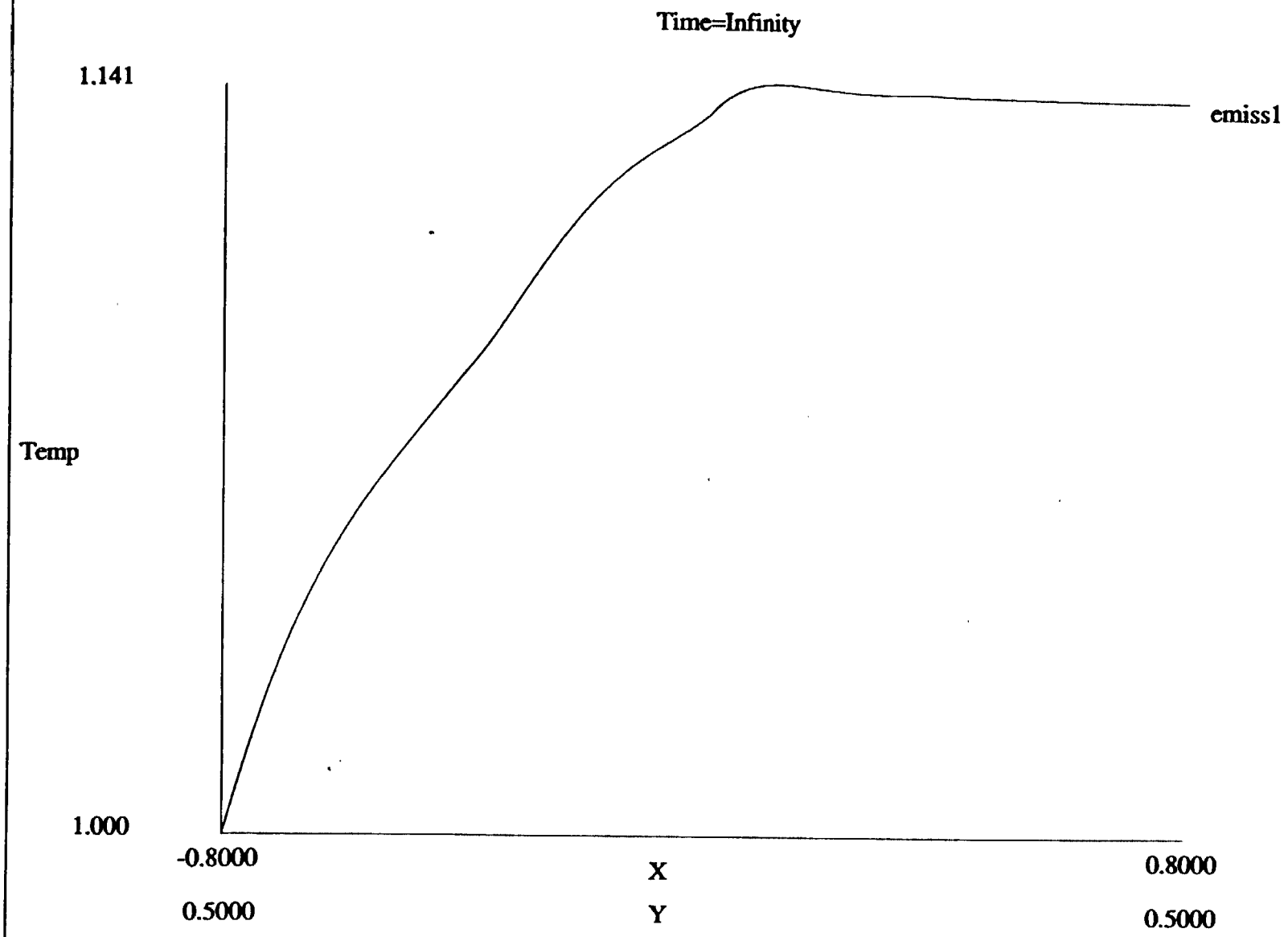

Figure 7c e=1 Temperature Profile along C

NEKTON V 2.7	Session Name: emiss1
	Postnek Results
	Dec 17 15:36 1990

Chapter 4

Soret Effects

OBJECTIVE:

The result achieved in this report period was to implement the Soret effect capability for passive scalars in NEKTON and to demonstrate its effects on the chemical mass concentration species for calculations in a CVD rotating pedestal reactor geometry.

BACKGROUND:

The chemistry in the gas phase in CVD reactors and, therefore, the concentration of each species of mass involved in the reaction is important in finding the overall rates of deposition and the spatial uniformity of that deposition. The high temperatures and large temperature gradients inside CVD reactors cause a coupling effect between the heat transfer and the mass diffusion to become significant. The effect of temperature gradients on mass flux is known as "thermal diffusion" or the "Soret Effect". The inverse effect of mass concentration gradients on heat flux is known as the "Dufour Effect". In MOCVD calculations, [1,2] the Soret effect is significant in effecting the deposition rate while the Dufour effect is not. We therefore concentrate our efforts

on implementing the Soret effects in order to increase the accuracy of our MOCVD calculations.

IMPLEMENTATION :

The implementation in NEKTON is valid for two- and three-dimensional as well as axisymmetric calculations. As most MOCVD applications are in axisymmetric geometries, we will use the axisymmetric form of the convection-diffusion equations to illustrate the implementation of these in NEKTON.

The mass balance and associated boundary conditions for the transport of chemical species are, then:

$$\frac{\partial c_{TMG}}{\partial t} + c\left(v_r \frac{\partial x_{TMG}}{\partial r} + v_z \frac{\partial x_{TMG}}{\partial z}\right) = \frac{1}{r}\frac{\partial}{\partial r}\left(cD_{TMG,H_2} r\left[\frac{\partial x_{TMG}}{\partial r} + k_T \frac{\partial \ln T}{\partial r}\right]\right) + \frac{\partial}{\partial z}\left(cD_{DMG\ H_2}\left[\frac{\partial x_{TMG}}{\partial z} + k_T \frac{\partial \ln T}{\partial z}\right]\right). \tag{7}$$

$$D_{TMG,H_2}\left[\frac{\partial x_{TMG}}{\partial z} + k_T \frac{\partial \ln T}{\partial z}\right] = k x_{TMG}\Big|_{surface} \tag{8}$$

Here D is diffusivity, c is concentration, x is mass fraction, k is a constant. The subscripts TMG, and H_2 represent the species to which the subscripted variable refers.

The Soret effect consists of the term of the form

$$-\nabla \cdot (K \nabla \varphi) = f \quad \text{IN } \Omega$$

where k is a constant, φ is a scalar field, and f is a forcing term, here the Laplacian of the log of the temperature. Here this is expressed in the "strong" form. Using the standard finite element approach, we convert this to the weak form by multiplying by a test function v, and integrating over the domain Ω.

$$\int_{\Omega} -\nabla \cdot (k \nabla \varphi) v \, d\Omega = \int_{\Omega} f v \, d\Omega$$

Integrating the left hand side by parts, yields

$$\int_{\partial\Omega} -k \frac{\partial \varphi}{\partial n} v \, ds + \int_{\Omega} k \nabla \varphi \nabla v \, d\Omega = \int_{\Omega} f \cdot v \, d\Omega$$

Note that the surface (boundary) term on $\partial\Omega$ from this integration is exactly equal to the additional boundary condition imposed by the original strong statement of the Soret equation. Thus, imposition of the variational approach and its "natural" boundary conditions handles the Soret term very consistently.

TEST CASES

We demonstrate Soret effect with two test cases. The first test case is in a very simple geometry. This is to demonstrate the mechanics of the operation of the program and to have a result simple enough to be amenable to theoretical analysis.

In case I, we impose a temperature onto the concentration such that the log(T) is the parabolic function log(T) = (X-X**2)/2 of figure Ia. The Soret effects constant is set at 1.0. The initial concentration was C=1.0. The boundary conditions were no mass flux on all boundaries. The simulation was run out to a nondimensional time of 10, which was 10x the characteristic diffusion time of the system.

These conditions resulted in the steady concentration plotted in figure Ib. An integration of the concentration yields a total mass in the domain within 1% of the original mass, with the discrepancy attributable to time stepping errors. While the concentration gradients are nonzero at the boundaries, implementation of the associated boundary conditions yields no net flux. This is consistent with the no-flux boundary conditions imposed and allows the concentration to in fact reach this steady state. This is required for simulations to be physically realistic.

The quantitative comparison requires that for steady state, the dC/dx = - d(log(t))/dx. Comparision of the plots Ia and Ib indicate that C and log(t) are parabolic profiles whose magnitude are both 0.125 and whose orientation are reversed, which verifies this requirement.

The second test case is in the axisymmetric rotating pedestal CVD reactor geometry of figure II. Here we impose the dimensionless temperature of 1.0 at inlet and flux of 1.0 at the pedestal surface. The resultant temperature profile we plot in figure III along A-B is essentially linear. We impose the value of 1.0 concentration at the inlet and 0.0 at the pedestal surface. In figure IVa we plot the concentration contours. In figure IVb we plot the profile of concentration along segment A-B. Note the essentially linear nature of the concentration profile where diffusion is the primary mechanism of mass transfer.

In figures Va and Vb we plot the results of the same calculation with the Soret effects enabled. The thermal diffusion is driven by the temperature field calculated in the heat transfer module of NEKTON. Here the essentially linear temperature profile results in log(T) convex in x, giving a concentration profile with the expected concave profile in x of figure Vb.

REFERENCES

1. Ouazzani, Jalil, Chiu, Kuan-Cheng, and Rosenberger, Franz: "On the 2D modelling of Horizontal CVD Reactors and its Limitations", Journal of Crystal Growth 91 (1988) 497-508.

2. Dimitrios Fotiadis, Anthony Kremer, Donald McKenna, Klavs F. Jensen : "Complex Flow phenomena in Vertical MOCVD Reactors; Effects on Deposition Uniformity and Interface Abruptness", Journal of Crystal Growth 85 (1987) 154-164.

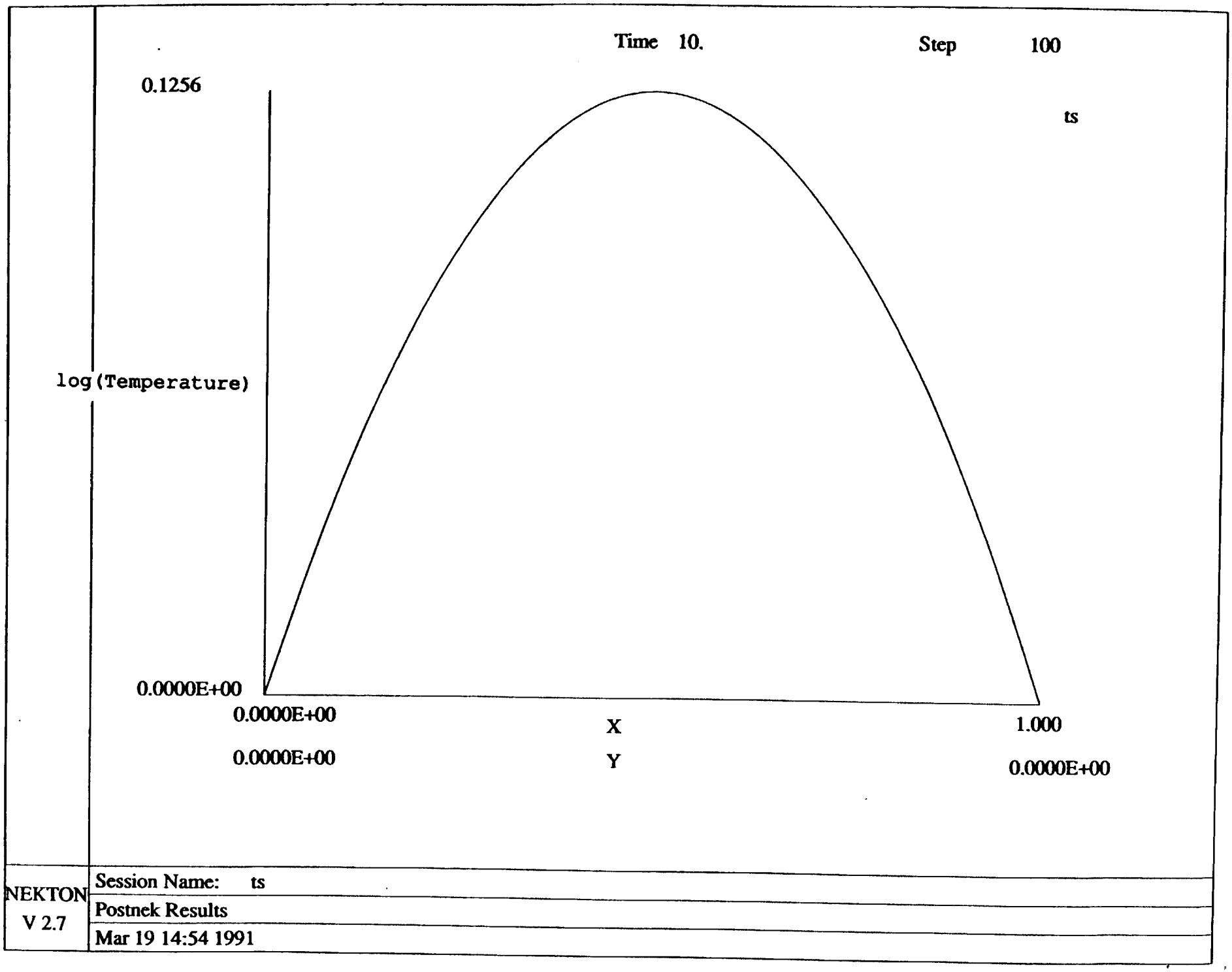
Time 10.
Step 100
0.1256
ts
log(Temperature)
0.0000E+00
0.0000E+00
X
1.000
0.0000E+00
Y
0.0000E+00
NEKTON
V 2.7
Session Name: ts
Postnek Results
Mar 19 14:54 1991

Figure I a)

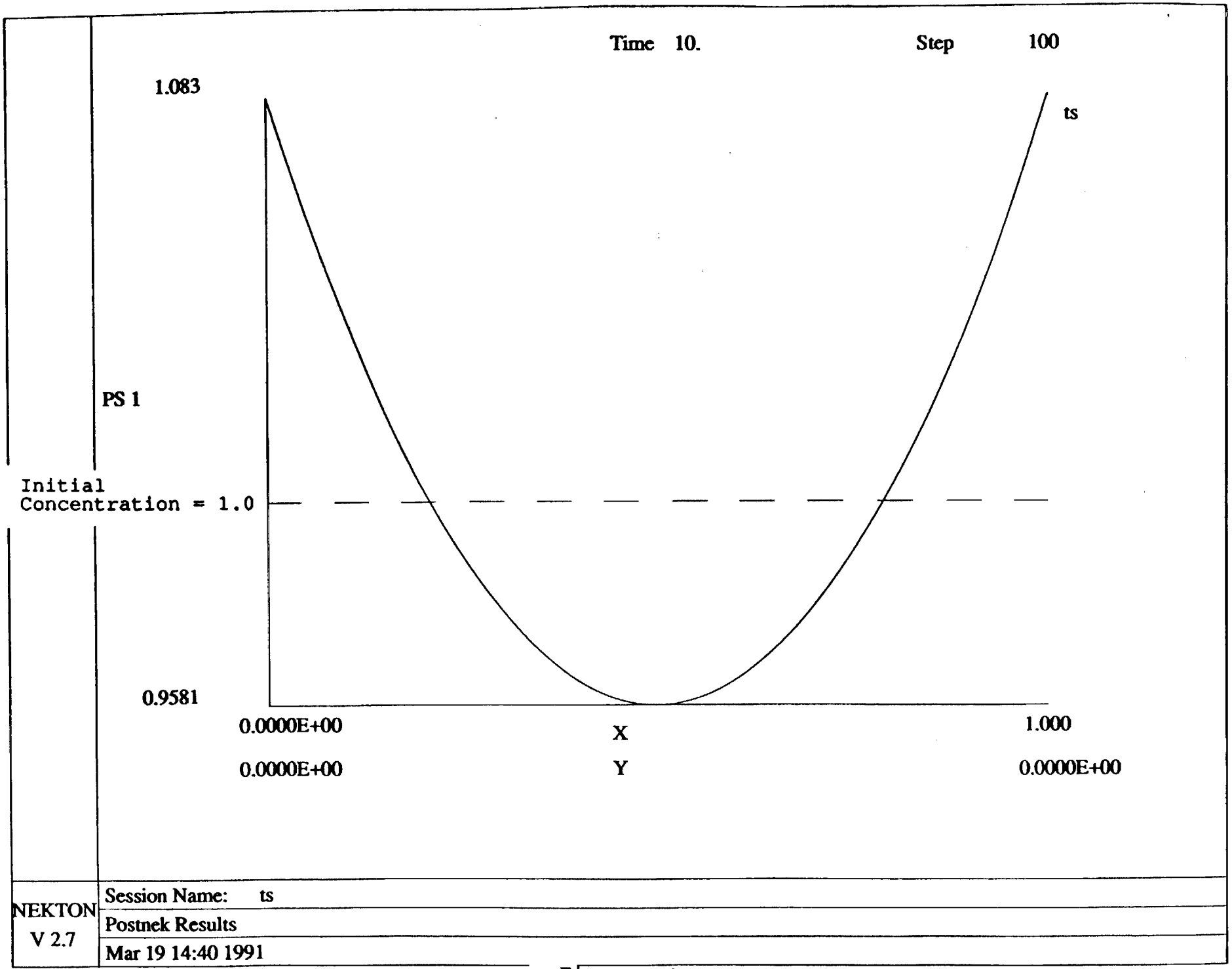
Time 10.
Step 100
1.083
ts
PS 1
Initial
Concentration = 1.0
0.9581
0.0000E+00
X
1.000
0.0000E+00
Y
0.0000E+00
NEKTON
V 2.7
Session Name: ts
Postnek Results
Mar 19 14:40 1991

Figure I b)

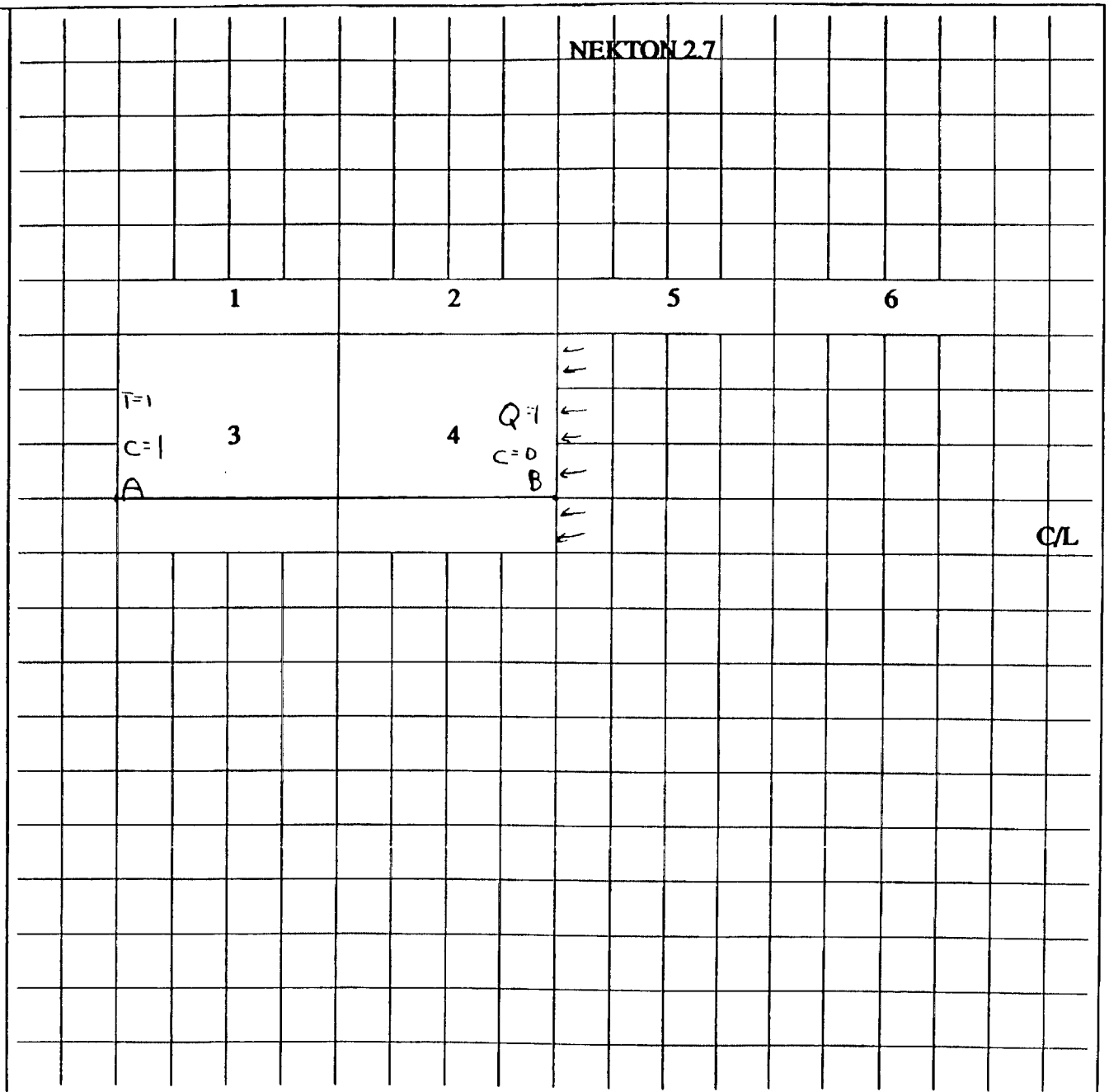

NEKTON V 2.7	Session Name: MESH
	Spectral Element Mesh from Prenek
	Mar 21 13:04 1991

Figure II

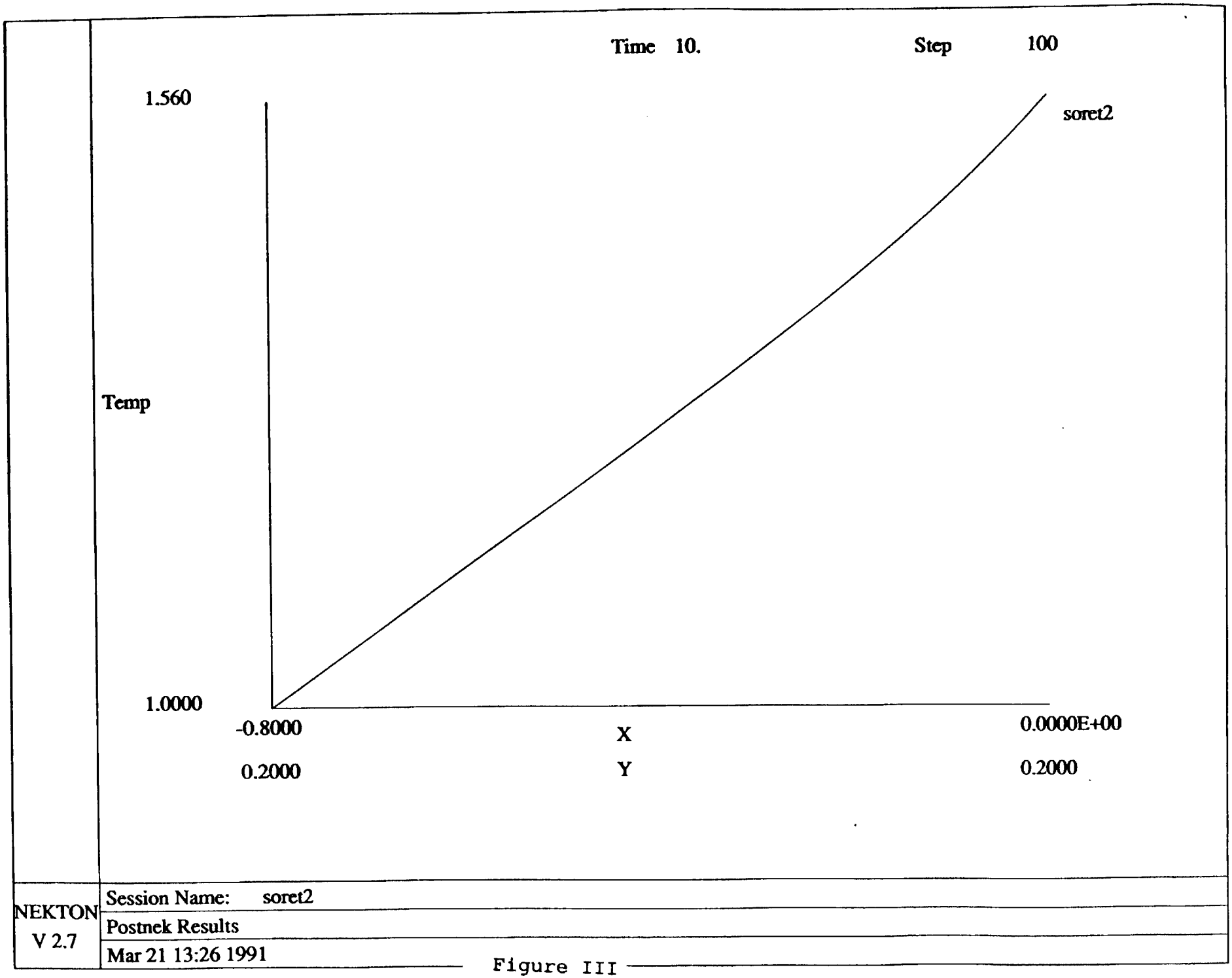
Time 10.
Step 100
1.560
soret2
Temp
1.0000
-0.8000
0.2000
X
Y
0.0000E+00
0.2000
NEKTON
V 2.7
Session Name: soret2
Postnek Results
Mar 21 13:26 1991

Figure III

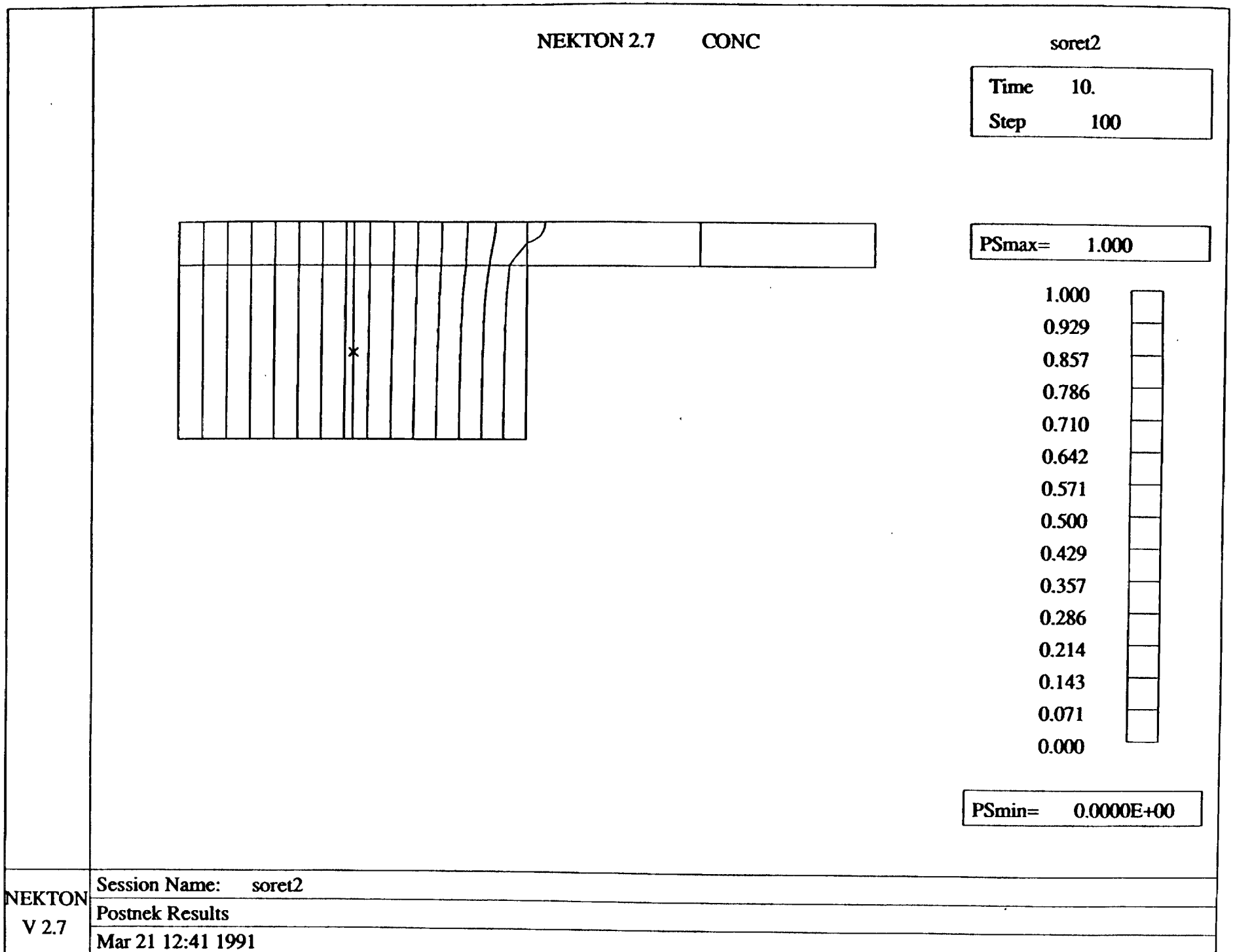
NEKTON 2.7 CONC
soret2
Time 10.
Step 100
PSmax= 1.000
1.000
0.929
0.857
0.786
0.710
0.642
0.571
0.500
0.429
0.357
0.286
0.214
0.143
0.071
0.000
PSmin= 0.0000E+00
NEKTON
V 2.7
Session Name: soret2
Postnek Results
Mar 21 12:41 1991

Figure IV a)

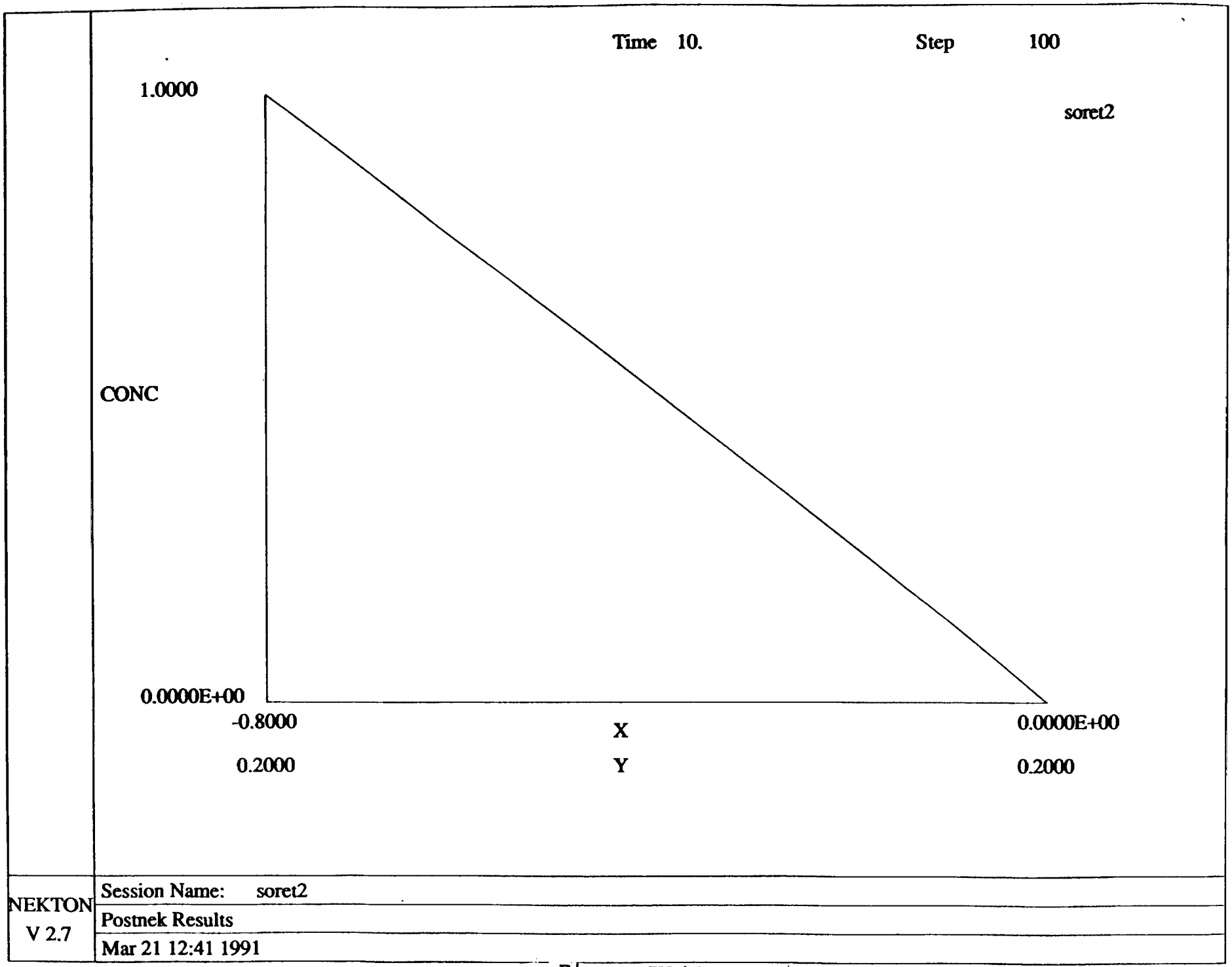
Time 10.
Step 100
1.0000
soret2
CONC
0.0000E+00
-0.8000
X
0.0000E+00
0.2000
Y
0.2000
NEKTON
V 2.7
Session Name: soret2
Postnek Results
Mar 21 12:41 1991

Figure IV b)

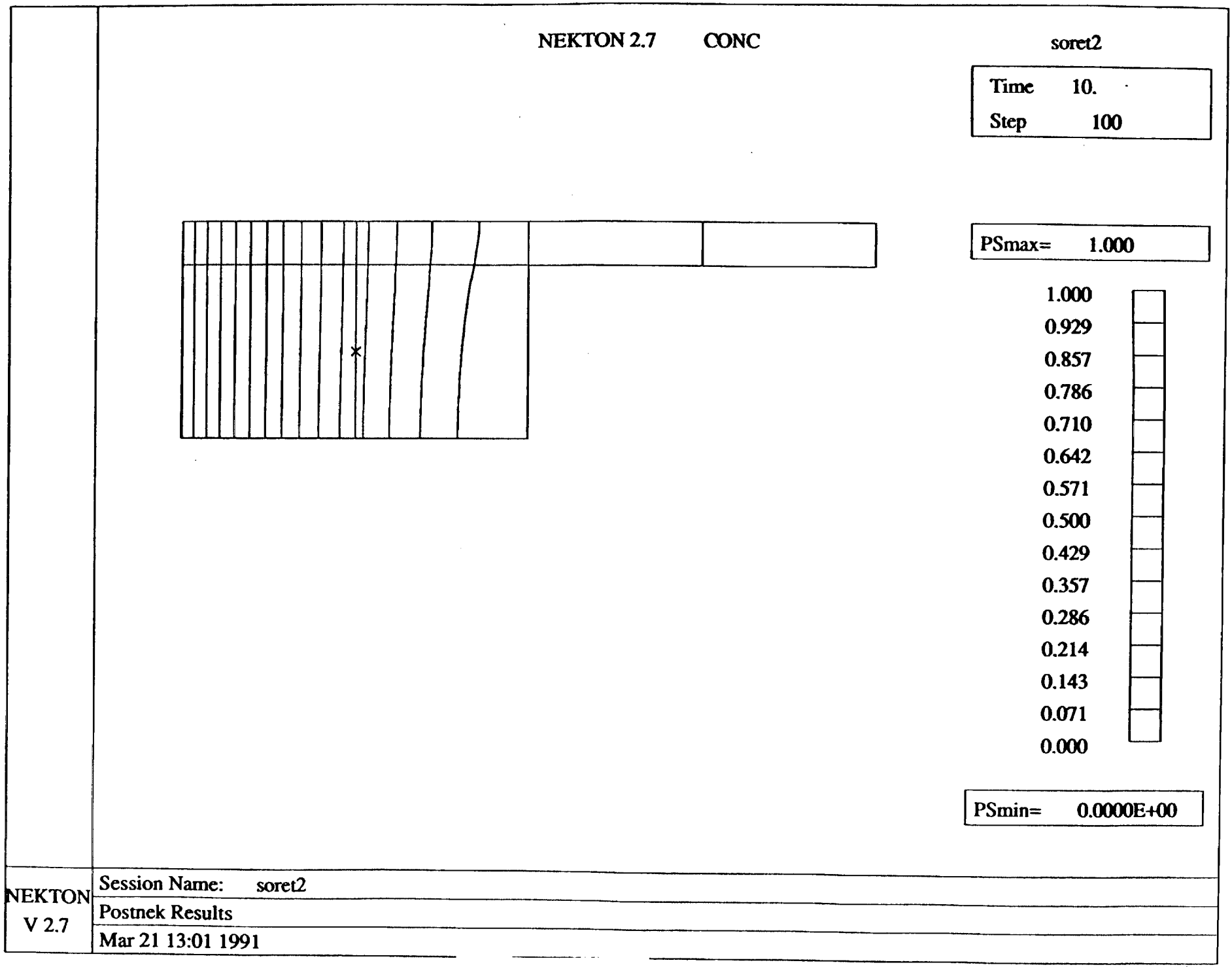
NEKTON 2.7 CONC
soret2
Time 10.
Step 100
PSmax= 1.000
1.000
0.929
0.857
0.786
0.710
0.642
0.571
0.500
0.429
0.357
0.286
0.214
0.143
0.071
0.000
PSmin= 0.0000E+00
NEKTON
V 2.7
Session Name: soret2
Postnek Results
Mar 21 13:01 1991

Figure V a)

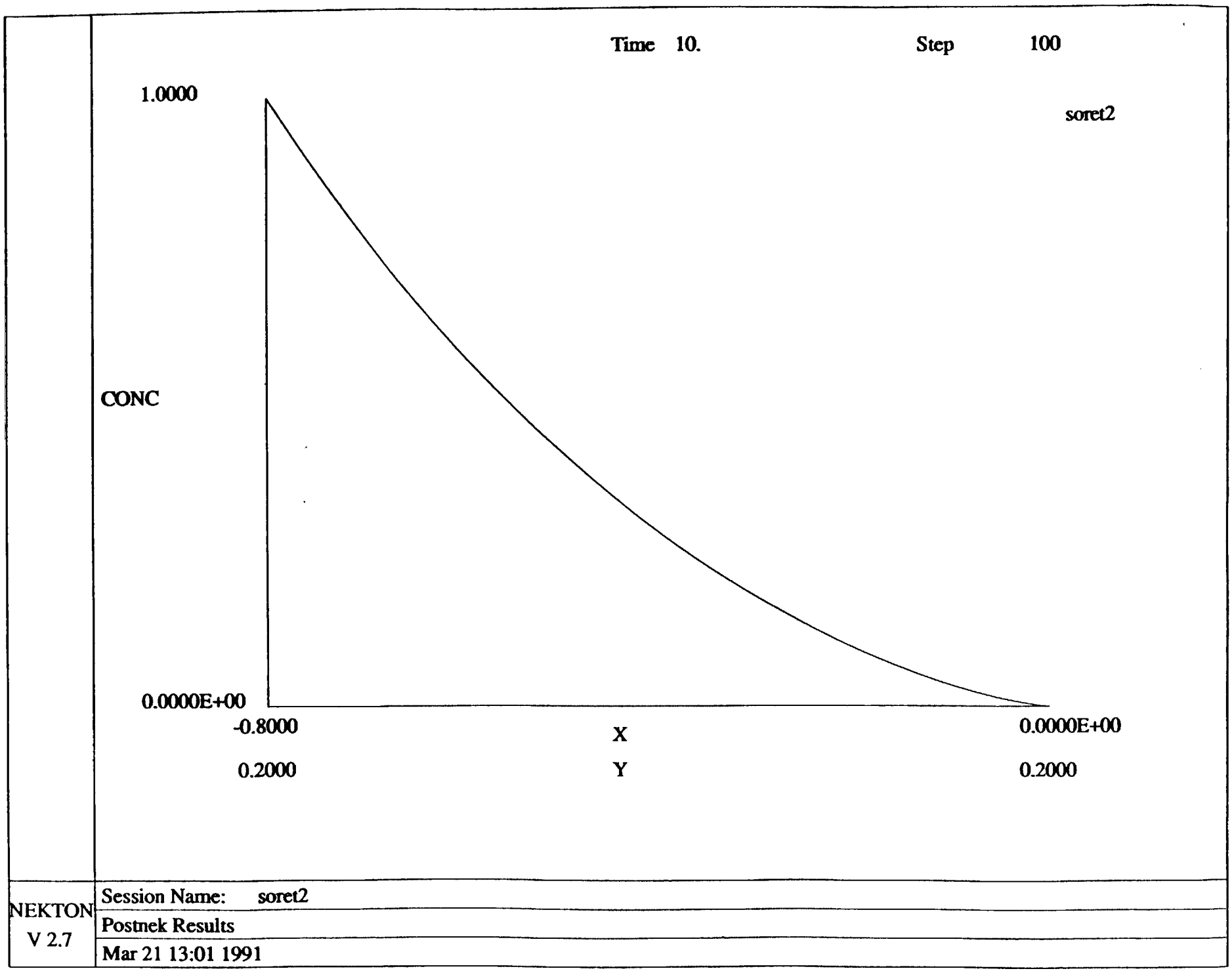
Time 10.
Step 100
1.0000
soret2
CONC
0.0000E+00
-0.8000
X
0.0000E+00
0.2000
Y
0.2000
NEKTON
V 2.7
Session Name: soret2
Postnek Results
Mar 21 13:01 1991

Figure V b)

Chapter 5

User Interface

OBJECTIVE:

The result achieved in this report period was to consolidate the implementation of the enhancements to the NEKTON user interface in order to accomodate the features (variable properties, need for easy axisymmetric and 3-D geometrical input, fast color fills, true 3-D scrollbar rotation, and scrollbar zoom) needed for CVD calculations and to provide enhanced ability to evaluate the results.

BACKGROUND:

Modern CAD and CAE packages rely increasingly on Graphical User Interfaces (GUI's) to support increasingly complex tasks done by the user. The object of these GUI's is to help the software developer produce a package that is intuitive, powerful, and easy to use. These GUI's also help to standardize the interfaces by providing guidelines for developers that result in coordination in the development of widely varying packages [1-7]. Thus, a user familiar with editting a file on a MacIntosh or with DecWindows will recognize some of the essential features in panning, zooming,

and pulldown menu selection in a code such as NEKTON.

We used Motif, which is the most popular, and, we believe, the most effective GUI system. Within this system we have adapted the current NEKTON user interface and added enhancements to achieve the above objectives.

Many powerful tools are becoming available to allow the software developer quickly generate Motif GUI's. Any description or list given here would no doubt be obsolete by the time this report reaches publication.

IMPLEMENTATION :

The implementation of the new user interface features in NEKTON are done in the context of the Motif graphical user interface. Motif consists of 3 parts: the Motif Window Manager, the Motif Interface Compiler, and the Motif Widget Library. NEKTON requires only the Motif Widget Library (libXm.a) and only when linking the graphical executables. Where this file is not part of the standard operating system, we ship precompiled and linked programs. Therefore, Motif requires no additional system resources for the new package.

While the new code can and has been installed on VMS systems, in doing so we have concluded that new releases will not be supported on VMS. There are several reasons for this. First, the code relies heavily on the X Windows windowing system. This is, in theory, a subset of DecWindows and supported on VAXes. However, in practice, the performance of both the graphics and floating point operations on the CISC systems is low, and bog down the system. With the emergence of very powerful and low-cost RISC systems, the investment of time and money in VMS is dubious. For example, the DecStation 3100 is approximately 10x as fast as the MicroVax II, and the DecStation 5000 is in turn, almost a factor of 2 as fast the 3100.

Moreover, while the VMS system has many advantages over UNIX, it is a different and proprietary system. Any enhancements taking advantage of these efforts can only be appreciated by a small group of users, and enhancements to UNIX (e.g., interprocess communication) would be curtailed to make it compatible with VMS. For all these reasons, it has been decided that VMS is an inappropriate platform on which a user should begin a committment to a new hardware/software package.

The use of Motif in the new interface has several benefits. First, interactive zoom and pan (scroll) are built-in to the geometry generator and postprocessor. The scrollbars

provide real-time "pulling" of the mesh, according to the standard conventions shared by Motif, MacIntosh software, and other window- based programs. The "look and feel" of the program is customizable by the user via attributes files.

EXAMPLE CASES

Mesh Generation

The ability to quickly and easily generate meshes is important in MOCVD applications. To facilitate this, we have incorporated the Motif pan/zoom capability into the PRENEK mesh generator. This enables quick and accurate input of meshes with elements with widely varying length scales, which are used, for example, in resolving thin boundary layers at the deposition surface of a rotating pedestal CVD reactor. In figures 1a and 1b we plot the whole mesh and the mesh zoomed in on a corner at which we refine to get higher resolution near the corner. Thus, in entering a mesh we can at times focus in on specific areas, retaining the accuracy in inputting and modifying very small elements with the mouse.

3-D Rotation

In figure 2 we plot a three dimensional mesh for a 3-D CVD reactor undergoing rotation. This rotation is done via the slider bars, which allow for independent adjustment of pitch, roll, and yaw as defined by the user (screen) orientated frame of reference. This system allows for easy intuitive rotation of the mesh, as well as the full access to each of the 3 degrees of freedom of the mesh. Previous to this, only 2 degrees of freedom were allowed.

Contour Lines

In figures 3a and 3b we plot the contours of temperature in a previous result of a CVD reactor undergoing g-jitter. This contour plot capability contains the same information as the color fill plots, but is nonetheless useful for black-and-white displays and for submission of results in publications.

Note also here that the zoom capability extends to all quantities and plot formats in

the post processor.

Pulldown Menu Structure

In figure 4 we plot the pulldown menu bar developed for POSTNEK. This menu bar structure enables easy access to all the capabilities of postnek. It minimizes the requirements for the user to read documentation on each function of the postprocessor. A scan through the POSTNEK menu bar and each of its submenus provides the user with an overview of the structure of POSTNEK and its capabilities. Moreover, this scan can be accomplished before committing to any action. In that sense, the process of selecting an item in a submenu is reversible. You can bring up the entire sequence of menus and submenus and decide at the bottom level whether to implement the action, or to abort the entire process without selecting the action. This is in contrast to more complex codes that present menus sequentially and only one level of the structure can be seen at a time.

Equation Menu Structure

In figure 5 we present the PRENEK set equation menu. This enables the various switches for the different aspects of the equation type to be switched on and off.

Numerical Constant Input

In figure 6 we show the Motif-style numerical input. This enables mouse-oriented editting of the default NEKTON constants. The standard click and double-click selection process, the cursor movement keys, and the delete operations work in a manner consistent with MacIntosh and other mouse-oriented application programs.

Scrollable Information Dialog Box

In the upper left of figure 6 the dialog box logs informational messages from PRENEK and POSTNEK. The size of the vertical scrollbar in relation to its box is proportional

to the size of the visible text window to the total text. Thus, messages which have scrolled off screen are still available and can be retrieved by movement of the scrollbar. This enables large amounts of messages to be generated for the user without sacrificing excessive screen area.

REFERENCES

1. McMinds, Donald L., **Mastering OSF/Motif Widgets**, Addison Wesley, 1992.

2. The Open Software Foundation, **The OSF/Motif Style Guide**, Prentiss Hall, 1990.

3. The Open Software Foundation, **The OSF/Motif User's Guide**, Prentiss Hall, 1990.

4. The Open Software Foundation, **The OSF/Motif Programmer's Guide**, Prentiss Hall, 1990.

5. The Open Software Foundation, **The OSF/Motif Programmer's Reference**, Prentiss Hall, 1990.

6. Nye, Adrian, **Xlib Programming Manual V11**, O'Rielly and Associates, Inc. 1990.

7. Nye, Adrian, editor, **Xlib Reference Manual V11**, O'Rielly and Associates, Inc. 1990.

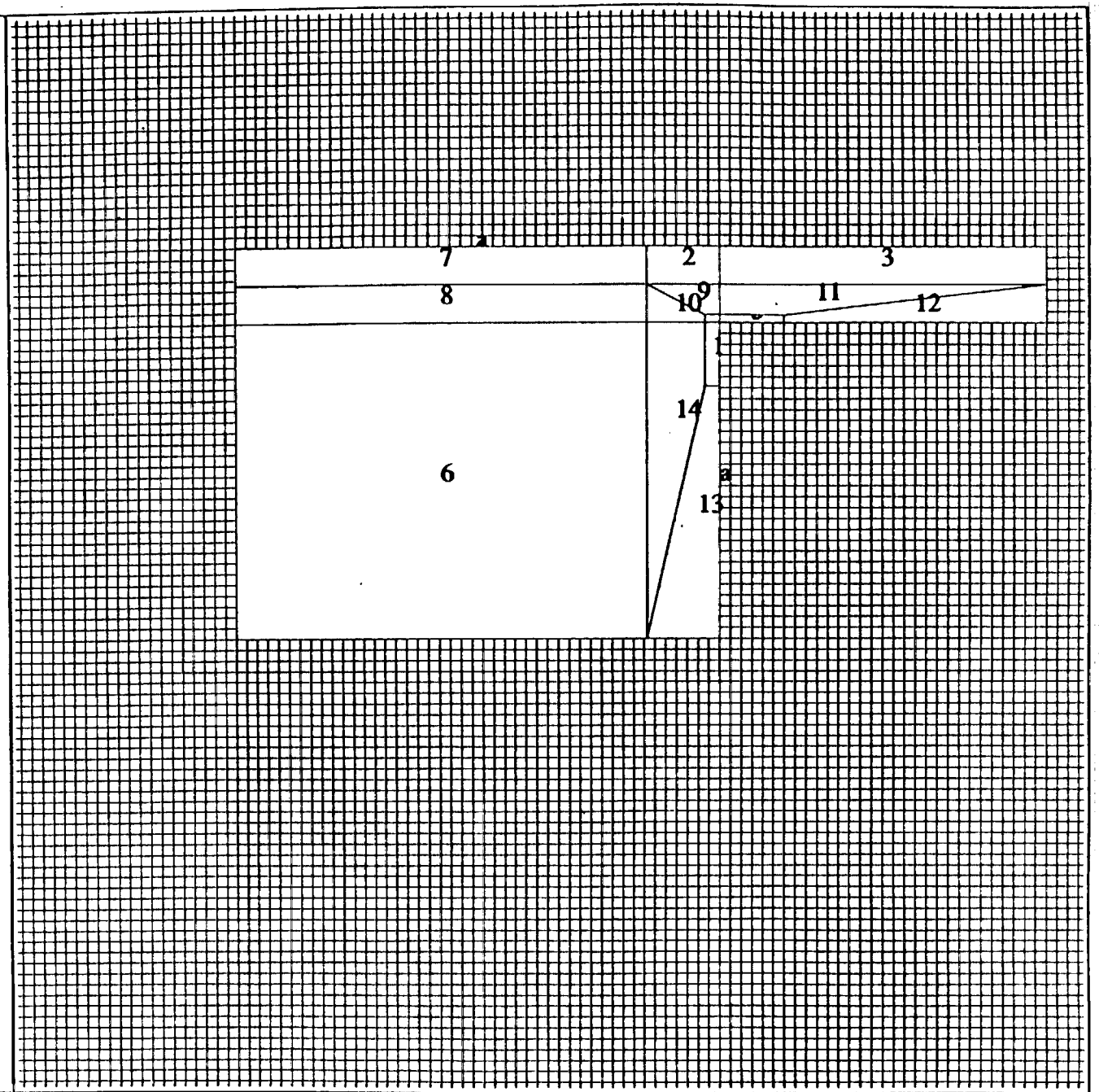
7
2
3
8
9
10
11
12
1
14
6
13
NEKTON
V 2.8
Session Name: axi
Spectral Element Mesh from Prenek
Jun 3 15:42 1991

Figure 1a

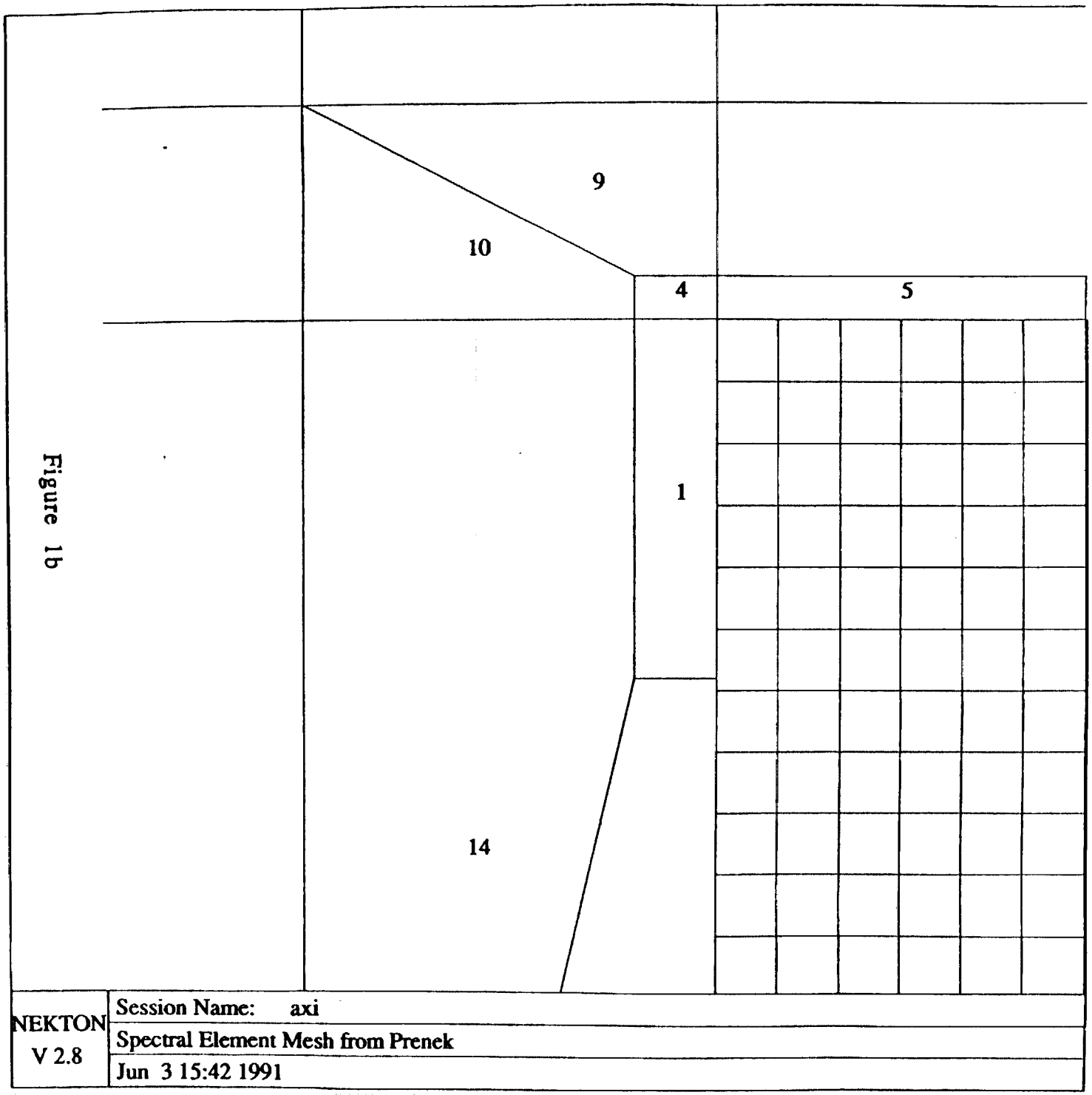
9
10
4
5
1
14
NEKTON
V 2.8
Session Name: axi
Spectral Element Mesh from Prenek
Jun 3 15:42 1991

Figure 1b

NEKTON 2.7
Rotate View
0
<- Roll Degrees ->
0
0
<- Yaw Degrees ->
Figure 2

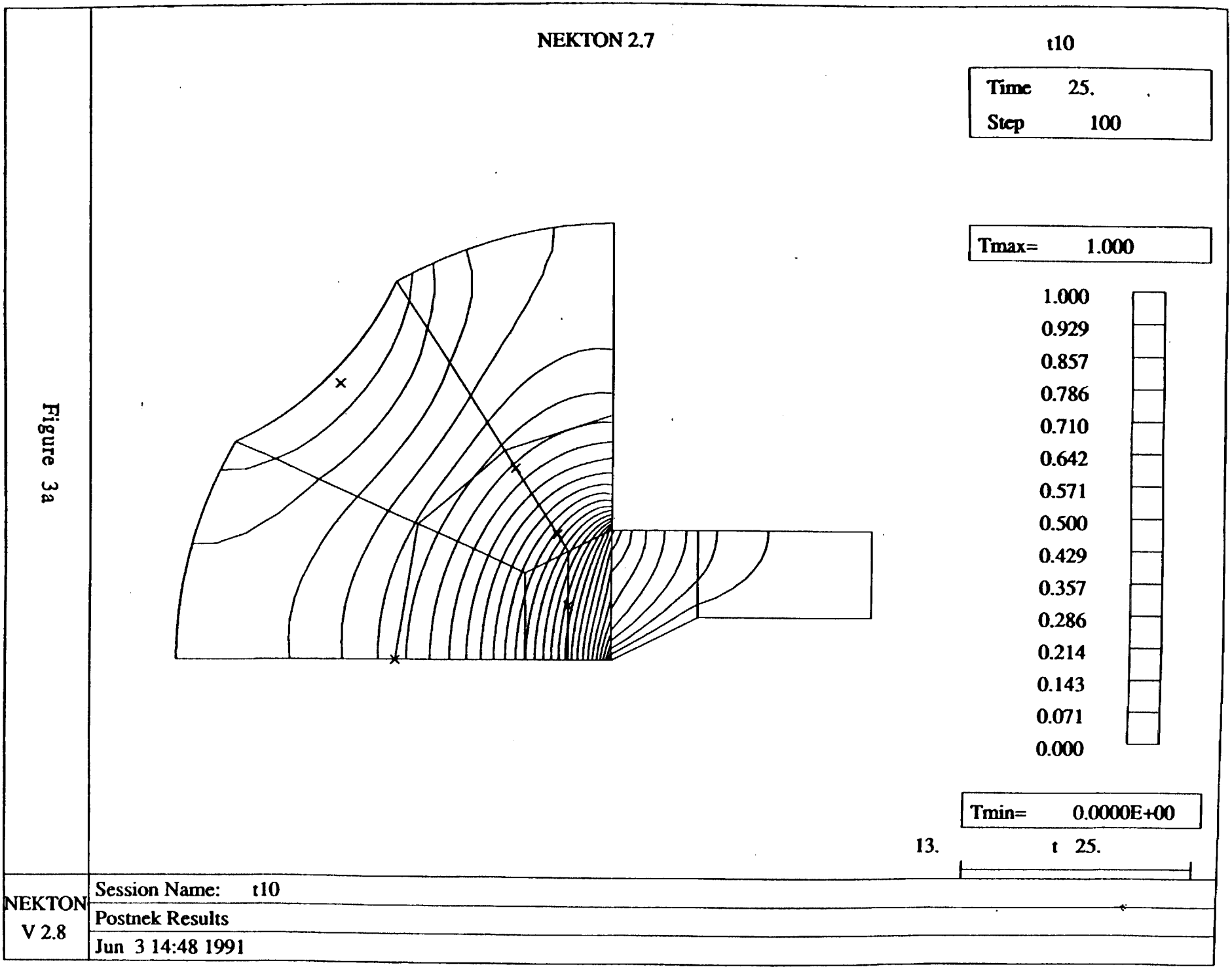
NEKTON 2.7
t10
Time 25.
Step 100
Tmax= 1.000
1.000
0.929
0.857
0.786
0.710
0.642
0.571
0.500
0.429
0.357
0.286
0.214
0.143
0.071
0.000
Tmin= 0.0000E+00
13.
t 25.
NEKTON
V 2.8
Session Name: t10
Postnek Results
Jun 3 14:48 1991

Figure 3a

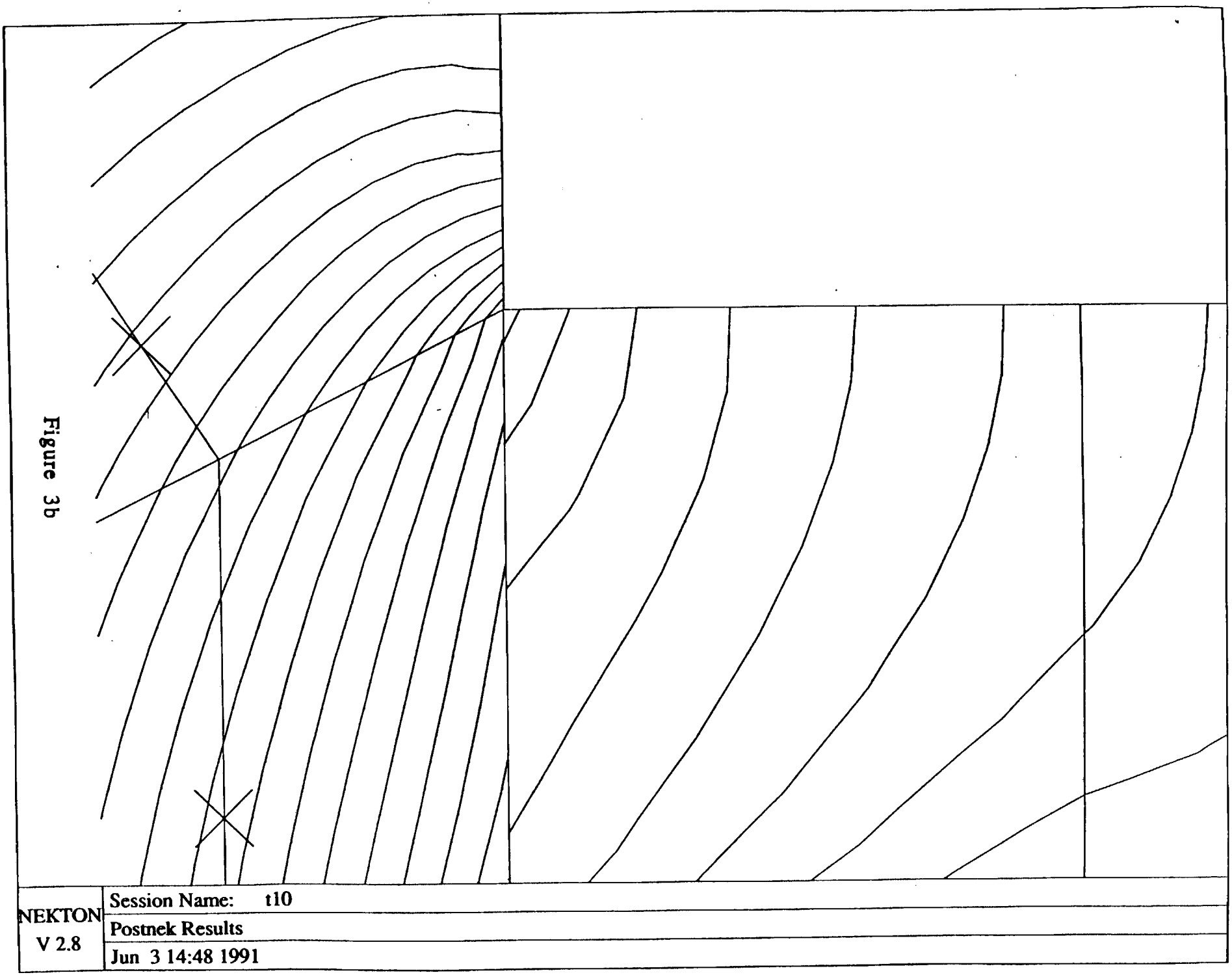

Figure 3b

Nekton 2.7
EXIT
CLEAR
PLOT
SET QUANTITY
SET LOCATION
SET PLOT FORMAT
SET ATTRIBUTE
SET SCREEN
DISPLAY OBJECT
NEKTON Version 2.7
Beginning Session problem1
Reading geometry from problem1
Reading History Data...
Read 1 History points
End of history data. Ready to begin.
1 Field dumps
VALUE AT POINT
X-Y PLOT
SURFACE PLOT
VALUES
HISTORY
INTEGRAL QUANTITY
STREAMLINE
PROFILE
SET OF PROFILES
HELP
Dump Screen
Nekton 2.7

Figure 4

NEKTON Version 2.7
Choose a Name for This Session:
Beginning Session problem2
Will Read Parameters From problem1.rea
CURRENT SETTING: STEADY TWO DIMENSIONAL HEAT TRANS
CURRENT SETTING: UNSTEADY TWO DIMENSIONAL HEAT TR
CURRENT SETTING: UNSTEADY TWO DIMENSIONAL STOKES
CURRENT SETTING: UNSTEADY TWO DIMENSIONAL NAVIER-
Time stepping scheme set to First Order
CURRENT SETTING: UNSTEADY TWO DIMENSIONAL NAVIER-
EQUATION TYPE
MOVING GEOMETRY N
ADVECTION Y
ACCEPT CURRENT SWITCHES
STRESS FORMULATION N
SPLIT FORMULATION Y
DIMENSION 2
TURBULENCE MODEL N
UNSTEADY Y
HEAT TRANSFER Y
FLUID FLOW Y
ADDL PASSIVE SCALARS 0
HELP
Dump Screen
Nekton 2.7

Figure 5

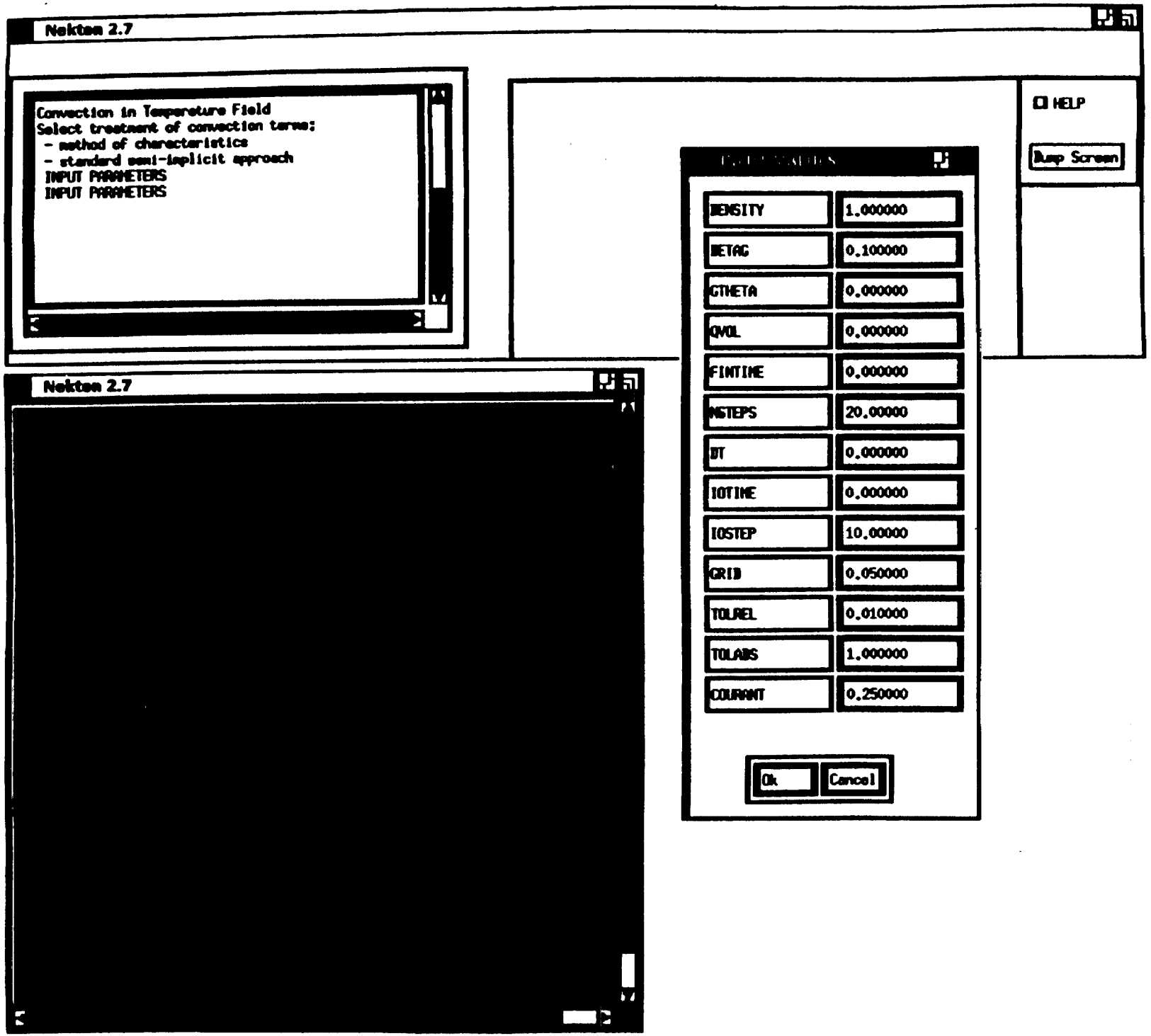
Nektan 2.7
Convection in Temperature Field
Select treatment of convection terms:
- method of characteristics
- standard semi-implicit approach
INPUT PARAMETERS
INPUT PARAMETERS
HELP
Dump Screen
DENSITY
1.000000
BETAG
0.100000
GTHETA
0.000000
QVOL
0.000000
FINTIME
0.000000
NSTEPS
20.00000
DT
0.000000
IOTIME
0.000000
IOSTEP
10.00000
GRID
0.050000
TOLREL
0.010000
TOLABS
1.000000
COURANT
0.250000
Ok
Cancel
Nektan 2.7

Figure 6

Chapter 6

Low Mach Number Compressibility

OBJECTIVE:

The objective in this report period was to implement the low Mach number compressibility into NEKTON and demonstrate this capability for CVD problems. We have shown the use of this accurately modelling the effects of compressibility due to the the effects of varying temperature. This is an improvement over the Boussinesq approximation which was previously used to model the effects of density changes. In this report period we have implemented this capabililty in NEKTON for general 2-D, 3-D and axisymmetric geometries. We have demonstrated this new capability in simple geometries with which we have verified our results through comparison with analytic solutions. We have also demonstrated this capability on realistic CVD geometries.

BACKGROUND:

Solution of the full time-dependent compressible Navier-Stokes equations presents

difficulties in combining the vastly differing acoustic and viscous time scales. In this approach we are able to decouple the acoustic compressibility, with its numerical and physical complexity which is irrelevant to CVD applications. We retain the thermal compressibility term which is crucial to accurate solution of CVD problems.

CVD problems typically involve absolute temperatures which can vary by a factor of two. The Mach numbers involved in CVD are typically of order 10^{-3} to 10^{-4}. This combination of parameters verifies that there is a need for a scheme which will account for the density variations due to temperature, and need not account for density changes due to momentum.

Torczynski [3] studied the inviscid problem in which a perfect gas is heated by means of energetic particles. He was able to confirm the validity of the acoustically filtered equations of motion for low Mach number by comparison with solution of the full gasdynamic problem. However, the inviscid assumption is valid when used as in most high Re aerospace applications where viscosity affects only thin boundary layers near walls or thicknesses of shock waves.

CVD applications, however, involve significant viscous and diffusive effects, and therefore require solution of the acoustically-filtered full Navier-Stokes equations. Additionally, as Makarov [4] noted, it is crucial to include the additional viscous and diffusive term associated with thermal gas expansion ("bulk viscosity") that arises in the compressible case. This is because in most CVD geometries a boundary layer forms normal to the deposition surface, and this viscous compressible term is significant in quantifying this boundary layer thickness and the resultant deposition rates.

This formulation offers significant advantages over solution of the full compressible Navier-Stokes equations. It greatly reduces the computational load presented by the presence of the viscous and convective time scales of order seconds and the acoustic

time scales of order fractions of milliseconds. With this formulation it is possible to concentrate on study of the real CVD problem without introducing the complexity of irrelevant and short-lived acoustic waves.

COMPRESSIBLE TRANSPORT EQUATIONS:

The development of compressible transport equations for low Mach numbers (characterisitic of CVD systems) stems from the need to fully capture the effect of temperature gradients in the system on the flow field in the reactor. Subsonic compressible flow models have been reported in [1,2,4-7]. More recently Strelets and co-workers [8] have extended this formulation to concentration convection and multi-component chemically reactive flows. The subsonic model takes advantage of the low Mach number of the system to eliminate acoustic waves and results in a system of equations similar to that of incompressible transport equations.

Non-dimensionalizing the length, velocity , time, pressure, temperature, and properties of the gas:

$$x, y, z, V, t, P, T, \rho, \mu, k$$

by system reference values

$$L^*, V^*, L^*/V^*, \rho^* RT^*, T^*, \rho^*, \mu^*, k^*,$$

respectively, results in the following equations:

$$\frac{D\rho}{Dt} + \nabla \cdot \rho V = 0 \tag{1}$$

$$\rho\frac{DV}{Dt} = -\frac{1}{\gamma M^2}\nabla P + \frac{gL^*}{V^{*2}}\rho\hat{e}_g + \frac{1}{Re}\tau \tag{2}$$

$$\rho\frac{DT}{Dt} = \frac{\gamma-1}{\gamma}\frac{dP}{dt} + \frac{1}{RePr}\nabla\cdot(k\nabla T) + \frac{1}{Re}(\gamma-1)(M^2)[2\mu(\nabla V + (\nabla V)^t) - \frac{2}{3}\nabla\cdot V^2\mathbf{I}] \tag{3}$$

$$P = \rho T \tag{4}$$

$$\tau = \mu[\nabla V + (\nabla V)^{\mathbf{T}} - \frac{2}{3}\nabla\cdot V\mathbf{I}] \tag{5}$$

In the above g is the gravity, γ the ratio of specific heats of the gas, M the Mach number $= V^*/c^*$, $\hat{e}_g$ unit gravity vector, Re the Reynolds number $= \rho^* V^* L^*/\mu^*$, Pr the Prandtl number, and $\mathbf{I}$ the identity matrix. Also the superscript $^{\mathbf{T}}$ denotes the transpose of the operator.

The subsonic model is based on two assumptions which are valid in CVD systems:

1. The Mach number $M = V^*/c^* << 1$.

2. The hydrostatic compressibility $\epsilon = gL^*/RT^* << 1$

In order to derive the subsonic compressible equations the field variables are expanded in terms of γM^2 and ϵ. For example, pressure is expanded as:

$$P = P^{(0)} + \gamma M^2 P^{(10)} + \epsilon P^{(01)} + ... \tag{6}$$

Inserting these expansions to eqs. (1)-(5), equating like-powers of the two perturbation parameters, and dropping the (0) superscript for all variables except pressure one obtains:

$$\nabla P^{(0)} = 0 \tag{7}$$

$$\frac{D\rho}{Dt} + \rho \nabla \cdot V = 0 \tag{8}$$

$$\rho \frac{DV}{Dt} = -(\nabla P^{(10)} + \frac{gL^*/RT^*}{\gamma M^2} \nabla P^{(01)}) + \frac{gL^*}{V^{*2}} \rho \hat{e}_g + \frac{1}{Re}(\tau) \tag{9}$$

$$\rho \frac{DT}{Dt} = \frac{\gamma - 1}{\gamma} \frac{dP^{(0)}}{dt} + \frac{1}{RePr} \nabla \cdot (k \nabla T) \tag{10}$$

$$P^{(0)} = \rho T \tag{11}$$

By recognizing that in equilibrium $\nabla P^{(01)} = \rho_s \hat{e}_g$, where ρ_s is the equilibrium density of the gas, eq. (9) can be rewritten as:

$$\rho \frac{DV}{Dt} = -\nabla P^{(10)} + \frac{gL^*}{V^{*2}} (\rho - \rho_s) \hat{e}_g + \frac{1}{Re}(\tau) \tag{12}$$

Equations (5)-(7), and (9)-(11) imply that in the subsonic model the pressure term splits into two terms: a thermodynamic pressure $P^{(0)}$ which is only a function of time (from eq. (7)) and enters the equation of state, and $P^{(10)}$ which is function of both space and time and accounts for the dynamic effects. In the subsonic formulation the viscous heating term of the energy equation is also dropped. By differentiating

the equation of state and using the above equations a new form of the continuity equation is obtained:

$$\nabla \cdot V = \frac{1}{P^{(0)}}[\frac{1}{RePr}\nabla \cdot (k\nabla T) - \frac{1}{\gamma}\frac{dP^{(0)}}{dt}] \tag{13}$$

For open systems the pressure term $P^{(0)}(t)$ is constant and one obtains the following set of equations:

$$\rho\frac{DV}{Dt} = -\nabla P^{(10)} + \frac{gL^*}{V^{*2}}(\rho - \rho_s)\hat{e_g} + \frac{1}{Re}(\tau) \tag{14}$$

$$\rho\frac{DT}{Dt} = \frac{1}{RePr}\nabla \cdot (k\nabla T) \tag{15}$$

$$\nabla \cdot V = \frac{1}{P^{(0)}}[\frac{1}{RePr}\nabla \cdot (k\nabla T)] \tag{16}$$

$$P^{(0)} = \rho T \tag{17}$$

The above sets of equations (for open CVD systems) is very similar to that of incompressible transport equations which are currently solved (in three space dimensions) by NEKTON. NEKTON has been modified to solve the above set of equations in order to correctly simulate the effect of local thermal expansion of gas during CVD processes. This reformulation of the governing equations takes advantage of the spectral-element discretization and iterative solvers already implemented in NEKTON.

IMPLEMENTATION :

The above procedure was implemented in NEKTON in the context of the current formulation for solving the elliptic equations associated with incompressible flow. The current implementation involves solving two problems: The Navier-Stokes equatons for viscous incompressible flow, and the energy equation for the temperature. The coupling of the convective terms was achieved by iterating between these two calculations in the process of time-stepping.

An essential difference in the calculation of low Mach number compressible flow in the enforcement of the divergence condition of the velocity. In the Navier-Stokes calculation the incompressibility condition enforced with $\nabla \cdot V = 0$ is replaced with a condition ($\nabla \cdot V = -CDT/dt$) relating the divergence to the total derivative of the temperature field. In this manner the methodology of the solving the (elliptic) system of equations guarantees that the pressure is solved globally in a coupled manner, without any local mechanisms which cause propagation of pressure (sound waves).

Additionally, modifications were made to the viscous stress tensor to include the extra viscous divergence terms and finally a body force proportional to density was added to replace the Bousinnesq approximation. The significant coding tasks involved in these changes were to implement and verify the above equations, and extensive changes from an assumed constant density to a variable density throughout the code, including the matrix preconditioners, etc.

We were able to introduce this capability in the context of the full code NEKTON. Thus this new capability can be used in two-and three-dimensional as well as axisymmetric geometries. Additionally, this compressibility can interact with the large set of boundary conditions available in NEKTON.

EXAMPLE CASES

In this section we present two classes of examples. In the first we present simplified geometries amenable to analytical analysis in order to demonstrate the validity and accuracy of the implementation. In the second class of problems we demonstrate the use of this method on CVD applications and compare the results of the compressible solution with that calculated using the Boussinesq approximation.

TEST GEOMETRIES

In the first we analyze the one-dimensional unsteady problem described in figure 1. Here we begin with a flow whose velocity, temperature, and pressure are unity. We set the Mach number to be 0.1, the Reynolds number to 100, and the Prandtl number to 1. We fix the inflow velocity and temperature to be unity at the left end of the domain and set the right edge of the domain to be outflow conditions with a pressure perturbation fixed at 0. Note that all pressures plotted are the perturbed (P_1) values; the constant pressure P_0 is fixed as input. Symmetry conditions ($d/dn = 0$) are used at the top and bottom boundaries. The thermal conductivity $k = 10^{-3}$, viscosity $\nu = 10^{-3}$, and domain length of 1. We input a heat flux of q=2k + 2/R (1-x). We expect an exact solution at steady state of

$$T = 1 + 2x - x^2$$

$$V = 1 + 2x - x^2$$

$$p = 8/3\mu(1 - x) = 2.66x10^{-3}(1 - x)$$

In figures 2-4 we plot the steady values of velocity, pressure, and temperature, respectively. In figures 5-7 we plot the time evolution of these quantities at the midpoint of the computational domain. In figures 8-10 we plot quantitatively the profiles of

these quantities along a line from inlet to outlet. At the midpoint of this line in figure 9 a small change in slope of the solution appears where the two elements of the computational domain meet. This error is associated with the finite spatial resolution and can be made arbitrarily small by increasing that resolution. In figure 11 we plot the L_2 error in these quantities as a function of time step magintude. These results confirm the accuracy of the solution and confirm that the scaling of the error with time step is linear, as expected in our first order stepping scheme.

In figure 12 we plot the geometry of a two-dimensional channel flow past a heated section of otherwise adiabatic walls for a Mach number of 0.1. In figure 13 we plot the streamlines of the steady flow past the heated section. In figure 14 we plot contours of the speed. Note the increase in speed as the density decreases downstream of the heat source. In figure 15 we plot perturbed pressure (P_1) contours. Note that the magnitude of this scales correctly (as Ma^2) confirming a one percent expected error (P_1/P_0) for Ma=0.1. In figure 16 we plot the temperature contours. In figure 16b we plot the coutours of divergence. Note the peaks in the divergence of steady flow are near peaks of temperature gradient, confirming the expected behavior of the flow divergence scaling with DT/dt. Finally in Figure 17 we plot the temperature history downstream of the heated plate, which shows the approach to steady state.

CVD REACTOR GEOMETRY

In figure 18 we plot the geometry of an axisymmetric CVD reactor. We use the following properties of H_2 and flow parameters:

H_2 Properties

$$\begin{aligned}
\mu &= 1.5 \times 10^{-5} \frac{Nt - s}{m^2} \\
R &= 8134 \frac{J}{kg - mol - ^\circ K} \times \frac{1kg - mol}{2kg} \\
&= 4157 \frac{J}{kg - ^\circ K} \\
C_p &= 14315 \frac{J}{kg - ^\circ K} \\
\gamma &= 1.4
\end{aligned} \tag{6.1}$$

Simulation Parameters

$$\begin{aligned}
Q &= 10 \;\; Std \;\; L/min \\
P_o &= 0.1 Atm \\
&= 1.01 \times 10^4 \frac{Nt}{m^2} \\
T_{in} &= 300^\circ K \\
T_{wafer} &= 1000^\circ K \\
\overline{T} &= \frac{300 + 1000}{2} = 650^\circ K \\
c &= \sqrt{\gamma R \overline{T}} = 1945 m/sec \\
D &= 0.1m \\
V_{inlet} &= 0.2m/sec \\
M &= V_{inlet}/c = 0.0001 \\
Re &= \frac{\rho V D}{\mu} = \frac{0.37 \times .2 \times .1}{1.5 \times 10^{-5}} = 5 \\
\overline{\rho} &= \frac{P}{R\overline{T}} = .0037 kg/m^3 \\
Pr &= 0.7 \\
k &= \frac{C_p \mu}{Pr} = .307 \frac{W}{m^\circ K}
\end{aligned} \tag{6.2}$$

$$\overline{\alpha} = \frac{k}{\overline{\rho} C_p} = .0058$$

$$\overline{\nu} = \frac{\mu}{\overline{\rho}} = .0040$$

$$\frac{R}{P_o} = .412$$

Note that the low Mach number of 10^{-4} justifies our assumption for the accuracy of the low Mach number assumption for CVD applications. We compare cases using the incompressible code and that with the low Mach number compressibility. In figures 19 and 20 we plot the velocity vectors and temperature contours using the incompressible assumption with properties based on the average temperature. In figures 21 and 22 we plot these same quantities using the low Mach number approximation. Note the large difference in peak velocity (1.2 vs. 0.5), resulting from the large volumetric expansion of the gas from 300 K to near 1000 K.

CONCLUSION

We have demonstrated that the low Mach number approximation is appropriate for CVD applications. In this report period we have concluded work on the development and implementation of the low Mach number scheme in NEKTON. We have demonstrated this new capability on theoretical problems and on problems in CVD.

REFERENCES

1. Forester, C.K., and Emery, A.F., "A Computational Method for Low Mach Number Compressible Free Convective Flows", Journal Comp. Phys. **10**, 487-502 (1972).

2. Paolucci, S, "On the Filtering of Sound from the Navier-Stokes Equations", Sandia National Labs Report SAND82-8257, December, 1982.

3. Torczynski, J.R., "On the Motion of a gas experiencing range-dependent volumetric heating", J. Fluid Mech **201**, 167-188, (1989).

4. Makarov, Y. N., and Zhmakin, A.I., "On the flow Regimes in VPE Reactors", Journal of Crystal growth **94** (1989), 537-550.

5. H. Moffat and K. F. Jensen, J. Cryst. Growth, **77** (1986) 108

6. J.E. Meyer, Nucl. Sci. Eng. 10(1961)267.

7. C.K. Forester and A.F. Emery, J. Comput. Phys. 10(1972)487.

8. J.D. Ramshaw and J.A. Trapp, J. Comput. Phys. 21(1976)438.

9. A. E. Kuznetsov, O.A. Nekhamkina and M.K. Strelets, High Temp. 22(1984)862.

10. Rehm, R.G., and Baum, H.R. "The Equations of Motion for Thermally Driven, Buoyant Flows", Journal of Research of the National Bureau of Standards, **83:3**, May-June, 1978.

11. Schlicting, H, *Boundary Layer Theory*, McGraw-Hill, 1979.

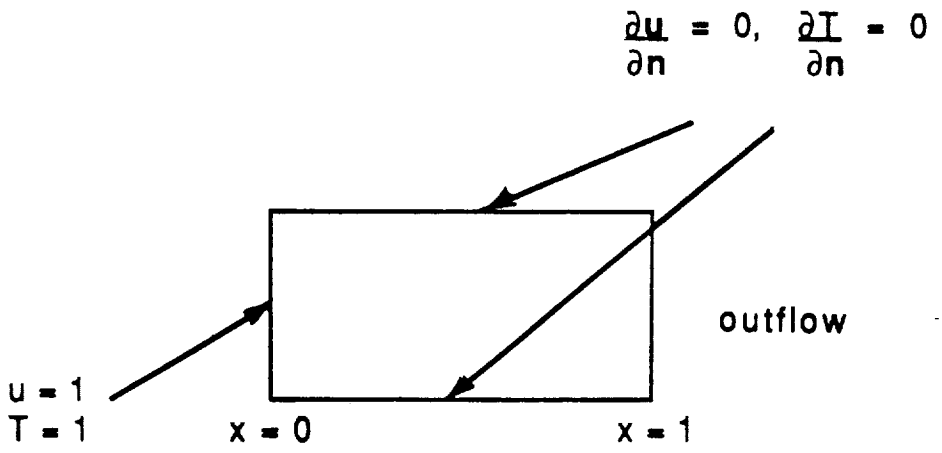

Figure 1 Case 1: Unsteady One Dimensional Compressible Flow Problem Geometry

NEKTON 2.8

comss4

Time 2.5
Step 300
Max Velocity
1.993

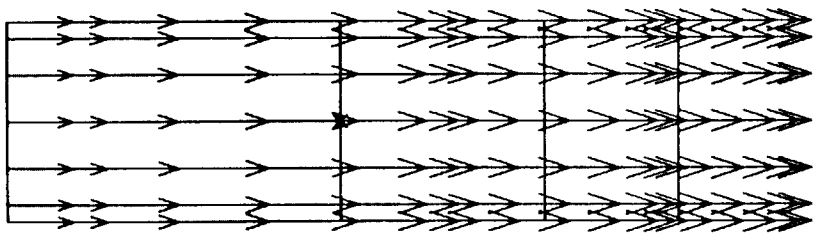

Figure 2 Case 1 Velocity

0.41 t 2.5

NEKTON V 2.8

Session Name: comss4
Postnek Results
Oct 1 09:45 1991

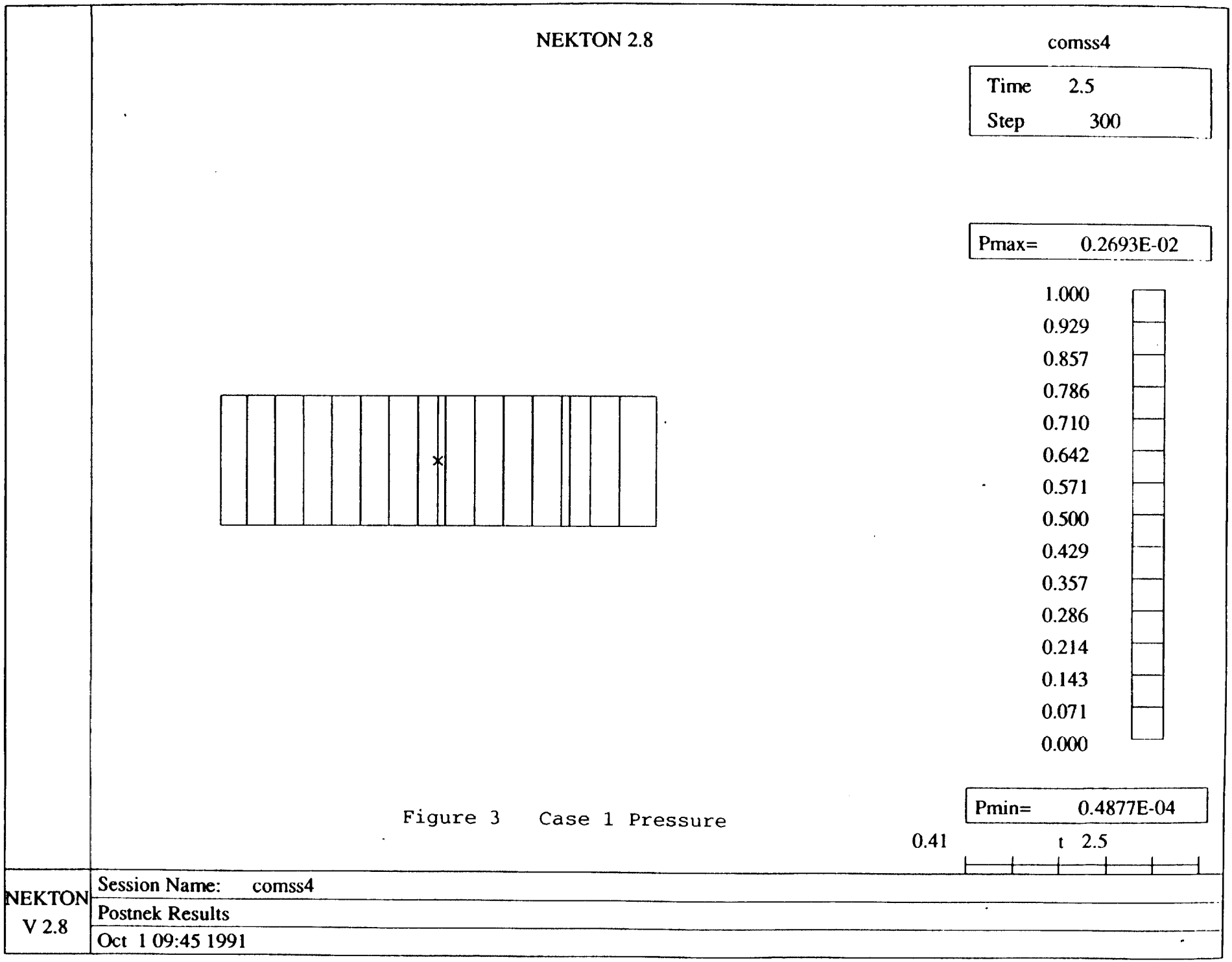

Figure 3 Case 1 Pressure

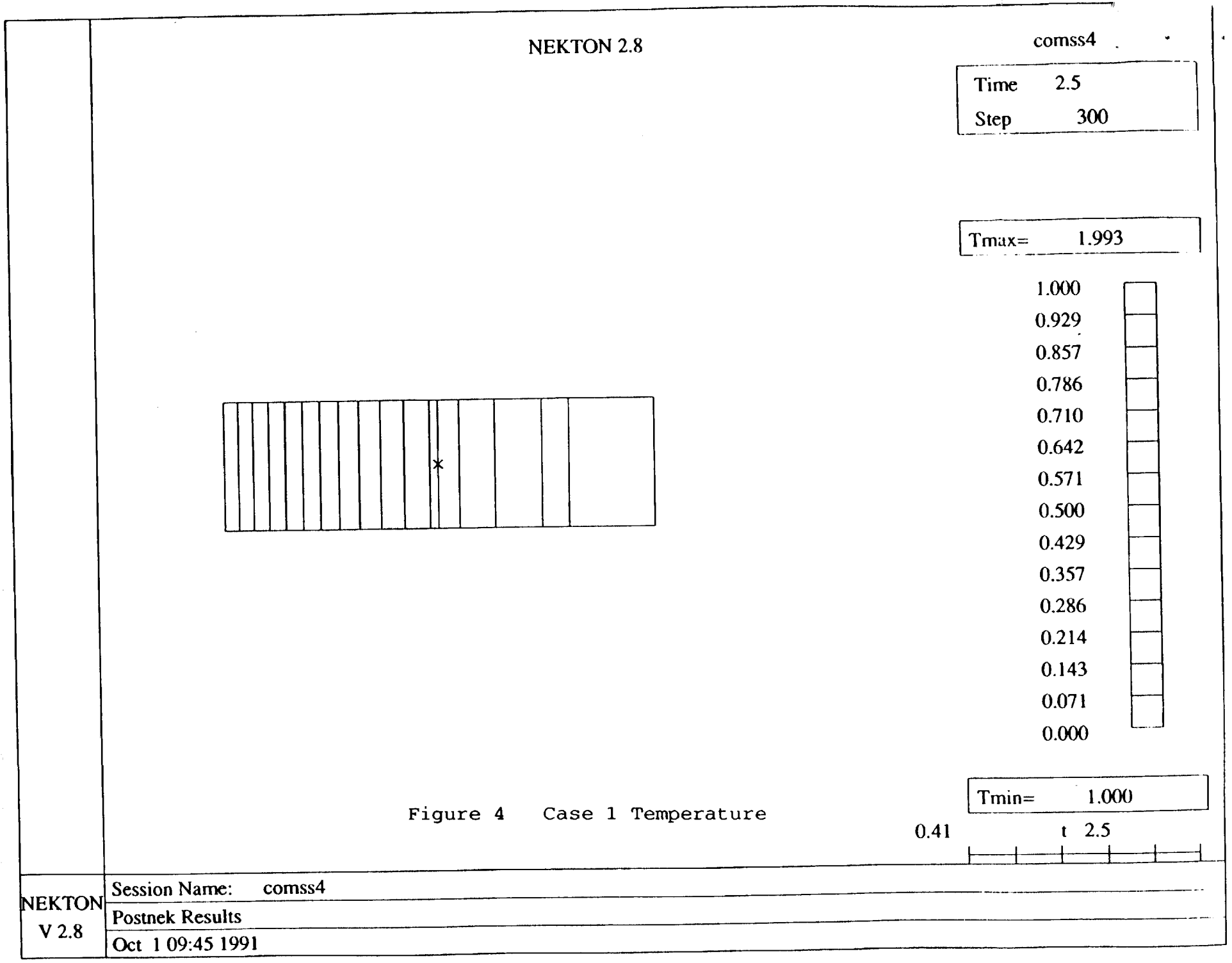

Figure 4 Case 1 Temperature

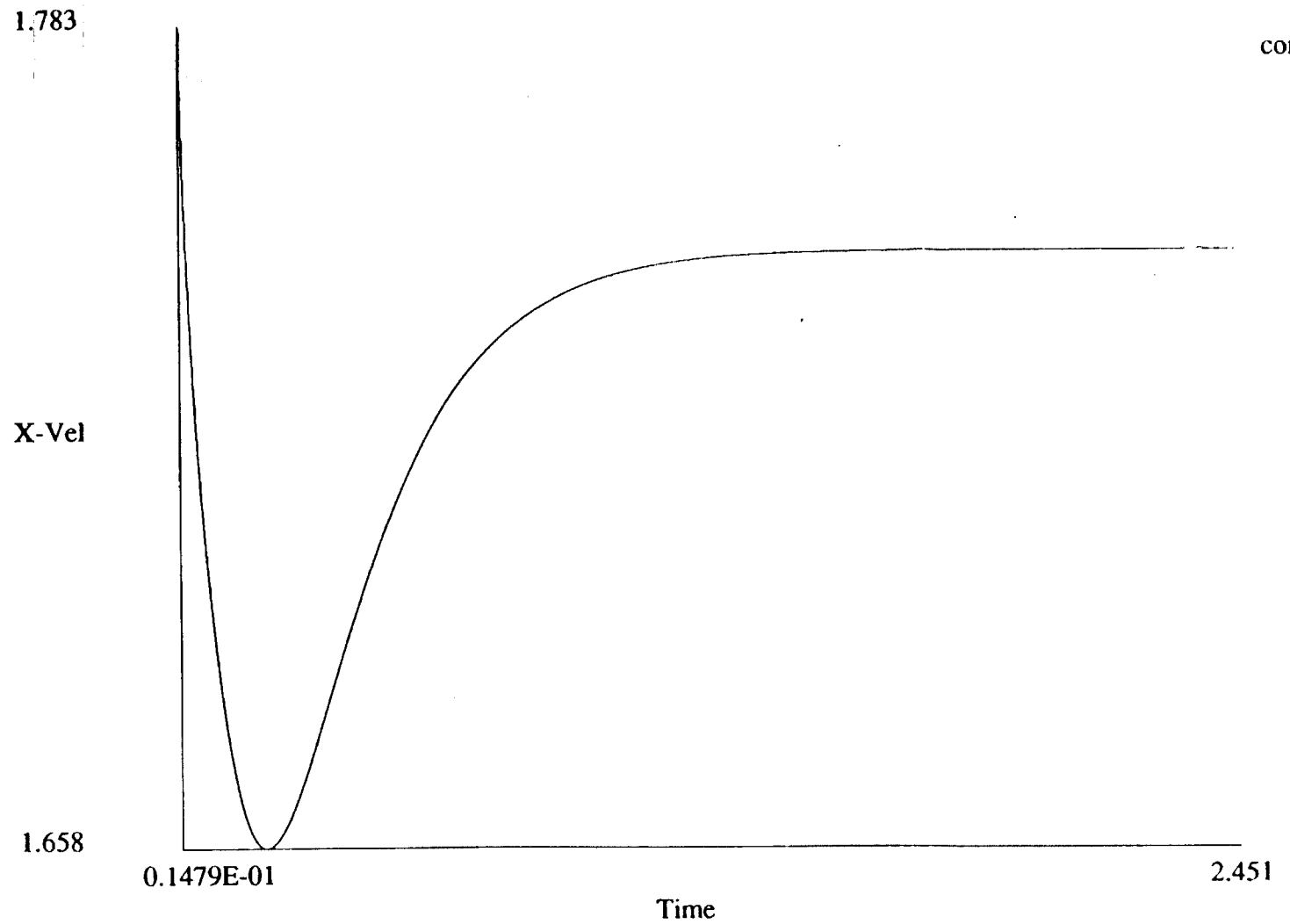

Figure 5 Case 1 Velocity History at X=0.5

NEKTON V 2.8	Session Name: comss4
	Postnek Results
	Oct 1 09:45 1991

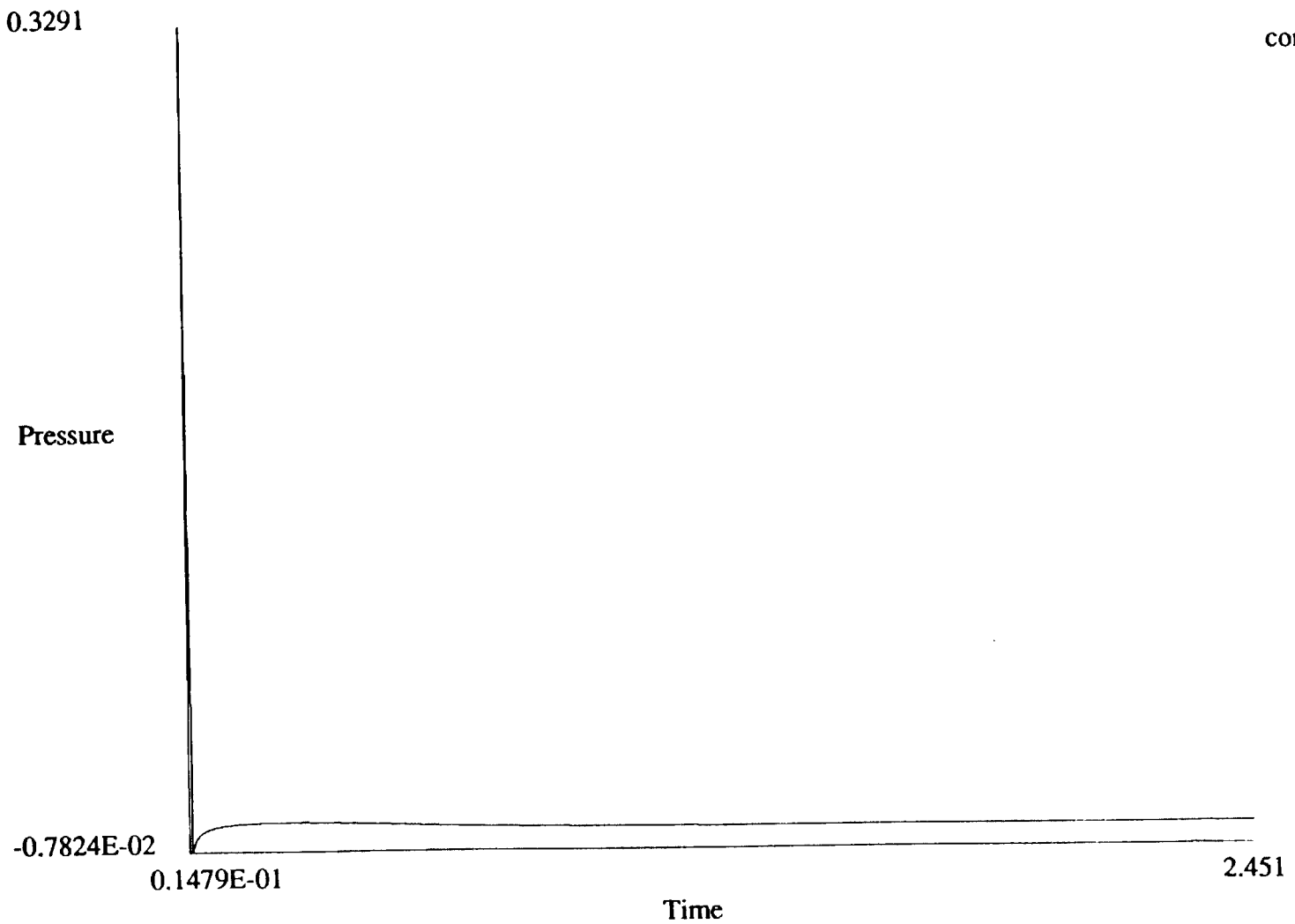

Figure 6 Case 1 Pressure History at X=0.5

NEKTON V 2.8	Session Name: comss4
	Postnek Results
	Oct 1 09:45 1991

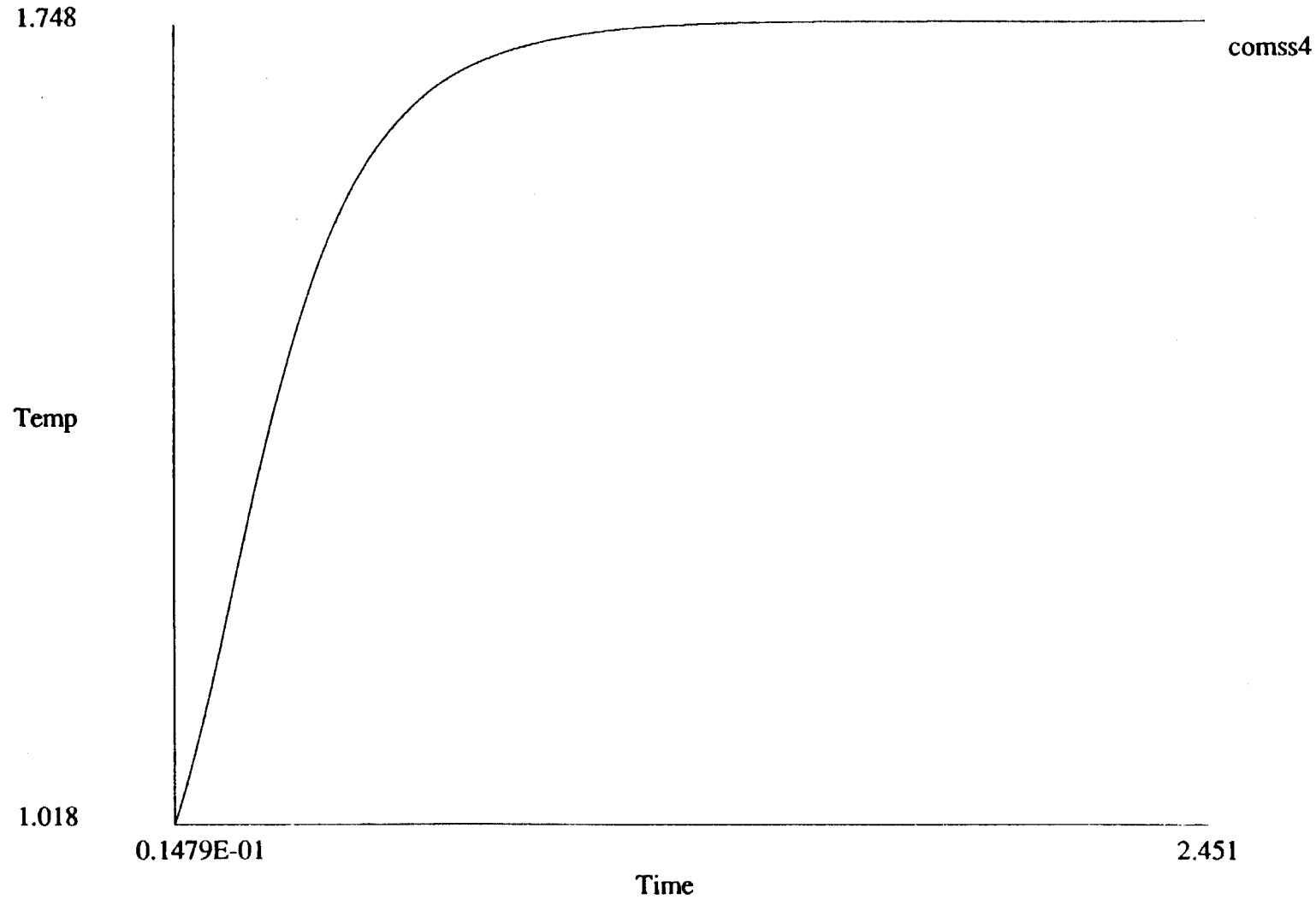

Figure 7 Case 1 Temperature History at X=0.5

NEKTON V 2.8	Session Name: comss4
	Postnek Results
	Oct 1 09:45 1991

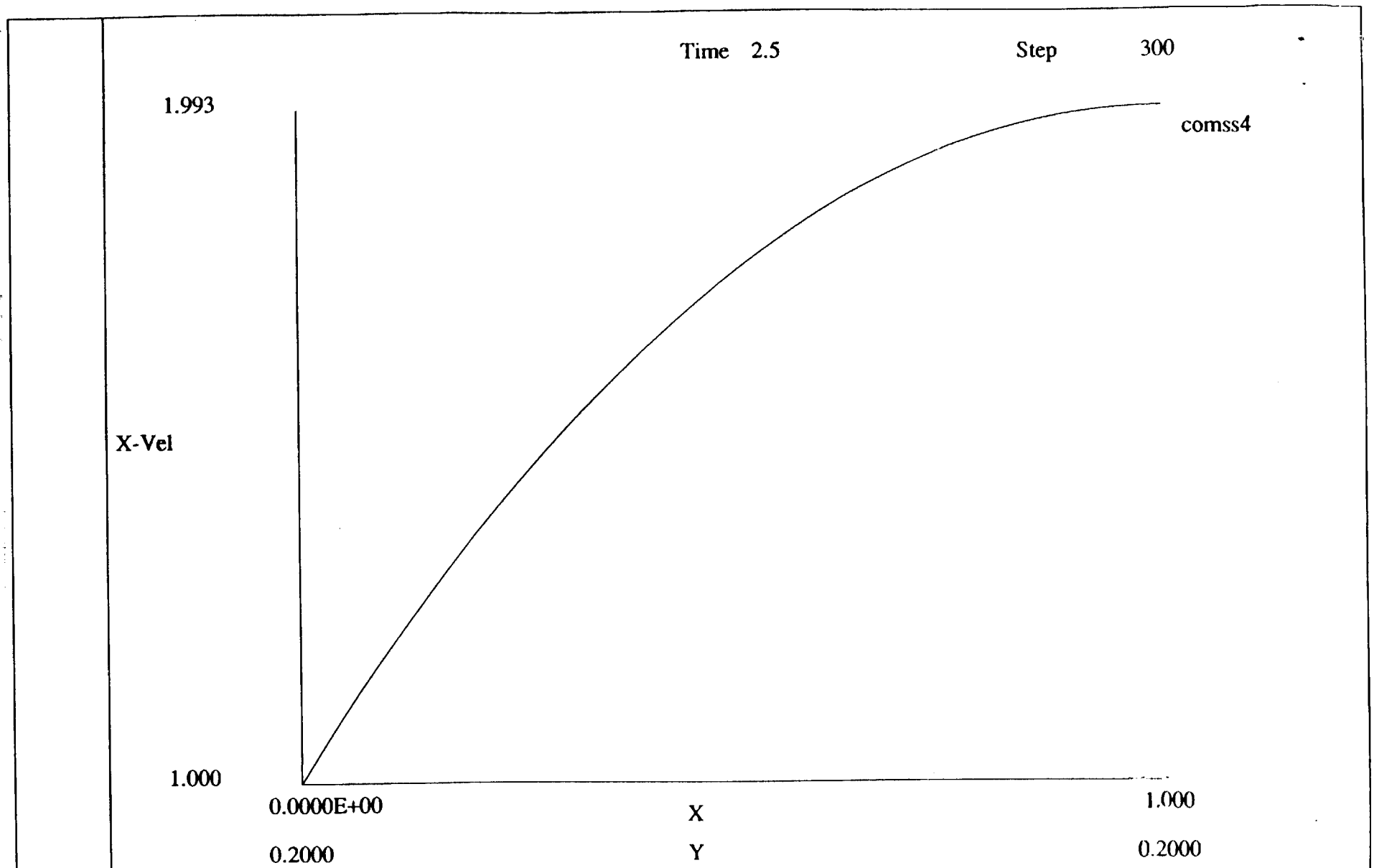

Figure 8 Case 1 Velocity

NEKTON V 2.8	Session Name: comss4
	Postnek Results
	Oct 1 09:45 1991

C-2.

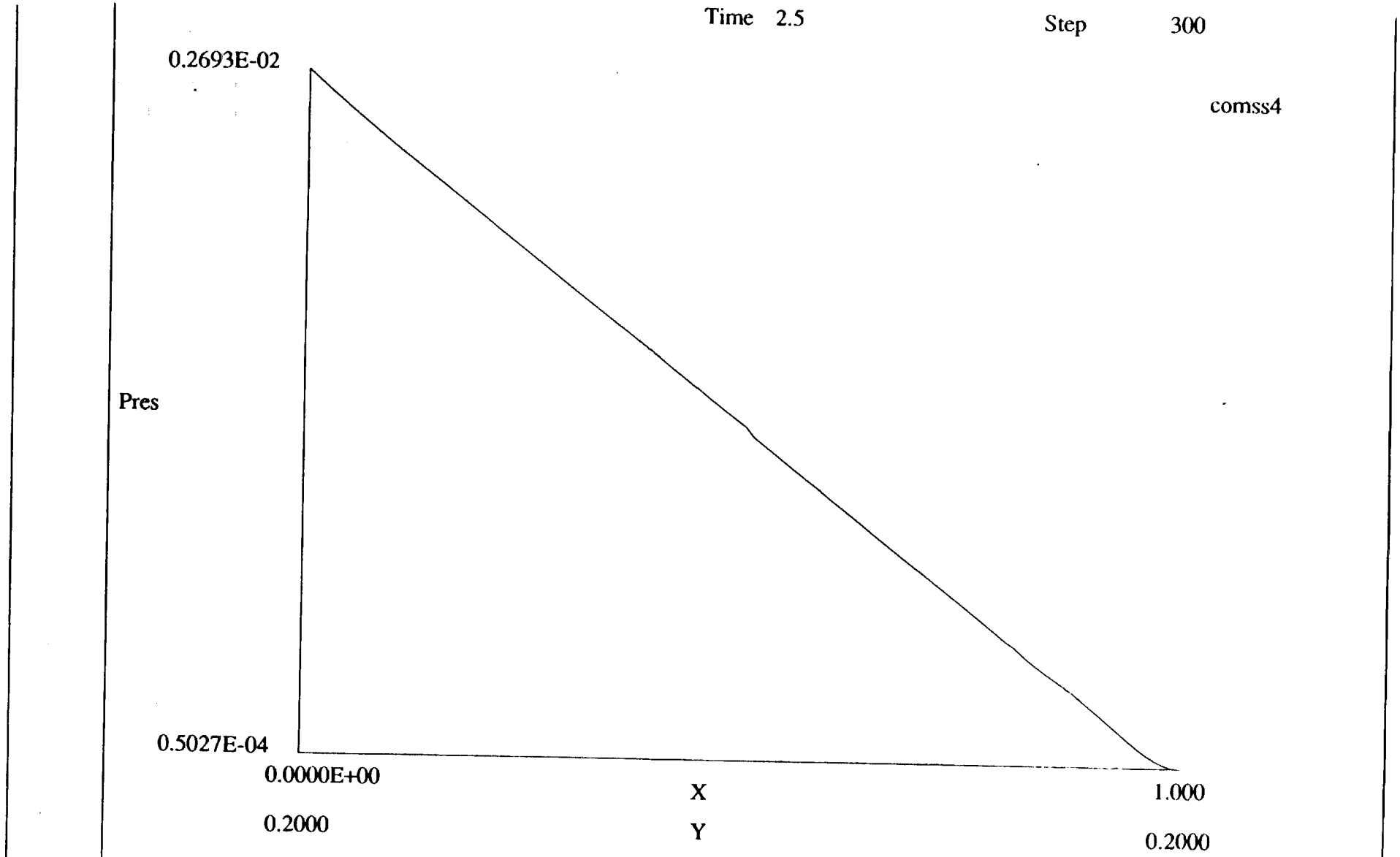

Figure 9 Case 1 Pressure

NEKTON V 2.8	Session Name: comss4
	Postnek Results
	Oct 1 09:45 1991

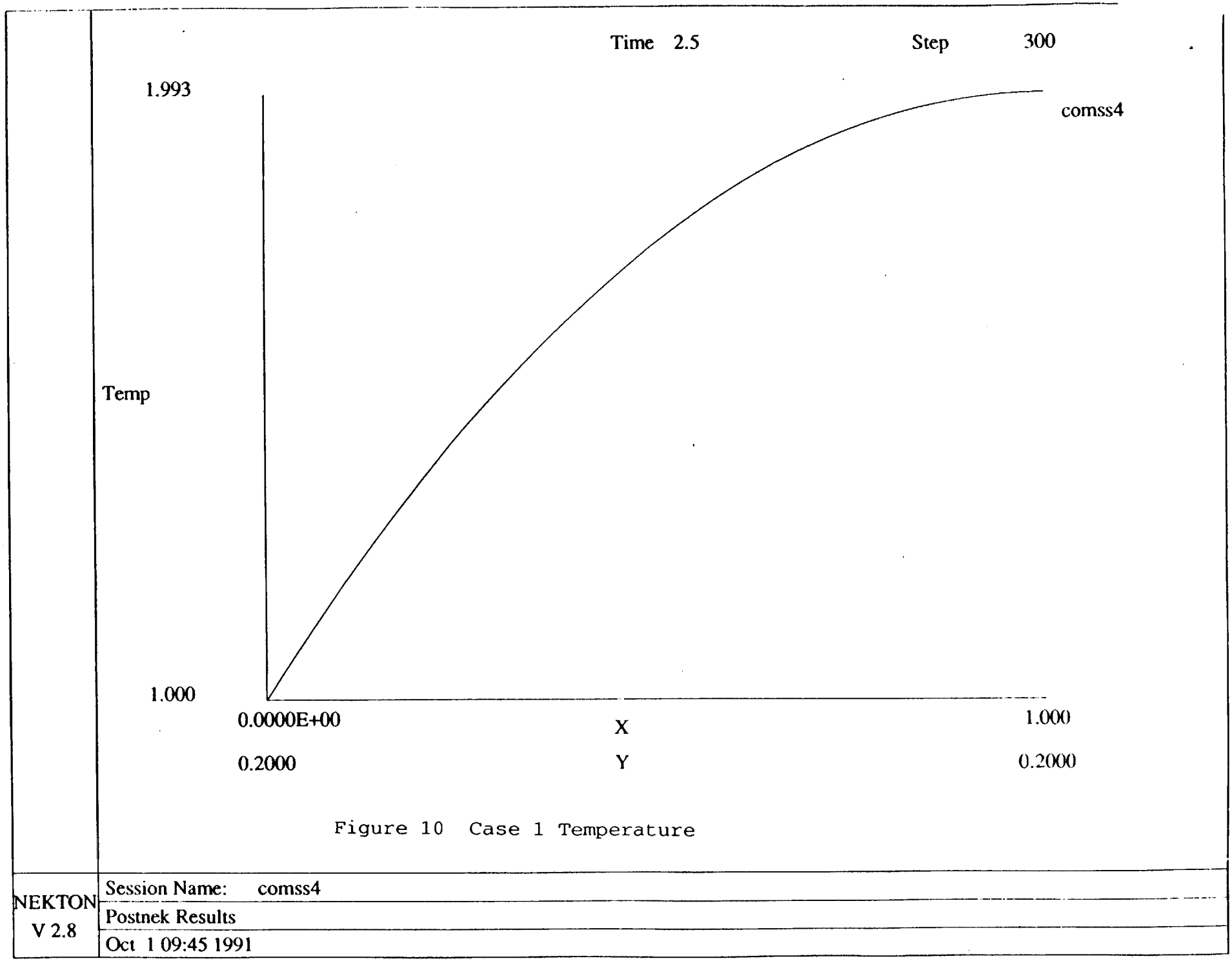

Figure 10 Case 1 Temperature

NEKTON V 2.8	Session Name: comss4
	Postnek Results
	Oct 1 09:45 1991

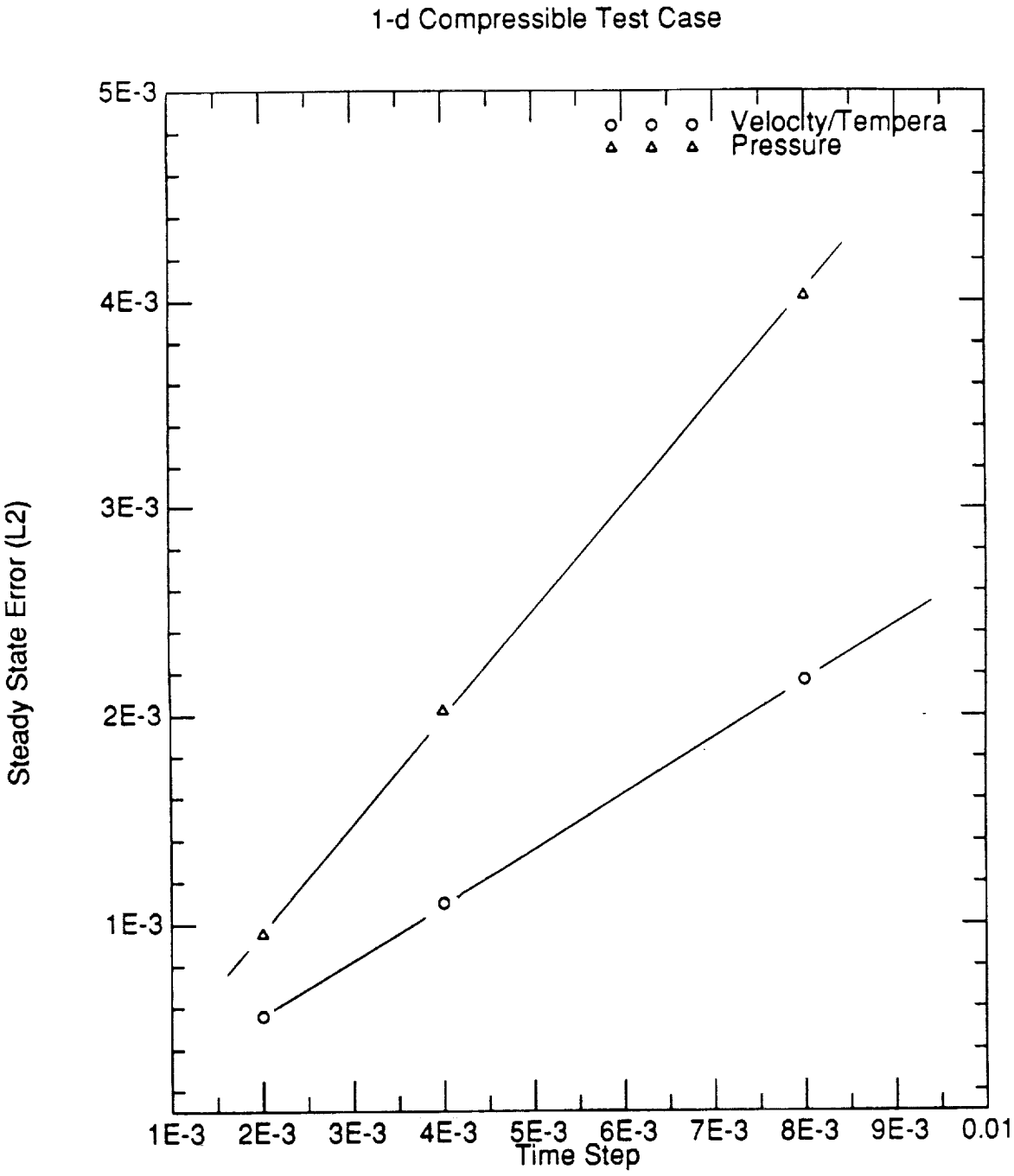
1-d Compressible Test Case
Velocity/Tempera
Pressure
Steady State Error (L2)
5E-3
4E-3
3E-3
2E-3
1E-3
1E-3
2E-3
3E-3
4E-3
5E-3
6E-3
7E-3
8E-3
9E-3
0.01
Time Step

Figure 11

Open System,

$P_0 = 1$

$M_0 = 0.1$

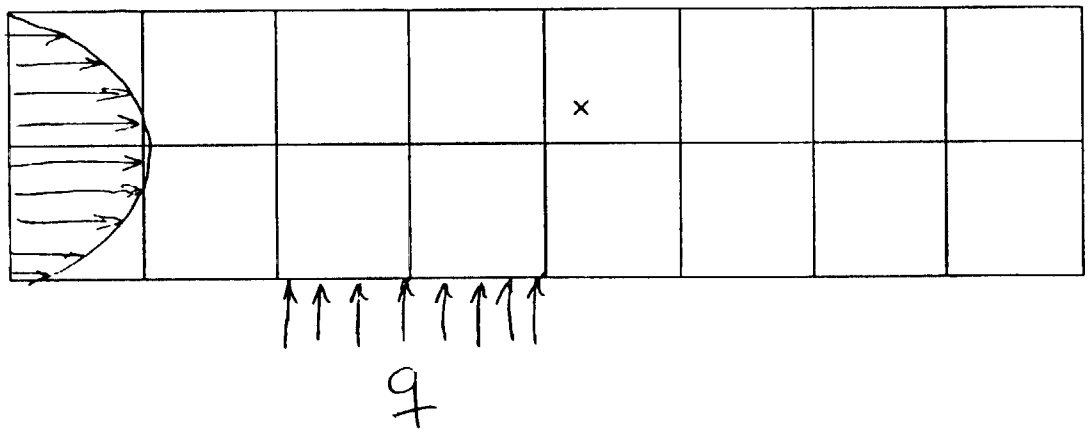

Figure 12 Case 2: Compressible Heated Channel Flow

$Re = 100$

$Pr = 1$

2.7 t 10.

NEKTON V 2.8

Session Name: box2

Postnek Results

Oct 1 12:50 1991

NEKTON 2.8

box2

Time 10.
Step 400

Max Velocity
1.712

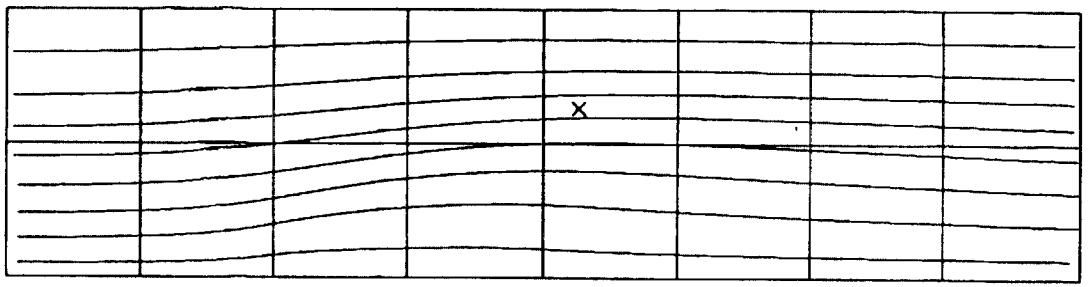

Figure 13 Case 2 Streamlines

2.7 t 10.

NEKTON V 2.8

Session Name: box2
Postnek Results
Oct 1 13:22 1991

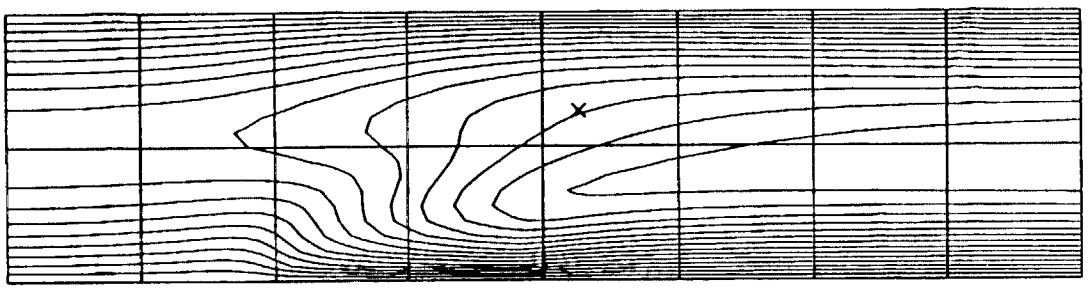

Figure 14 Case 2 Speed Contours

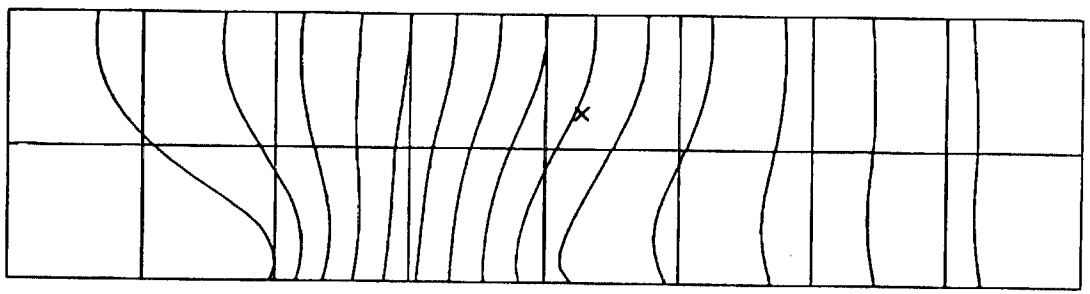

Figure 15 Case 2 Pressure Contours

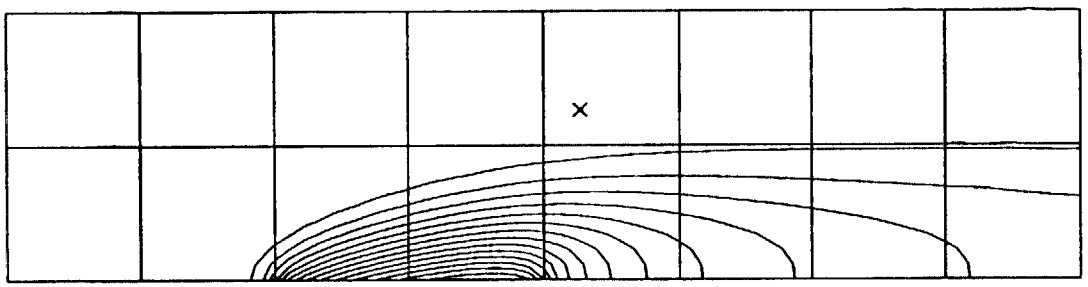

Figure 16 Case 2 Temperature Contours

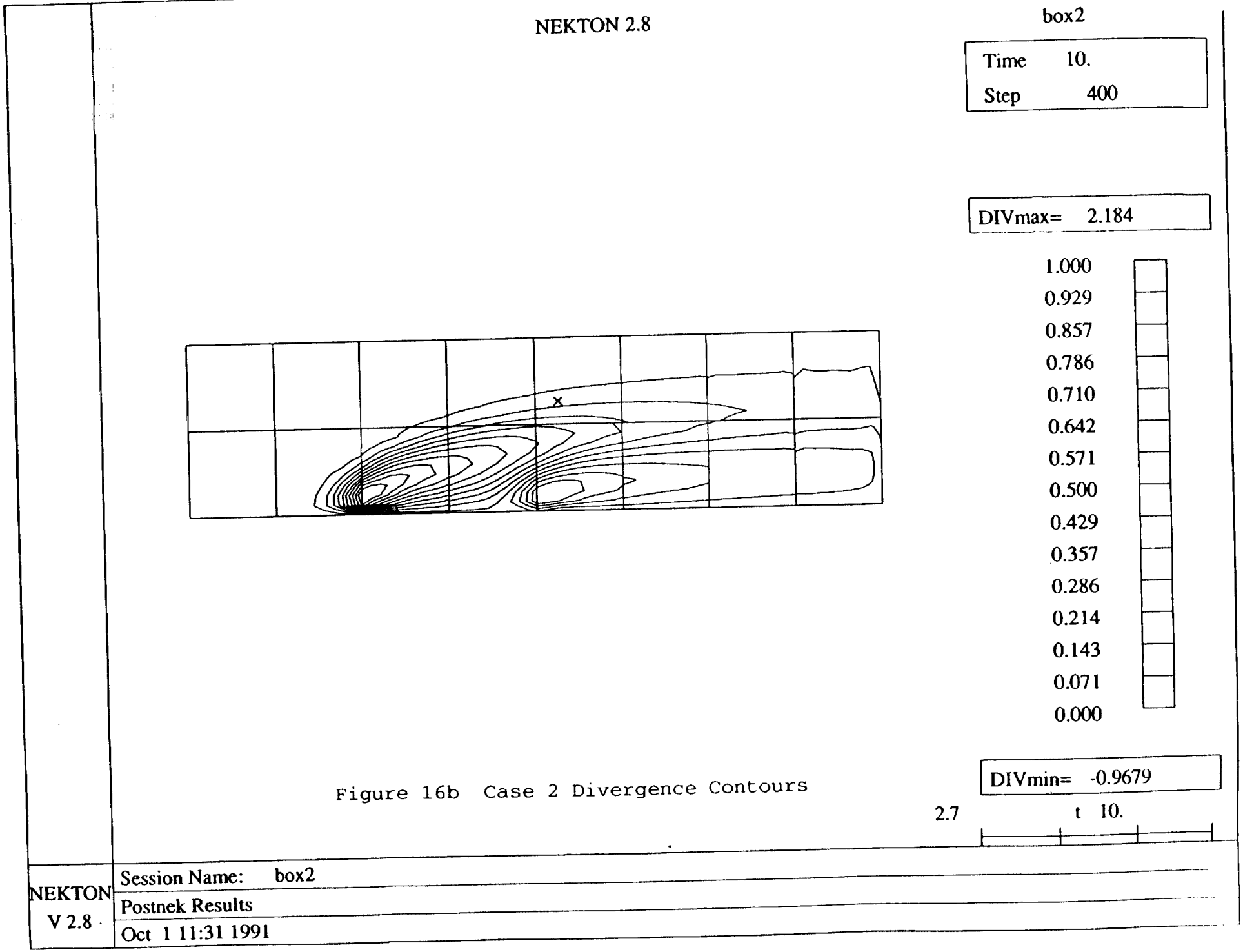

Figure 16b Case 2 Divergence Contours

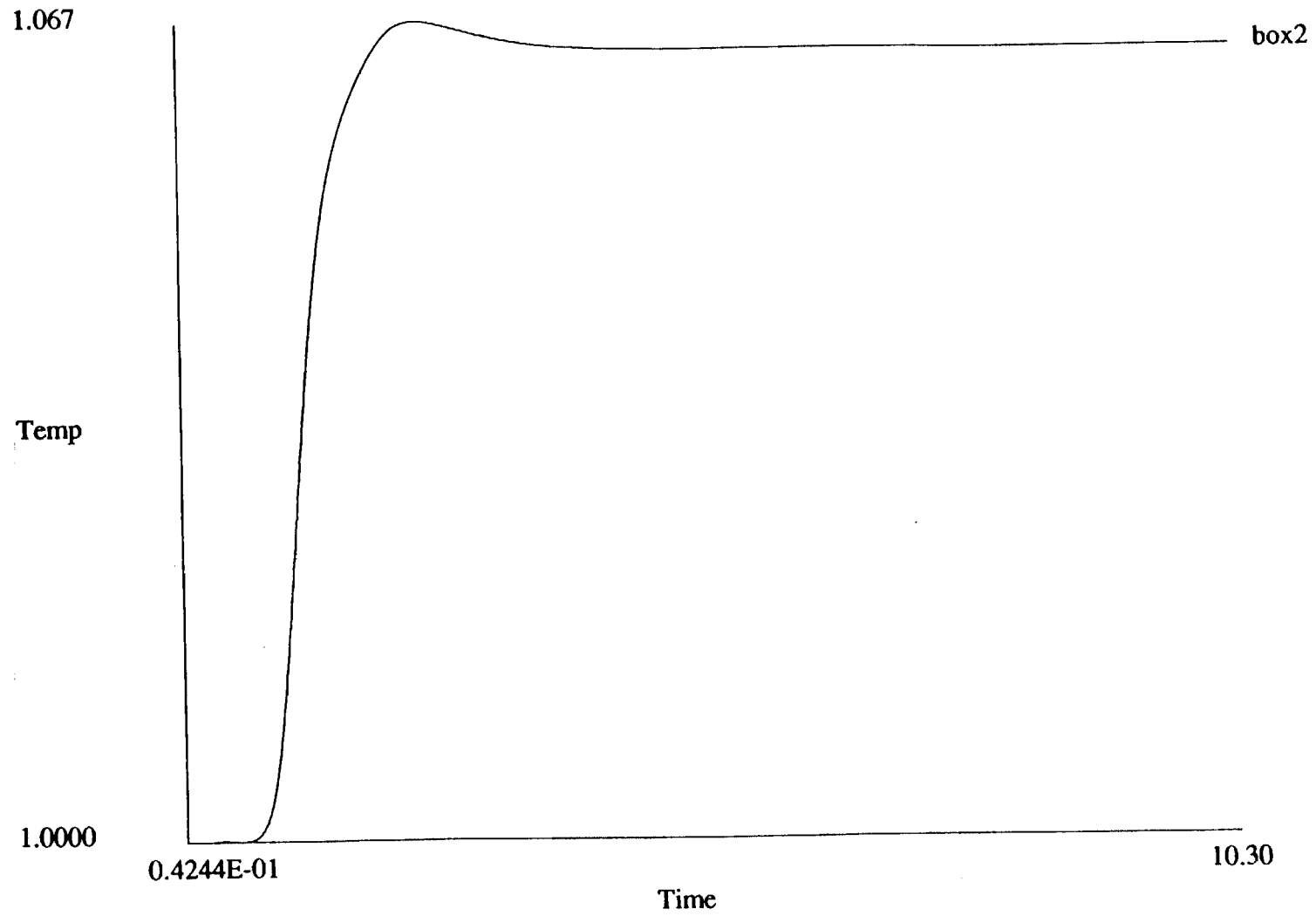

Figure 17 Case 2 Temperature History

NEKTON V 2.8	Session Name: box2
	Postnek Results
	Oct 1 11:31 1991

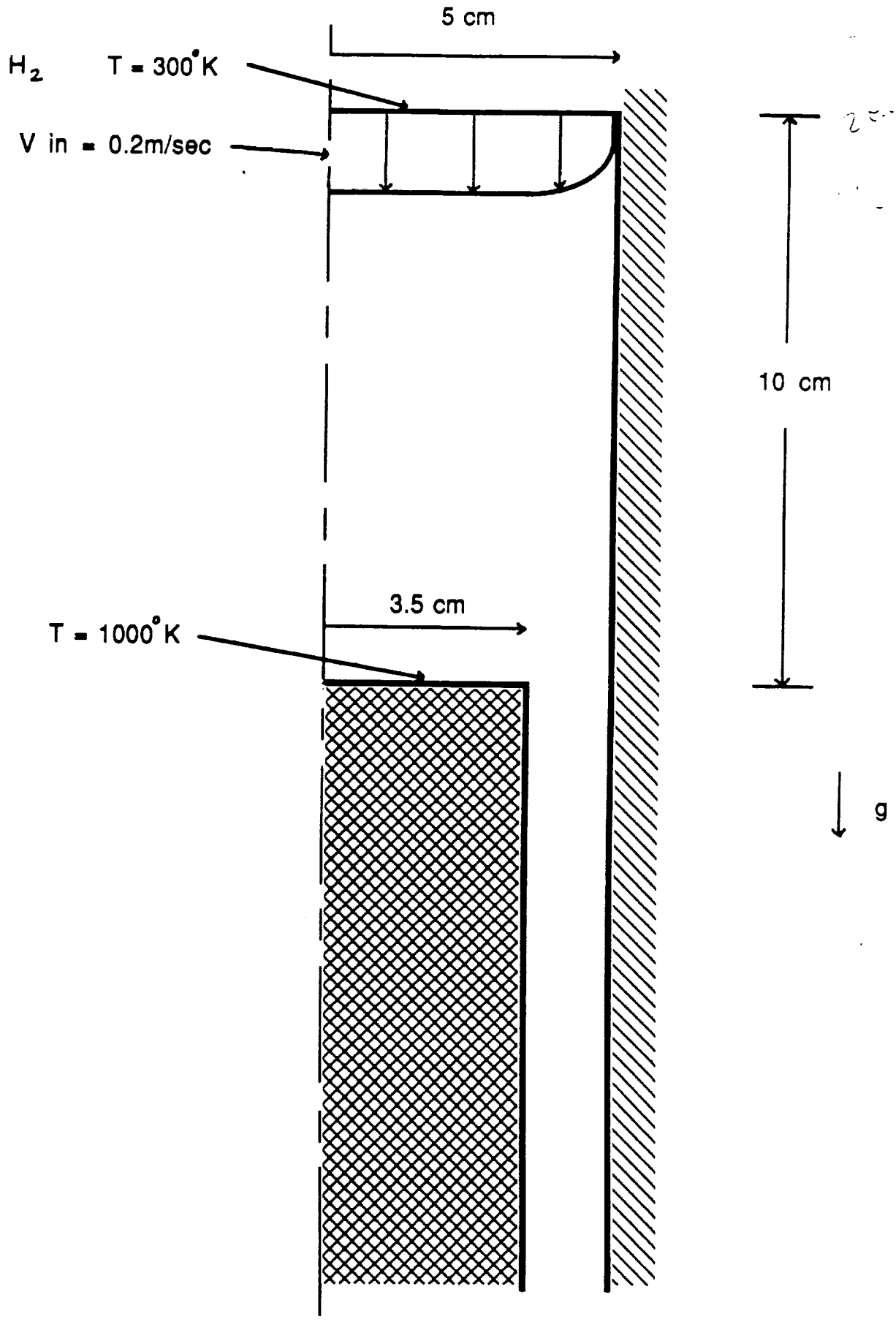

Figure 18 Case 3: Cylindrical Rotating Pedestal MOCVD Reactor

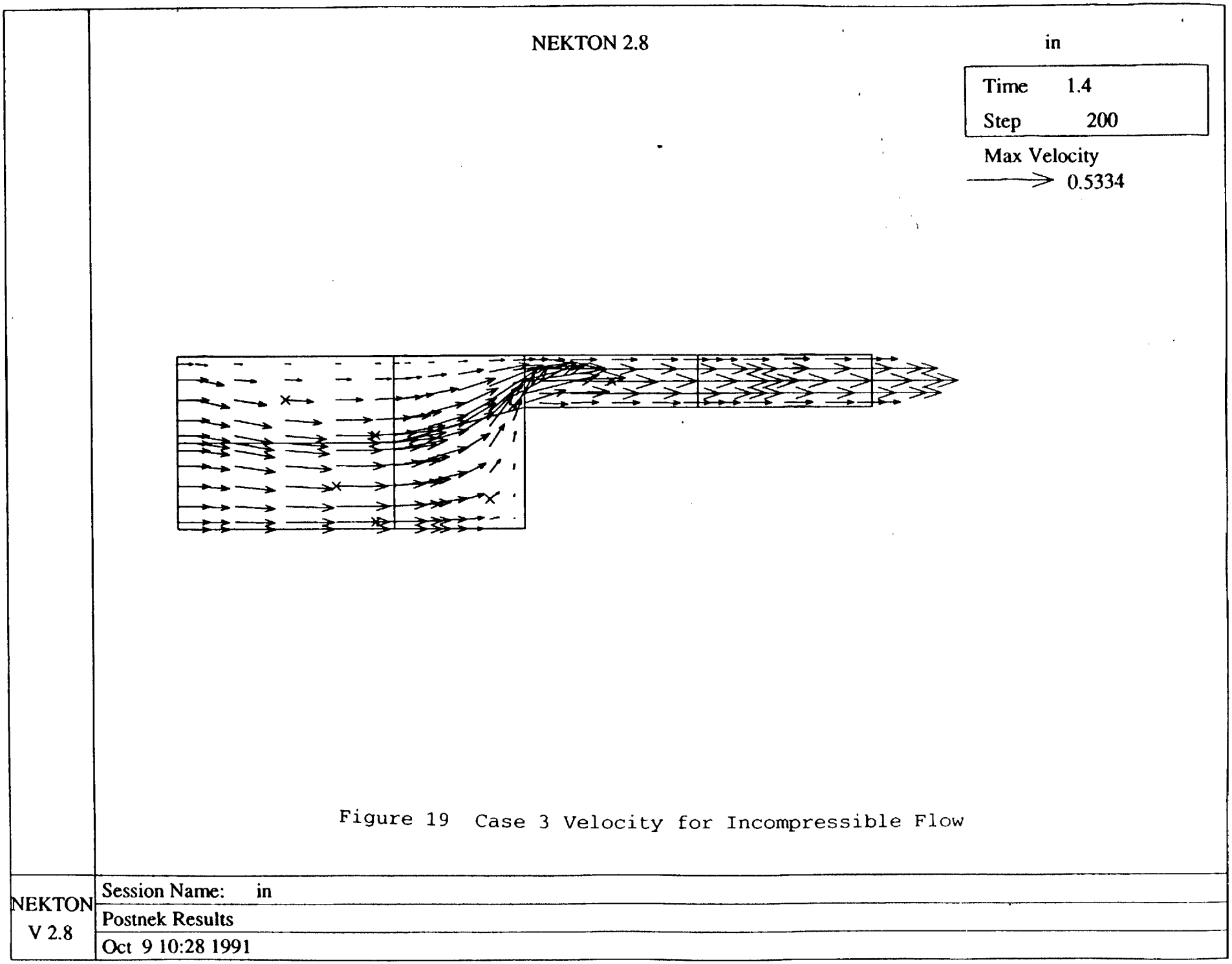

Figure 19 Case 3 Velocity for Incompressible Flow

NEKTON 2.8

in

Time 1.4
Step 200

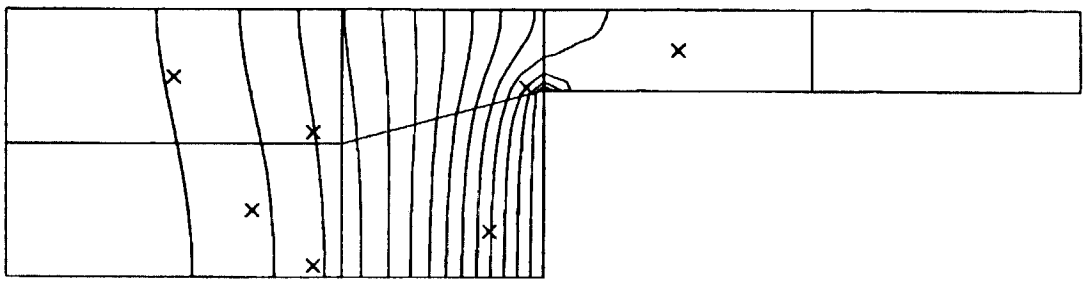

Tmax= 1000.

1.000
0.929
0.857
0.786
0.710
0.642
0.571
0.500
0.429
0.357
0.286
0.214
0.143
0.071
0.000

Tmin= 300.0

Figure 20 Case 3 Temperature Contours for Incompressible Flow

NEKTON V 2.8

Session Name: in
Postnek Results
Oct 9 10:28 1991

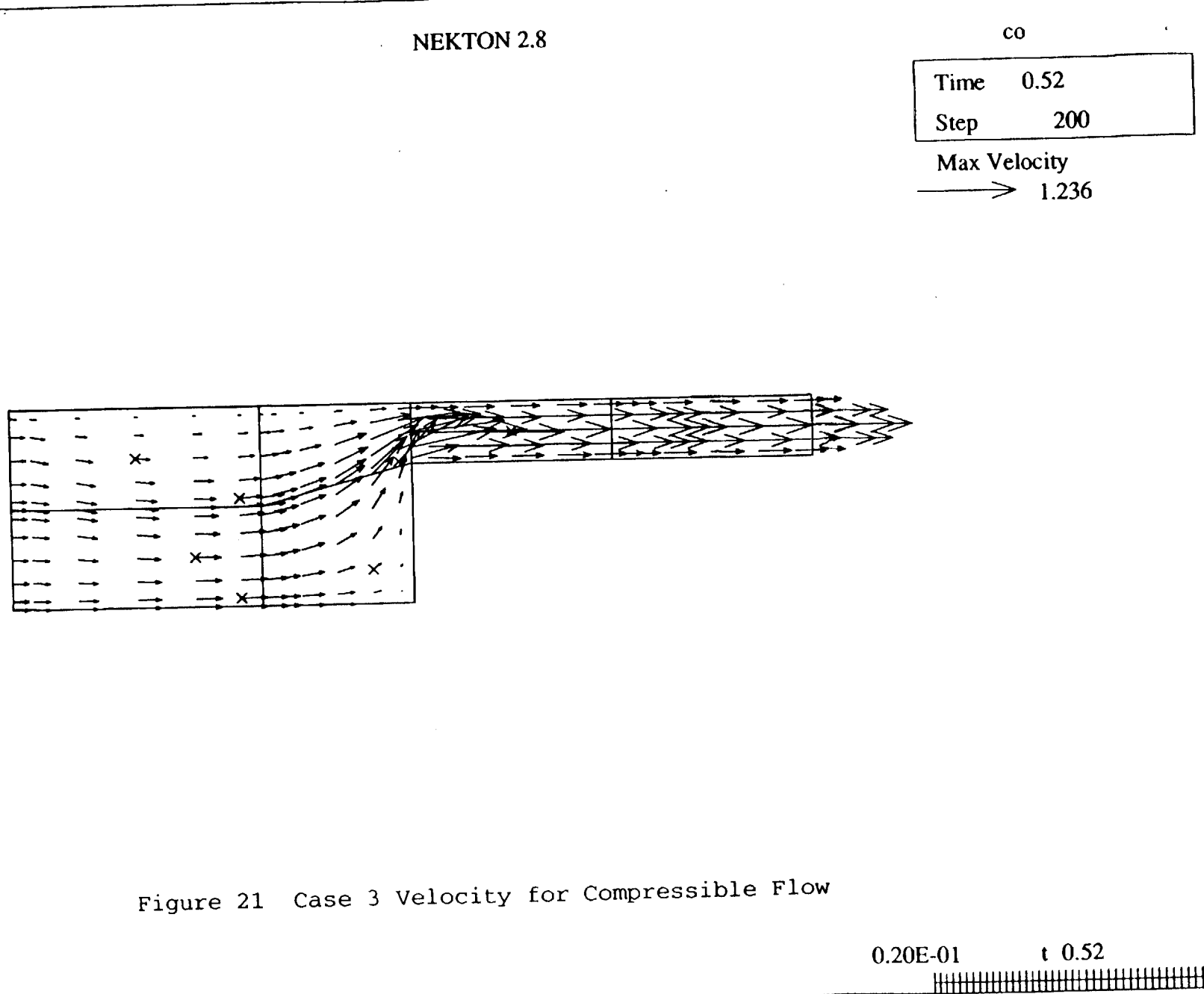

Figure 21 Case 3 Velocity for Compressible Flow

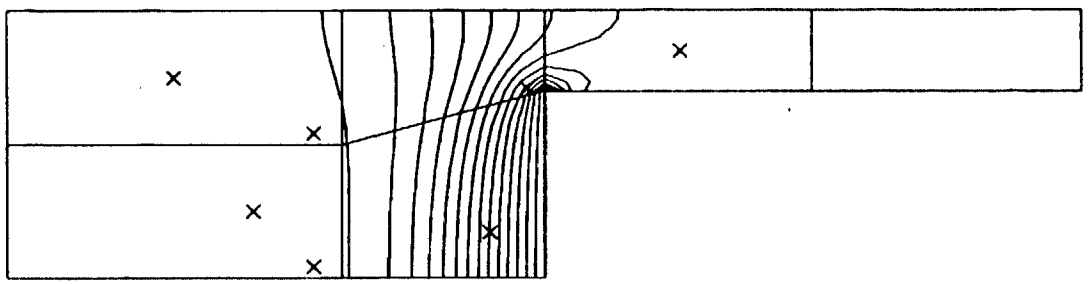

Figure 22 Case 3 Temperature Contours for Compressible Flow

Chapter 7

Point-Implicit Integration

OBJECTIVE:

The objective in this report period was to implement an implicit time integration of the chemical reactions into NEKTON. This was to be done using the point-implicit method described by Bussing and Murman [1].

In this report period we have implemented this capabililty in NEKTON for general 2-D, 3-D and axisymmetric geometries. We have demonstrated this new capability in simple geometries with which we have verified our results through comparison with analytic solutions. We have also demonstrated this capability on realistic CVD geometries.

BACKGROUND:

In many cases, solution of chemically reacting flows is made difficult by wide separation in the time scales involving the diffusive and convective fluid effects and the rates of chemical reactions. In typical MOCVD problems, the reactions can occur in time scales which are orders of magnitudes faster than the fluid effects. The physical

interpretation of this is that the reactions are diffusion-limited, that is, the reactants are quickly depleted locally and the reaction is governed by the slower time scales associated with transport of new reactants to the reaction site. These reactions result in a stiff numerical problem, with the stiffness usually defined by the ratio of the smallest time scale to the largest time scale,

$$Stiffness = \tau_{largest}/\tau_{smallest}$$

Bussing and Murman [1] developed a point-implicit method for use in solving these stiff problems for use with Euler equation calculations using finite volume methods. We have adapted this point-implicit method for use in solving the compressible and incompressible Navier-Stokes equations in NEKTON.

EXAMPLE CASES

To test the consistency, time-accuracy, and accuracy in the steady-state solution, two test problems were chosen. These were chosen to be relatively simple problems which had analytic solutions, but were nonetheless representative of calcualtions required for MOCVD. Each reaction has the form of:

$$R = kS$$

where the reaction rate constant k for a species of concentration S was given values of 1 and 100. This problem was run in a reaction/diffusion environment described by:

$$\frac{DS}{Dt} = -kS + \nabla^2 S$$

For this the steady solution is of the form

$$S = C_1 e^{10x} + C_2 e^{-10x}$$

and

$$S = C_1 e^{x} + C_2 e^{-x}$$

TEST RESULTS

These calculations were run in the domain x=[0,1] with S(0,t)=1; S(1,t)=2; and S(x,0) = 1.0. the resultant steady solution is:

$$S = 0.6944e^{x} + 0.3056e^{-x}$$

$$S = 9.07978E-5e^{x} + 0.999909202e^{-x}$$

The steady concentration solution calculated by NEKTON corresponding to the fast and slow reactions is plotted in Figures 1 and 2, respectively.

The error in the steady result (as measured by concentration at the domain midpoint) is summarized as follows:

Time Step	Fast Reaction		Slow Reaction	
	SS Soln	SS Error	SS Soln	SS Error
0.001	1.33023	0	0.0202140	0
0.01	1.33023	0	0.0202140	0
0.1	1.33024	10^{-5}	0.0202128	10^{-6}
1.0	1.33024	10^{-5}	0.0202128	10^{-6}
10.0	1.33024	10^{-5}	0.0202122	10^{-6}
100.0	1.33024	10^{-5}	0.0202122	10^{-6}

The time histories of the approach to the steady solution is plotted in figures 3a-4c. Figures 3 a,b, and c represent the history of the concentration in the fast reaction as it approches its steady value with time steps of 0.001, 0.01, and 0.1, respectively. Figures 4a, b, and c represent the same for the slow reaction.

DISCUSSION

In as much as it is possible, this scheme preserves the time accuracy of the algorithm. For those component reactions whose characteristic time τ is small compared to the time step, a time-accurate calculation of its contribution is done. For those parts of the simulation whose characteristic time τ is large compared to the time step, a *stable* iteration occurs which leads it to the correct steady state. This process results in a coupled calculation in which the faster processes are solved in a quasi-steady iterative scheme, and the unsteadiness is governed by the time-accurate calculation of the slower system components to which the fast process is coupled. For problems in which the time step is much greater than the characteristic time (e.g., DT=0.1 for a reaction with time scales of 0.01, figure 3c), the time stepping algorithm effectively becomes an iteration scheme, with the species converging to steady state in a few time steps. The advantage is in that many less iterations are required in this pseudo time-stepping scheme than actual time steps required in the standard time-stepping scheme.

CONCLUSION

We have demonstrated that the point-implicit method in NEKTON for solution of stiff chemically reacting flows. It has been demonstrated to give full time-accurate solutions for those problems which are temporally resolved, that is, for problems in which the time step is small enough to capture the time scales for the physics of interest. It has been demonstrated to reach accurate steady state solutions for those

problems that are not temporally resolved. Where both fast and slow time scales exist in a coupled problem, the enhanced NEKTON gives time-accurate solutions for the slow components and smears the fast reactions across a few time steps.

REFERENCES

1. Bussing, Thomas R.A. Forester, and Murman, Earll M., "Finite Volume Method for the Calculation of Compressible Chemically Reacting Flows", AIAA Journal, VOL 26, NO. 9, 1070-1078.

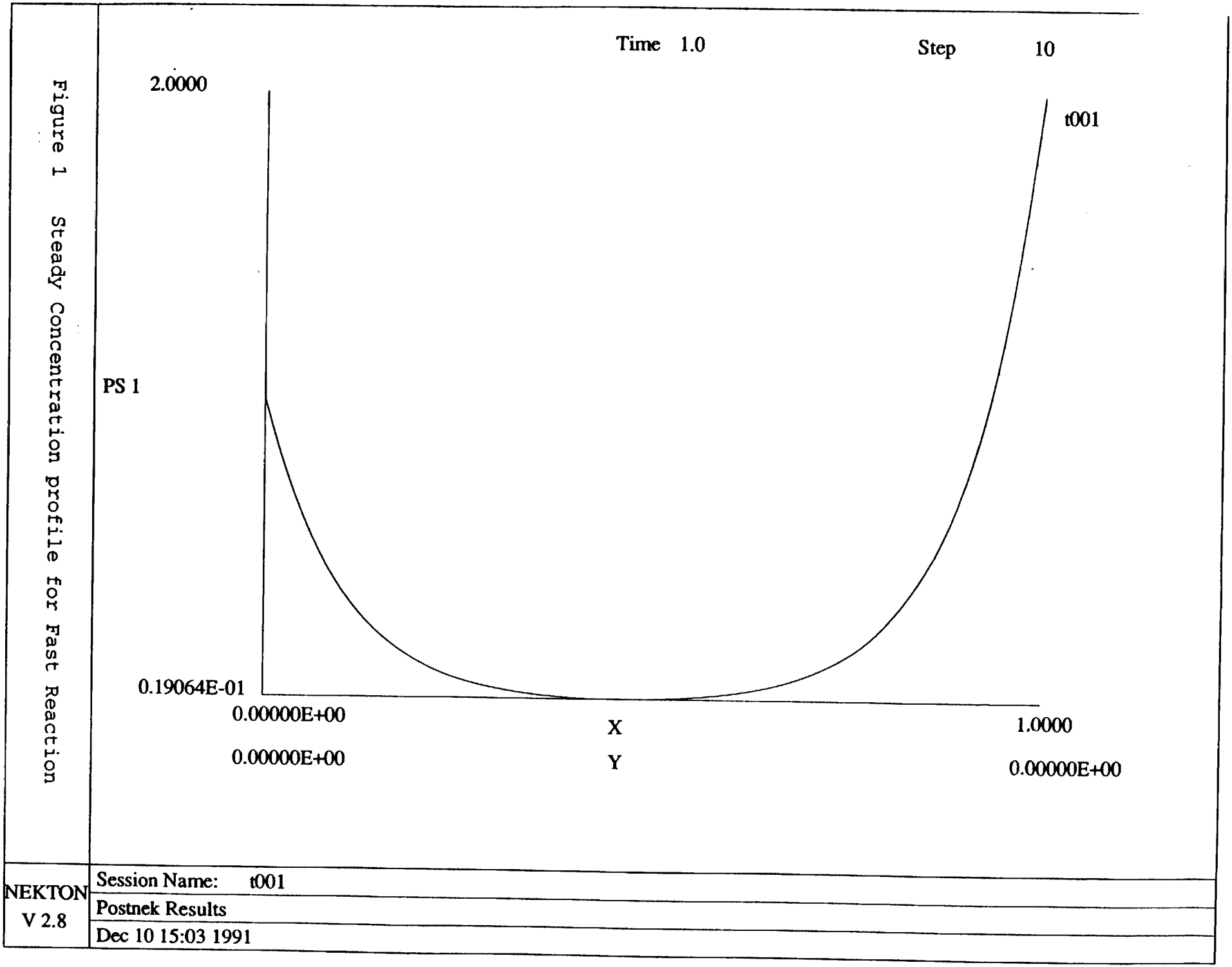

Figure 1 Steady Concentration profile for Fast Reaction

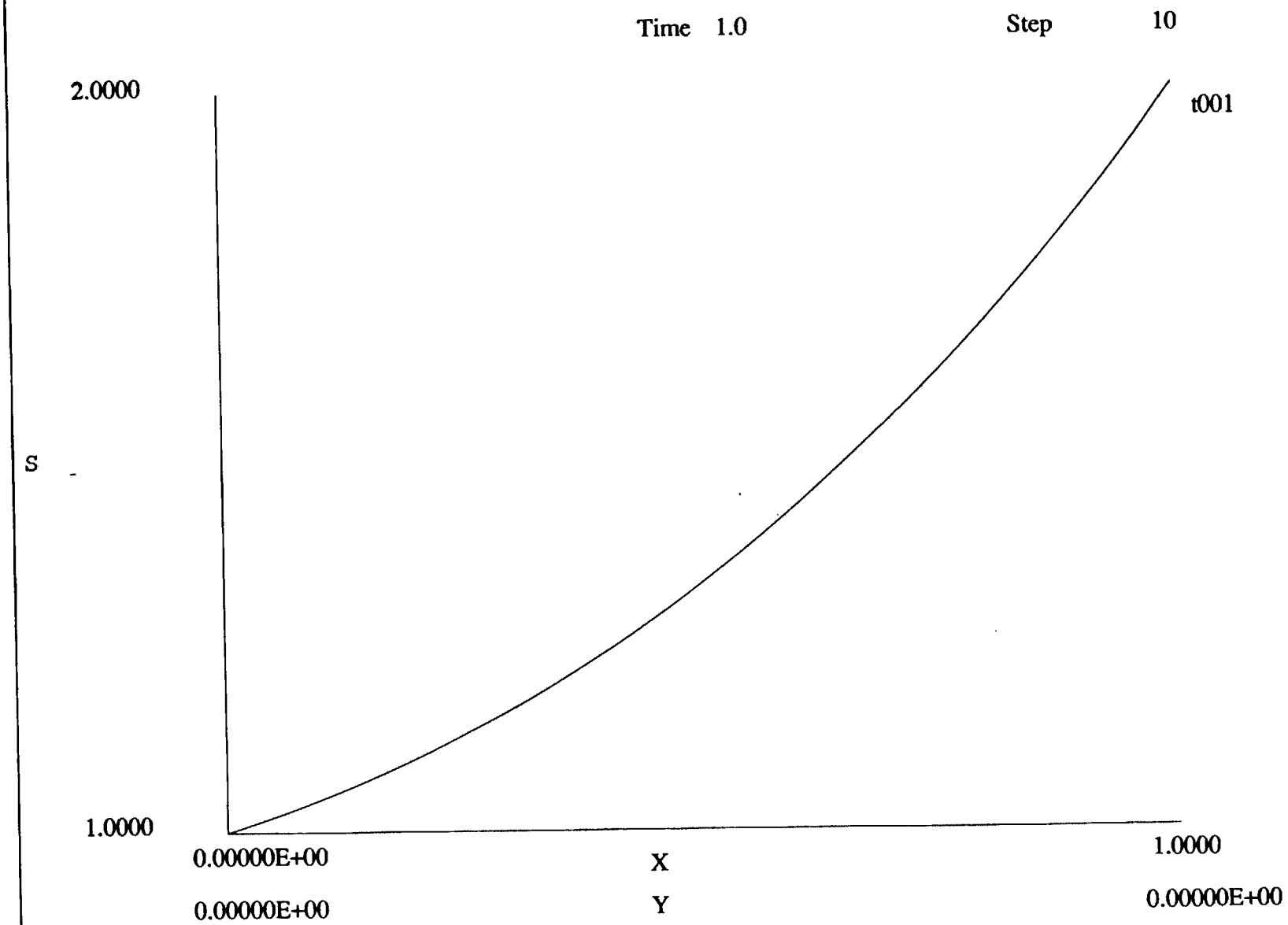

Figure 2 Steady Concentration profile for Slow Reaction

NEKTON V 2.8	Session Name: t001
	Postnek Results
	Dec 10 15:03 1991

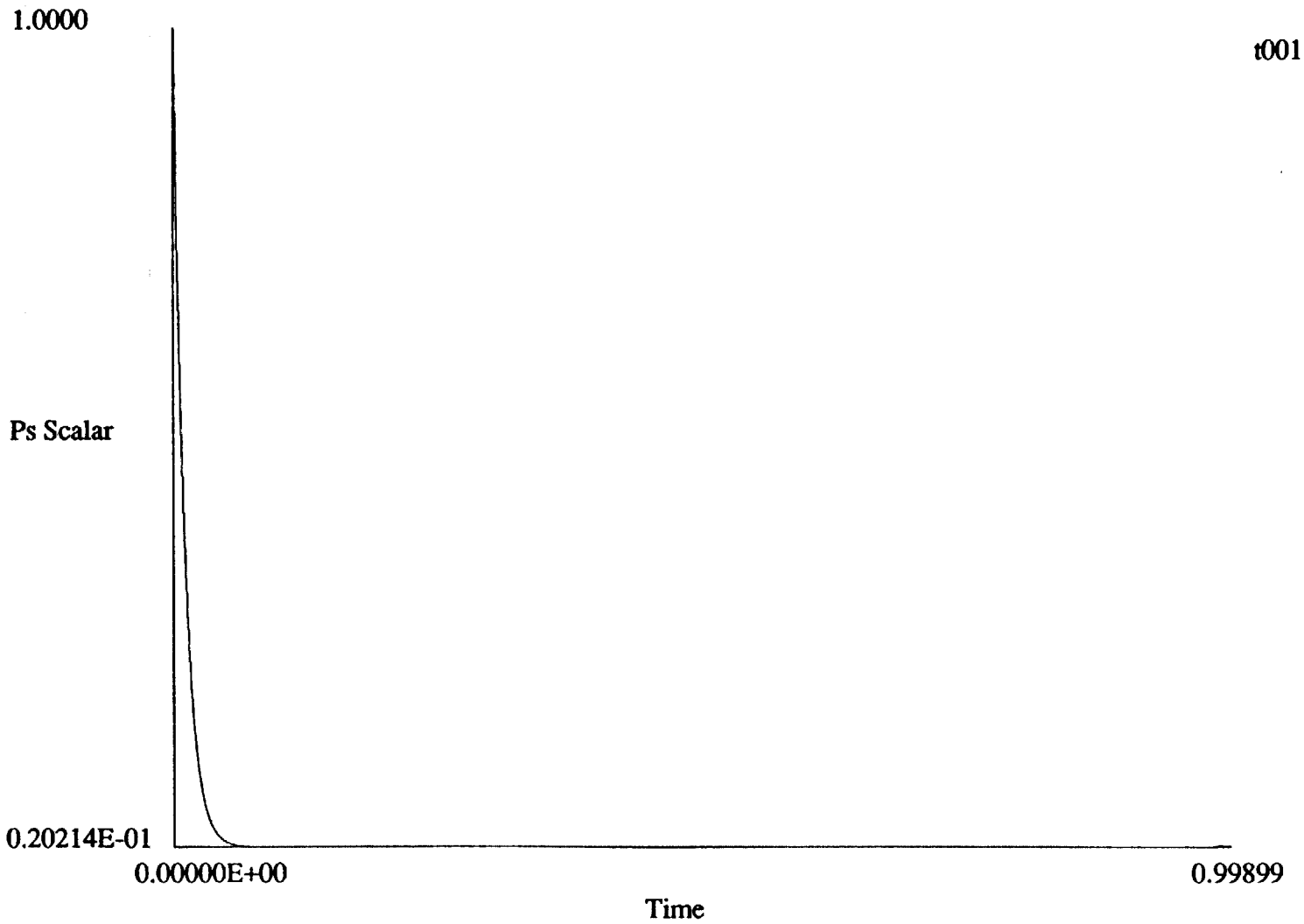

Figure 3a Concentration history for Fast Reaction DT = 0.001

NEKTON V 2.8	Session Name: t001
	Postnek Results
	Dec 10 11:03 1991

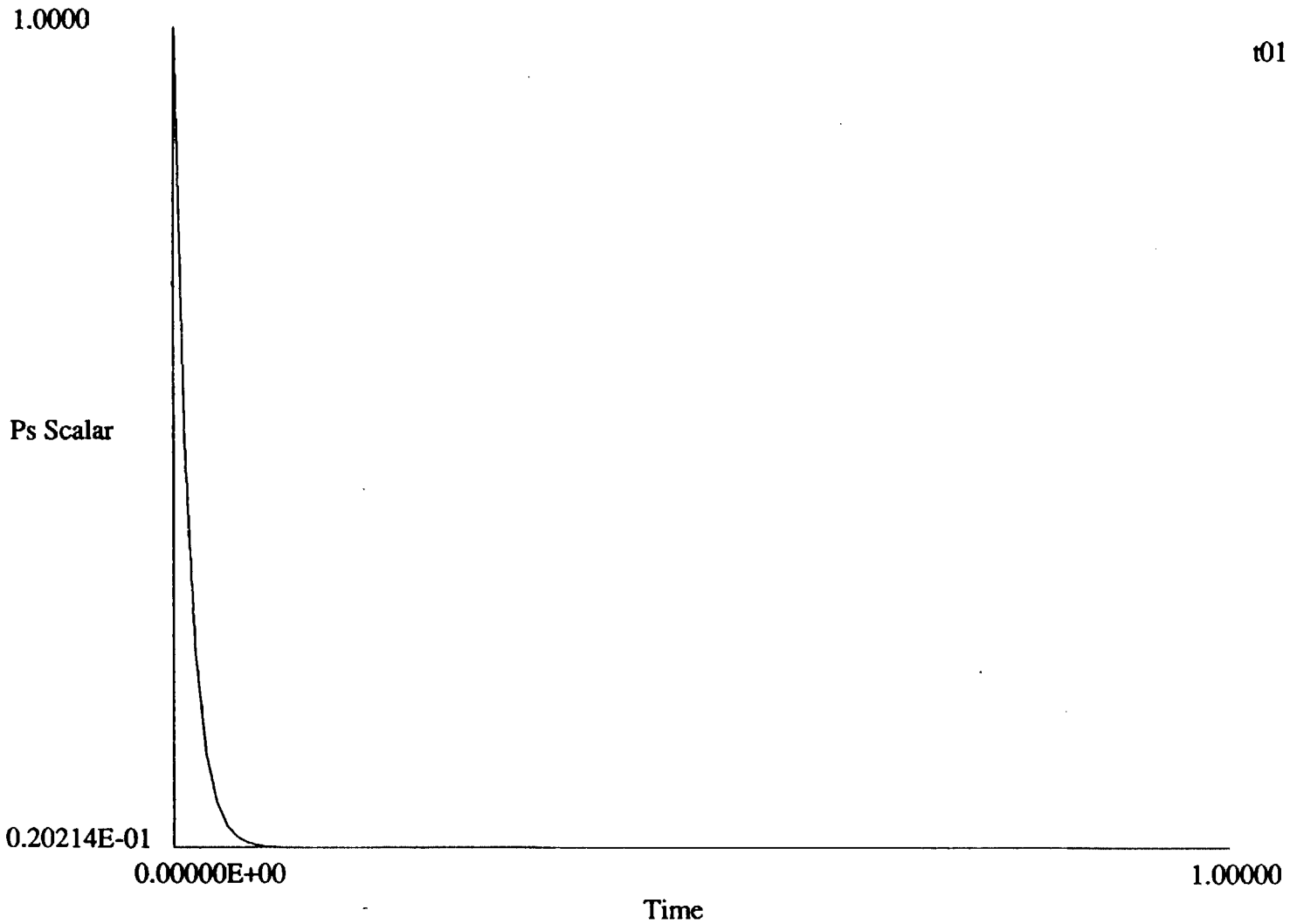

Figure 3b Concentration history for Fast Reaction DT = 0.01

NEKTON V 2.8	Session Name: t01
	Postnek Results
	Dec 10 11:05 1991

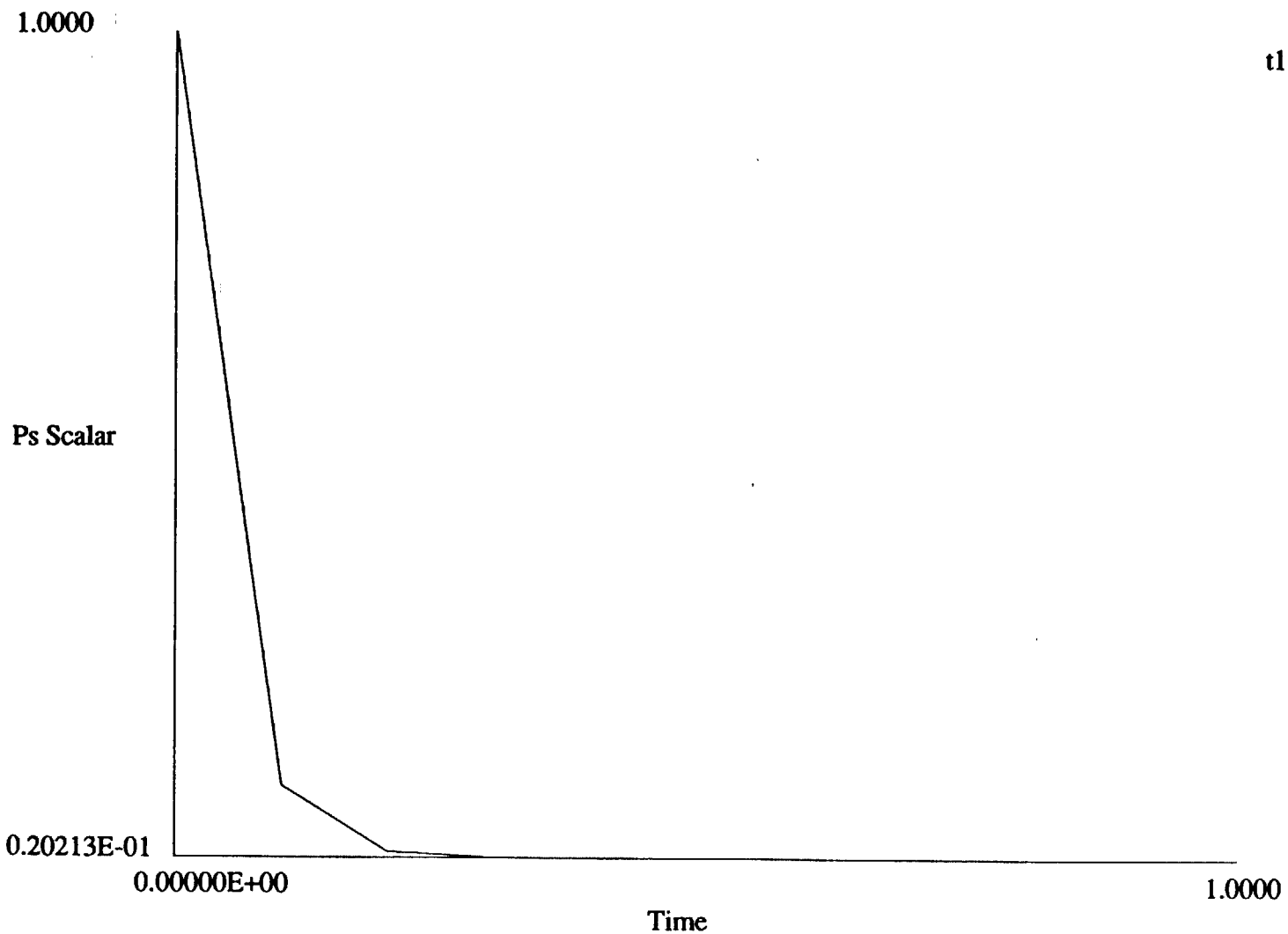

Figure 3c Concentration history for Fast Reaction DT = 0.1

NEKTON V 2.8	Session Name: t1
	Postnek Results
	Dec 10 11:07 1991

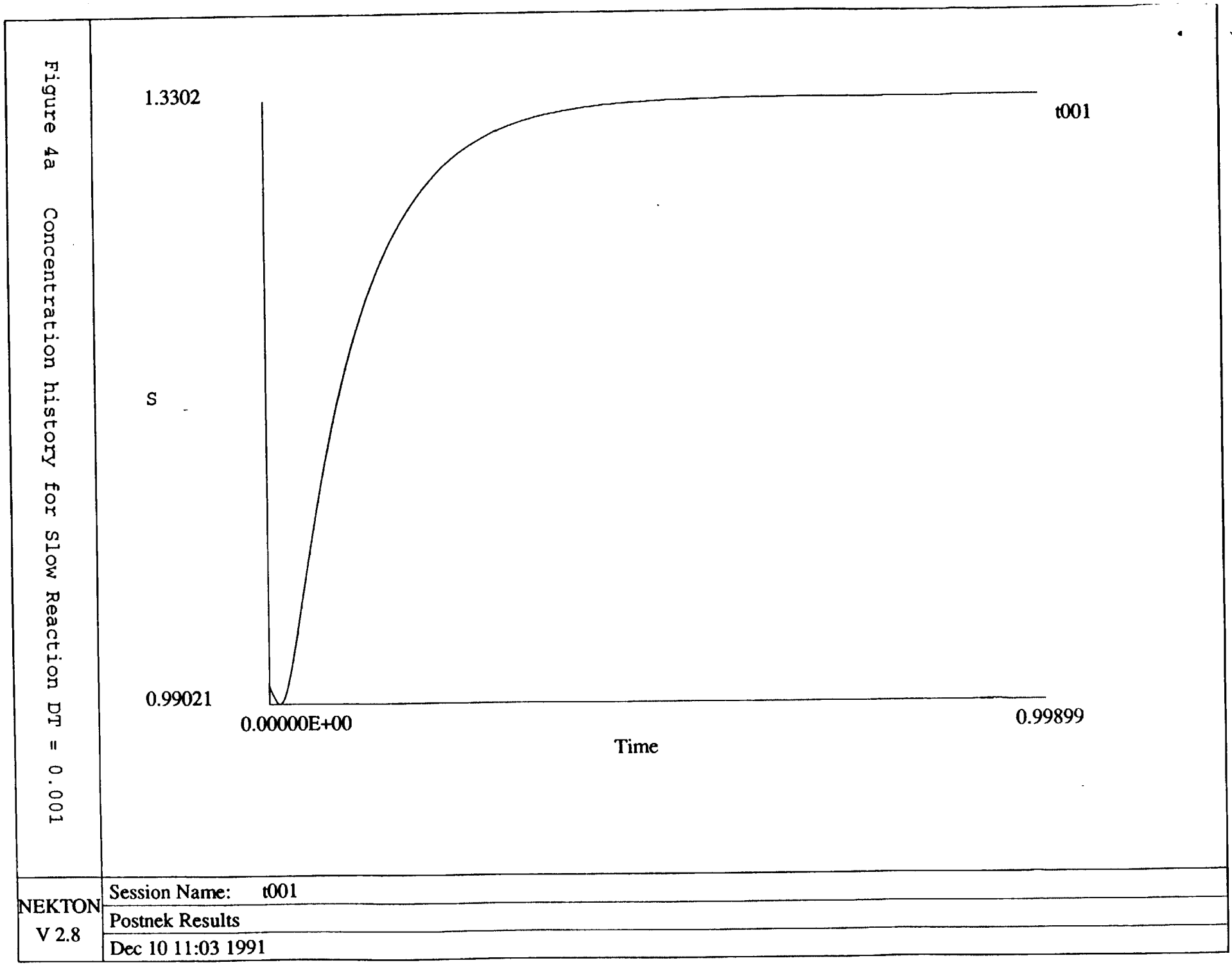
Figure 4a Concentration history for Slow Reaction DT = 0.001
1.3302
t001
S
0.99021
0.00000E+00
0.99899
Time
NEKTON
V 2.8
Session Name: t001
Postnek Results
Dec 10 11:03 1991

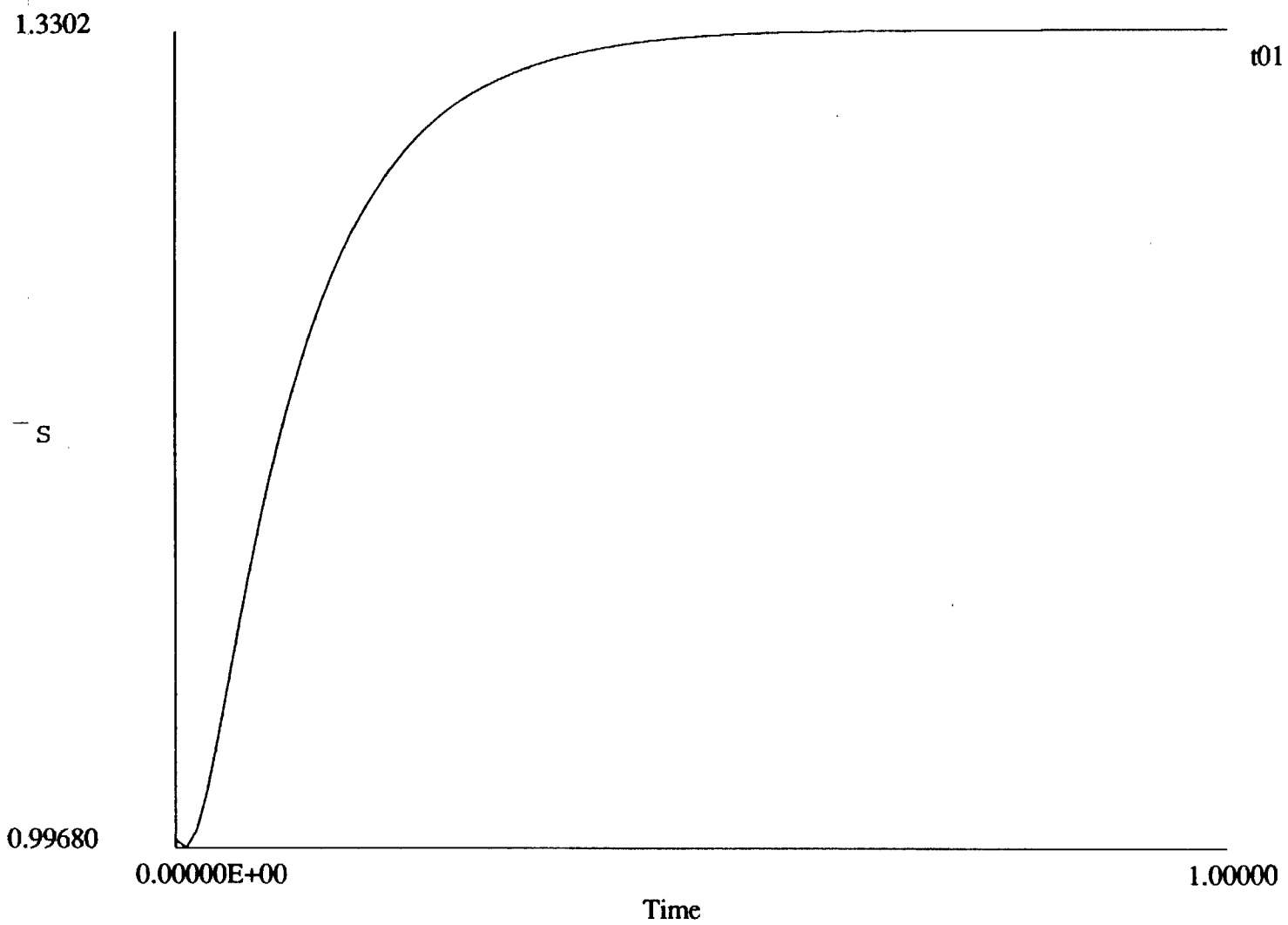

Figure 4b Concentration history for Slow Reaction DT = 0.01

NEKTON V 2.8	Session Name: t01
	Postnek Results
	Dec 10 11:05 1991

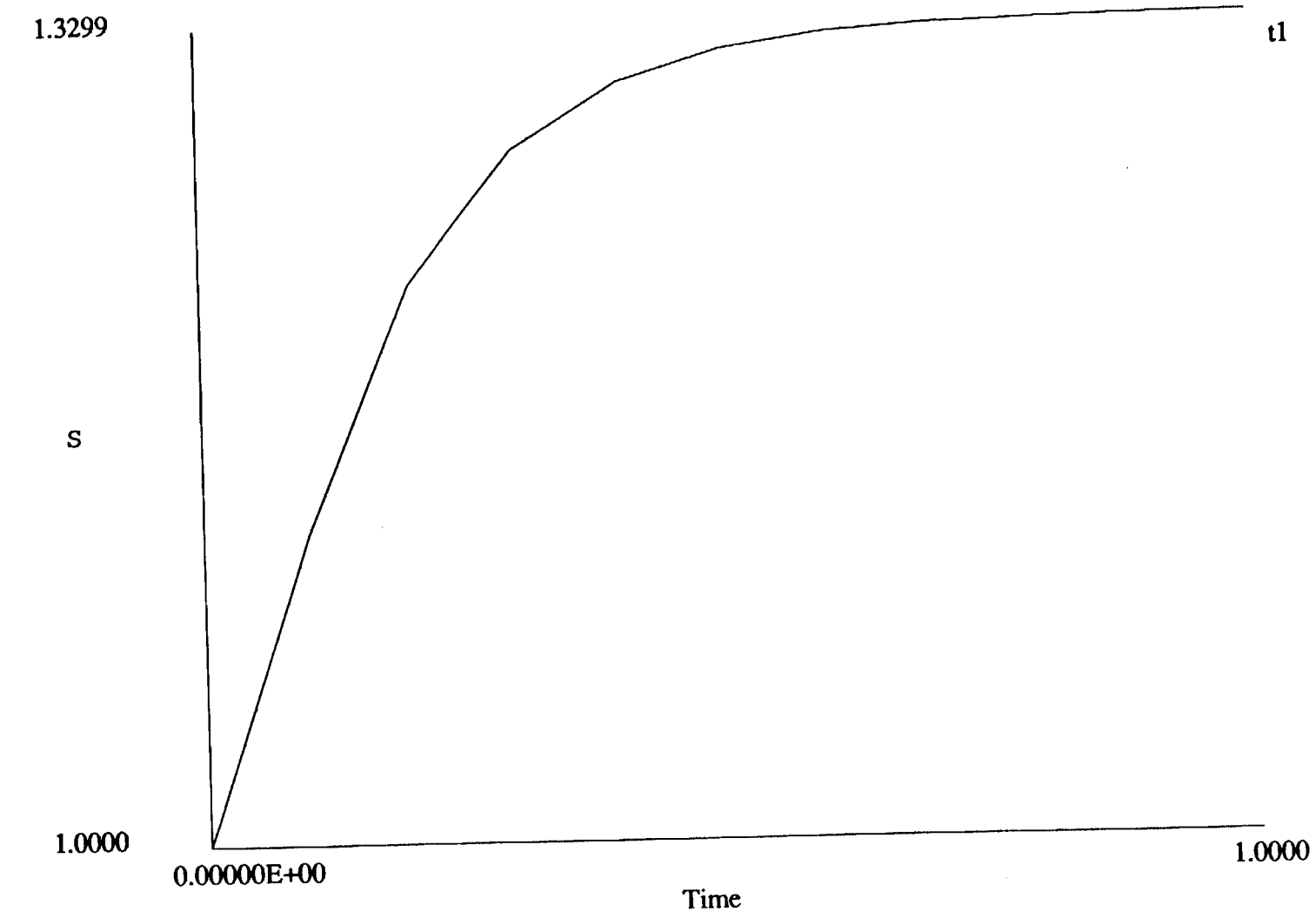

Figure 4c Concentration history for Slow Reaction DT = 0.1

NEKTON V 2.8	Session Name: t1
	Postnek Results
	Dec 10 11:07 1991

Chapter 8

Non-dilute Mixtures

OBJECTIVE:

The result achieved in this report period was to implement the effects of non-dilute mixtures in the convection-diffusion equations in NEKTON.

BACKGROUND:

The chemistry in the gas phase in CVD reactors and the concentration of each species of mass involved in the reaction is important in finding the overall rates of deposition and the spatial uniformity of that deposition. The standard diffusion equations used when small concentrations of contaminants diffuse through background media passively (without affecting the background media) break down when the concentrations become large.

IMPLEMENTATION :

We begin with the relations for multicomponent nondilute mixtures developed in White (1). We have a mixture of n fluids, with individual total masses $m_1, m_2, m_3, \ldots$ contained in volume v. The density of this mixture would be defined as:

$$\rho = \frac{m}{v} \tag{1}$$

where

$$m = \sum_{i=1}^{n} m_i \tag{2}$$

and

$$\rho_i = \frac{m_i}{v} \tag{3}$$

where

$$\rho = \sum_{i=1}^{n} \rho_i \tag{4}$$

we define ω as the mass fraction:

$$\omega_i = \frac{m_i}{m} = \frac{\rho_i}{\rho} \tag{5}$$

which sum to one:

$$\sum_{i=1}^{n} \omega_i = 1 \tag{6}$$

The velocity $\mathbf{V}$ is defined as

$$\mathbf{V} = \frac{1}{\rho} \sum_{i=1}^{n} \rho_i \mathbf{V}_i = \sum_{i=1}^{n} \omega_i \mathbf{V}_i \tag{7}$$

where $\rho_i \mathbf{V}_i \equiv \mathbf{f}_i$, the mass flux of species i.

The difference between the mass averaged velocity and the species velocity of component i is the diffusion velocity of component i, $(\mathbf{V}_i - \mathbf{V})$. The diffusion mass flux is:

$$\mathbf{j}_i = \rho_i (\mathbf{V}_i - \mathbf{V}) \tag{8}$$

The net diffusion mass flux sums to zero:

$$\sum_{i=1}^{n} \mathbf{j}_i = 0 \tag{9}$$

The implications of this in implementation of these equations in NEKTON is as follows. The boundary condition for absorption of a given species is $\rho_i \mathbf{V}_i = \mathbf{f}_i$. The

boundary condition for a given species that is not absorbed is $\rho_i \mathbf{V}_i = \mathbf{f}_i = 0$. In the vector quantities used here and in what follows, the coordinate system used is local, with all vector quantities (fluxes, velocities) represent components oriented normal to the surface with the convention that quantities oriented outward from the domain are positive. From (7), the velocity at the surface can be calculated as:

$$\mathbf{V} = \frac{1}{\rho} \sum_{i=1}^{n} \mathbf{f}_i = \frac{1}{\rho} \sum_{i=1}^{n} \rho_i \mathbf{V}_i \tag{10}$$

Note that in cases in which one or more species are being absorbed, i.e., $\mathbf{f}_i \neq 0$, the velocity at the wall is *nonzero.*

The mass balance and associated boundary conditions for the transport of chemical species is, then:

Knowing $\mathbf{V}$ and $\mathbf{V}_i$, The diffusion mass flux at the surface is:

$$\mathbf{j}_i = \rho_i(\mathbf{V}_i - \mathbf{V}) = D_i \nabla \rho_i \tag{11}$$

This mass flux can be input as a surface flux.

Continuity Equations:

The continuity equation for a single component gas under low Mach number compressibility is

$$\nabla \cdot \mathbf{V} = \frac{1}{T} \frac{dT}{dt} \tag{12}$$

With a mixture of ideal gases the effective gas law constant for the mixture is:

$$\overline{R} = \frac{1}{\rho} \sum_{i=1}^{n} \rho_i R_i \tag{13}$$

The continuity equation for the gas mixture under low Mach number compressibility is

$$\nabla \cdot \mathbf{V} = \frac{1}{T}\frac{dT}{dt} + \frac{1}{\overline{R}}\frac{d\overline{R}}{dt} = \frac{1}{T}\frac{dT}{dt} + \frac{1}{\sum_{i=1}^{n}\rho_i R_i}\sum_{i=1}^{n} R_i \frac{d\rho_i}{dt} \tag{14}$$

while the momentum equation becomes:

$$\frac{\mathbf{DV}}{\mathbf{Dt}} = -\frac{\nabla P}{\overline{\rho}} + \nu\nabla^2\mathbf{V} + f \tag{15}$$

SCALINGS:

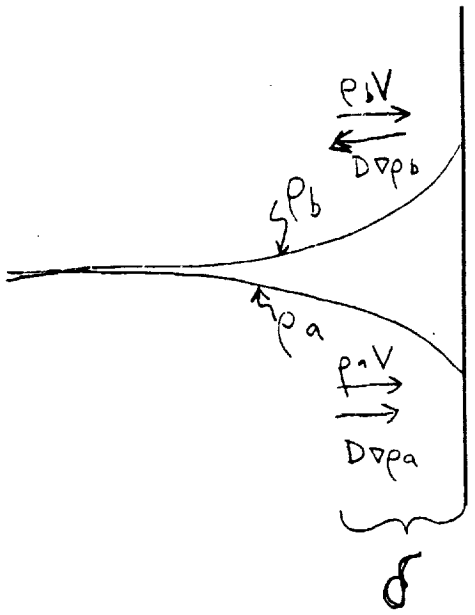

For a binary mixture of gases a and b in which a is being absorbed and the b is not, we have the following:

$$\mathbf{V} = \frac{1}{\rho}\sum_{i=1}^{n}\mathbf{f}_i = \frac{1}{\rho}\rho_a\mathbf{V}_a \tag{16}$$

The diffusion mass flux of b at the surface is:

$$\mathbf{j}_b = \rho_b(\mathbf{V}_b - \mathbf{V}) = D_b\nabla\rho_b \tag{17}$$

Since $\mathbf{V}_b = 0$, we have

$$-\rho_b\mathbf{V} = D_b\nabla\rho_b \tag{18}$$

Fo a boundary layer thichness δ, the conentration gradient $\nabla\rho_b$ scales as $1/\delta$, so that

$$\delta \sim \frac{D_b}{\mathbf{V}}, \tag{19}$$

e.g., the dimensionless boundary layer thickness$\left(\delta/L\right)$scales as $\frac{1}{ReSc}$, where $Sc \equiv \frac{\nu}{D}$ and $ReSc = \frac{\mathbf{V}L}{D}$.

REFERENCES

1. White, Frank M., **Heat and Mass Transfer** Addison-Wesley, 1988.

Chapter 9

Project Summary

CHEMICAL VAPOR DEPOSITION FLUID FLOW SIMULATION MODELLING TOOL

Chemical Vapor Deposition (CVD) processes combine problems from several disciplines. They require solution of the flow problem to model the transport of heat and chemical species, as well as solution of the chemical kinetics problem within the flow. Modeling of the of the flow field requires solution of the Navier-Stokes and energy partial differential equations which are coupled through thermal expansion, buoyancy, and convection. The principal effect of the flow field on deposition is that it affects the transport of the species to the reaction sites and their temperatures. Modelling of the chemistry consists of solution of a set of ordinary differential equations governing the (local) reaction chemistry.

To these sets of problems, we have applied the spectral element method (SEM) using the code NEKTON. The SEM combines the methodology of the standard finite element with high-order (spectral) techniques. In this way the accuracy of

spectral techniques can be combined with the geometric flexibility of finite element methods.

NEKTON incorporates additional innovative features in its design that maintain it at the leading edge of the state of the art in numerics. It is the first commercial CFD code to be intrinsically designed for use on parallel processors. It is, to our knowledge, the only major commercial CFD package which can effectively utilize parallel processors. Its locally structured, globally unstructured spectral element mesh is naturally suited to a geometry-based parallelism in which each spectral element (or group of spectral elements) is mapped to a separate processor/memory, with the individual processor/memory units linked by a relatively sparse communications network. This structure makes for high parallel efficiency. Another innovation is that it is designed to be inherently three-dimensional, so that features implemented in two dimensions are automatically available in the three-dimensional code.

In modifying NEKTON to address issues in CVD modelling, we have made progress in three essential areas: First, e have implemented a number of features into the code which aid in the analysis of CVD problems. Second, we have developed improved and robust numerical methods. Third, we have identified methods of programming methodology that will result in future codes that are more portable, modular, and maintainable.

The capabilities implemented were specific to CVD and especially to CVD in microgravity applications. We first implemented the capability of solution of problems in which the "g-jitter" typically found in microgravity applications was a significant influence on the convective transport. This was done through user specification of an arbitrary time-dependent and orientation dependent gravity vector.

The major task in this project was the implementation of low-Mach num-

compressibility. Whereas most analyses of CVD processes assume a Boussinesq approximation for thermal expansion, Makarov and Zhmakin [1] have recently shown that this approximation can result in errors of the order of 100%. In contrast, we have shown that the low-Mach number approximation gives errors of less than 1% through the range of CVD problems. This approximation takes advantage of the fact that the compressibility in CVD applications is essentially due to thermal expansion, and that compressibility due to the momentum equation is negligible. This gives the important advantage in solution of CVD problems in reduced physical and numerical complexity. Additionally, the stiff numerical problems associated with the widely disparate time scales of the fully compressible Navier-Stokes equations are avoided.

Another important feature for CVD was the ability to solve problems in which the properties (thermal and mass diffusivities) vary with temperature and species concentration.

A feature crucial for rotating pedestal CVD reactors is the ability to include swirl (azimuthal velocity) in the calculations. The swirl calculation enables rotational pumping of the flow by the rotating pedestal to be included in the model. The swirl velocity is coupled to the planar axisymtric velocities in the reactor via the coriolis and centrifugal forces.

An additional feature has been implemented into the code. While the code is inherently iterative and unsteady, we have identified some CVD problems for which a steady, direct solver is more appropriate.

We have also tested modules for multi-body radiation, Soret effects, and nondilute mixtures. We have to date included into the commercial code several numerical capabilities developed in this project. The major developmental goal of this project, compressible transport in the gas phase, has been fully integrated into

the code. We have also incorporated single-body radiation, the steady solver, the ability to put in arbitrary and time- and orientation-dependent gravitational forces in order to model g-jitter.

The programming advances that resulted from this project were as follows. The implementation of the direct solver presented memory requirements that were substantially larger than the iterative solvers. Moreover, the memory for the direct solver varied as square of the the number of degrees-of-freedom, rather than linearly, resulting in huge variations in memory requirements for different problems. We have developed the capability in our commercial code of mixing C routines with the FORTRAN which makes up the bulk of the code. The C code functions to allocate memory during run-time to pass to the FORTRAN subroutines. This approach was so successful and attractive that we are currently in the process of a complete rewrite of the code into the C language. Additional benefits of C are modularity, encapsulation of data, and natural transition to the object-oriented language C++.

In the Phase III commercialization of this code we expect to incorporate the remainder of the features developed under this program into the commercial NEKTON. Using the newly developed programming techniques we expect the increased modularity of the code to enable us to re-use modules and retain a broad range of features in a rapidly evolving code.

REFERENCES

1. Y.N. Makarov and A.I. Zhmakin, J. Cryst. Growth, **77** (1986) 108.

REPORT DOCUMENTATION PAGE

Form Approved
OMB No. 0704-0188

1. AGENCY USE ONLY (Leave blank)	2. REPORT DATE	3. REPORT TYPE AND DATES COVERED
	June, 1992	Contractor Report

4. TITLE AND SUBTITLE
Chemical Vapor Deposition
Fluid Flow Modelling Tool

5. FUNDING NUMBERS
C NAS1-19102
WU 324-02-02

6. AUTHOR(S)
Edward T. Bullister

7. PERFORMING ORGANIZATION NAME(S) AND ADDRESS(ES)
Nektonics, Inc.
875 Main St.
Cambridge, MA 02139

8. PERFORMING ORGANIZATION REPORT NUMBER

9. SPONSORING / MONITORING AGENCY NAME(S) AND ADDRESS(ES)
National Aeronautics and Space Administration
Langley Research Center
Hampton, VA 23665-5225

10. SPONSORING / MONITORING AGENCY REPORT NUMBER
NASA CR-189648

11. SUPPLEMENTARY NOTES
Langley Technical Monitor: I. O. Clark
Final Report-SBIR Phase II

12a. DISTRIBUTION / AVAILABILITY STATEMENT
[redacted]
Subject Category 34

12b. DISTRIBUTION CODE

13. ABSTRACT *(Maximum 200 words)*

Accurate numerical simulation of chemical vapor deposition (CVD) processes requires a general purpose computational fluid dynamics package combined with specialized capabilities for high temperature chemistry. In this report we describe the implementation of these specialized capabilities in the spectral element code NEKTON. The thermal expansion of the gases involved is shown to be accurately approximated by the low Mach number perturbation expansion of the incompressible Navier-Stokes equations. The radiative heat transfer between multiple interacting radiating surfaces is shown to be tractable using the method of Gebhart. The disparate rates of reaction and diffusion in CVD processes are calculated via a point-implicit time integration scheme.

We demonstrate the use above capabilities on prototypical CVD applications.

14. SUBJECT TERMS	15. NUMBER OF PAGES
Materials Processing, Fluid Mechanics, Chemical Vapor Deposition, Spectral Element	135
	16. PRICE CODE

17. SECURITY CLASSIFICATION OF REPORT	18. SECURITY CLASSIFICATION OF THIS PAGE	19. SECURITY CLASSIFICATION OF ABSTRACT	20. LIMITATION OF ABSTRACT
Unclassified	Unclassified		